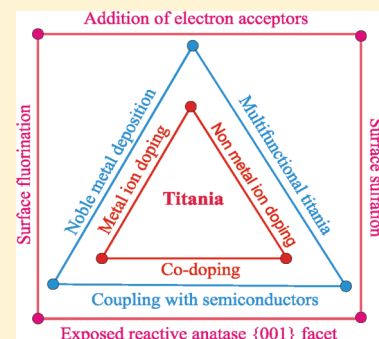


# Review on Modified TiO<sub>2</sub> Photocatalysis under UV/Visible Light: Selected Results and Related Mechanisms on Interfacial Charge Carrier Transfer Dynamics

S. Girish Kumar and L. Gomathi Devi\*

Department of Post Graduate Studies in Chemistry, Bangalore University, Central College City Campus, Dr. Ambedkar Street, Bangalore-560001, Karnataka, India

**ABSTRACT:** Titania is one of the most widely used benchmark standard photocatalysts in the field of environmental applications. However, the large band gap of titania and massive recombination of photogenerated charge carriers limit its overall photocatalytic efficiency. The former can be overcome by modifying the electronic band structure of titania including various strategies like coupling with a narrow band gap semiconductor, metal ion/nonmetal ion doping, codoping with two or more foreign ions, surface sensitization by organic dyes or metal complexes, and noble metal deposition. The latter can be corrected by changing the surface properties of titania by fluorination or sulfation or by the addition of suitable electron acceptors besides molecular oxygen in the reaction medium. This review encompasses several advancements made in these aspects, and also some of the new physical insights related to the charge transfer events like charge carrier generation, trapping, detrapping, and their transfer to surface are discussed for each strategy of the modified titania to support the conclusions derived. The synergistic effects in the mixed polymorphs of titania and also the theories proposed for their enhanced activity are reported. A recent venture on the synthesis and applications of anatase titania with a large percentage of reactive {001} facets and their band gap extension to the visible region via nonmetal ion doping which is a current hot topic is briefly outlined.



## 1.0. INTRODUCTION

Semiconductor nanostructure materials with superior physicochemical and optical properties are being employed for potential uses in diverse applications. The semiconductor acts as a photocatalyst for the light-induced photochemical reactions because of its unique electronic structure characterized by a filled valence band (VB) and an empty conduction band (CB). The prerequisite for an efficient photocatalyst is that the redox potential for the evolution of hydrogen and oxygen from water and for the formation of reactive oxygenated species (hydrogen peroxide, hydroxyl, and superoxide radicals) should lie within the band gap of the semiconductor. Since the photocatalytic reaction proceeds in an air-saturated and water-rich environment, the stability of the chosen photocatalyst is vital under these conditions. In 1972, Fujishima and Honda achieved UV light induced water cleavage using a TiO<sub>2</sub> photoanode in combination with a Pt counter electrode immersed in an aqueous electrolytic solution.<sup>1</sup> Since then, TiO<sub>2</sub> photocatalysis has attracted significant attention because of its promising applications in wastewater purification as well as solar energy conversion.<sup>2–10</sup> The excitation of TiO<sub>2</sub> by photons with light energy greater than the band gap is the primary process underlying its vast area of photochemistry and photoelectrochemistry. TiO<sub>2</sub> is used mainly due to its nontoxicity, water insolubility, hydrophilicity, cheap availability, stability and against photocorrosion and for its suitable flat band potential ( $V_{fb}$ ) that can induce the desired redox reactions without biased potential. Furthermore, TiO<sub>2</sub> can be

supported on various substrates such as glass, fibers, stainless steel, inorganic materials, sand, and activated carbon which allows its continuous reuse. However, the large band gap of TiO<sub>2</sub> (~3.2 eV for anatase and brookite, ~3.0 eV for rutile) requires an excitation wavelength that falls in the UV region. Given that less than ~5% of the solar flux incident at the earth's surface lies in this spectral regime (solar light consists of ~5% UV, ~43% visible, and ~52% harvesting infrared), utilization of natural solar light for a photocatalytic or photoelectrochemical process can thus be enhanced by tuning the band gap response of titania to the visible region. Thus, designing, fabricating, and tailoring the physicochemical and optical properties of titania is indispensable to utilize a large fraction of the solar spectrum and to realize the indoor applications of this photocatalyst. For this purpose, TiO<sub>2</sub> is modified by various strategies like coupling with a narrow band gap semiconductor, metal ion/nonmetal ion doping, codoping with two or more foreign ions, surface sensitization by organic dyes or metal complexes, surface fluorination, and noble metal deposition which exerts a substantial influence in modifying the electronic band structure and construction of favorable surface structure resulting in higher quantum efficiency and reaction rates for the degradation of organic pollutants under UV/solar light illumination. Although the physics behind the

**Received:** May 10, 2011

**Revised:** August 10, 2011

**Published:** September 15, 2011

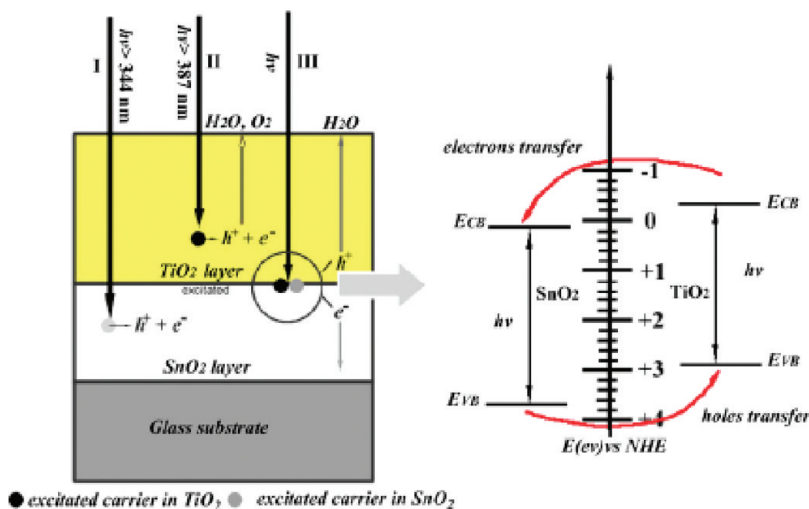


**Figure 1.** Schematic representation of the interfacial charge transfer processes in the  $\text{SnO}_2\text{--TiO}_2$  composite film. Reprinted with permission from Zhou, M.; Yu, J.; Liu, S.; Zhai, P.; Jiang, L. *J. Hazard. Mater.* 2008, 154, 1141–1148. Copyright Elsevier, 2008.

**Table 1. Activity of the  $\text{SnO}_2\text{--TiO}_2$  Composite for the Degradation of Monocrotophos under a Medium Pressure Mercury Lamp<sup>a,b</sup>**

SnO <sub>2</sub> content (wt %)					
0	1	3	5	10	
$\eta_1$ (%)	27.6	27.6	26.3	25.6	24.3
$\eta_2$ (%)	28.1	35.0	39.7	43.6	40.1

<sup>a</sup> Reprinted with permission from Shifu, C.; Lie, C.; Shen, G.; Gengyu, C. *Mater. Chem. Phys.* 2006, 98, 116–120. Copyright Elsevier, 2006.

<sup>b</sup> Experimental conditions:  $\eta_1$  without ball milling and  $\eta_2$  with ball milling.

separation of space charge carriers varies with different pollutants and also on the surface-electronic structure of the  $\text{TiO}_2$ , it is unambiguously accepted that the primary reactions responsible for positive photocatalytic effect are interfacial redox reactions of electrons and holes that are generated upon band gap excitation. So far, many insightful review articles have reported the recent advancement achieved in the field of  $\text{TiO}_2$ -based photocatalysis.<sup>11–30</sup> Because of the large volume of research papers available on the photochemistry of  $\text{TiO}_2$ , it is not possible for this review to be fully comprehensive, and hence only some selected and unique results are discussed. The strategies developed on the band gap engineering of titania for visible light response and to improve the charge carrier separation together with their photocatalytic activity for the degradation of organic pollutants are reviewed.

## 2.0. $\text{TiO}_2$ COUPLED WITH OTHER SEMICONDUCTORS

The fabrication, design, and tailoring of the semiconductor–semiconductor heterojunction for achieving better charge separation in a light energy conversion system has received significant attention. The vectorial charge transfer from one semiconductor to another with suitable band edge positions that is thermodynamically favorable can increase the lifetime of the charge carriers thus promoting the interfacial charge transfer and catalytic efficiency.<sup>31,32</sup> Coupling the  $\text{TiO}_2$  with a wide band gap semiconductor like  $\text{SnO}_2$  is reported to enhance the charge separation

and thus the photocatalytic activity.<sup>33,34</sup> Both  $\text{TiO}_2$  and  $\text{SnO}_2$  are n-type semiconductors with band gap energies greater than 3.0 eV and exhibit a strong absorption threshold in the UV region. The CB edges of anatase  $\text{TiO}_2$  and  $\text{SnO}_2$  are situated at  $-0.34$  and  $+0.07$  V, respectively, while the VB edge of  $\text{SnO}_2$  ( $+3.67$  V) is much more positive than that of anatase  $\text{TiO}_2$  ( $+2.87$  V) as shown in Figure 1.<sup>33,34</sup> The  $\text{SnO}_2\text{--TiO}_2$  composite films fabricated on transparent electro-conductive glass substrate showed superior activity for the degradation of Rhodamine B (RhB) due to the combined effects of low sodium content, better crystallization, appropriate phase composition of anatase (73.4%) and rutile (26.3%), and slower recombination rate of charge carriers.<sup>33</sup> Upon UV illumination, electrons flow into the  $\text{SnO}_2$  underlayer, while the hole diffuses oppositely to the  $\text{TiO}_2$  overlayer. Consequently, more holes reach the  $\text{TiO}_2$  surface to cause oxidation reactions, while electrons are consumed for dioxygen reduction at the band edge of the  $\text{SnO}_2$  film. The VB edge of  $\text{TiO}_2$  inhibits the interfacial hole transfer from  $\text{TiO}_2$  to  $\text{SnO}_2$ , thereby increasing the hole density in the  $\text{TiO}_2$  VB, and oxidizes the organic contaminant. The double-layered  $\text{SnO}_2\text{--TiO}_2$  film with both the components exposed to the surface prepared by plasma-enhanced chemical vapor deposition showed superior activity for phenol degradation. The activity of this bilayer film was highest when the deposition time of  $\text{TiO}_2$  on a  $\text{SnO}_2$  layer was 10 min and decreased thereafter. With an increase in the deposition time (30 min), electrons photogenerated on the  $\text{SnO}_2$  film had little chance to approach the adsorbed oxygen molecules, and hence the activity of this composite film was reduced.<sup>35</sup> Vinodgopal and Kamat<sup>36</sup> conducted a systematic approach and confirmed that the photogenerated electrons can accumulate on the  $\text{SnO}_2$ , and holes on the  $\text{TiO}_2$  in the  $\text{SnO}_2\text{--TiO}_2$  composite film under applied bias and the formation of  $\text{SnO}_2\text{--TiO}_2$  heterojunction interface result in higher quantum efficiency and better photocatalytic activity for Acid Orange 7 degradation. The enhancement in the activity was observed when the mass ratio of  $\text{SnO}_2$  to  $\text{TiO}_2$  was 2:1 and decreased when the dosage of  $\text{SnO}_2$  was lower than  $\text{TiO}_2$ .<sup>36</sup> The coupled  $\text{SnO}_2\text{--TiO}_2$  prepared by ball milling using  $\text{H}_2\text{O}$  as a disperser showed higher activity for the degradation of monocrotophos, compared to the  $\text{SnO}_2\text{--TiO}_2$  composite which was prepared without ball

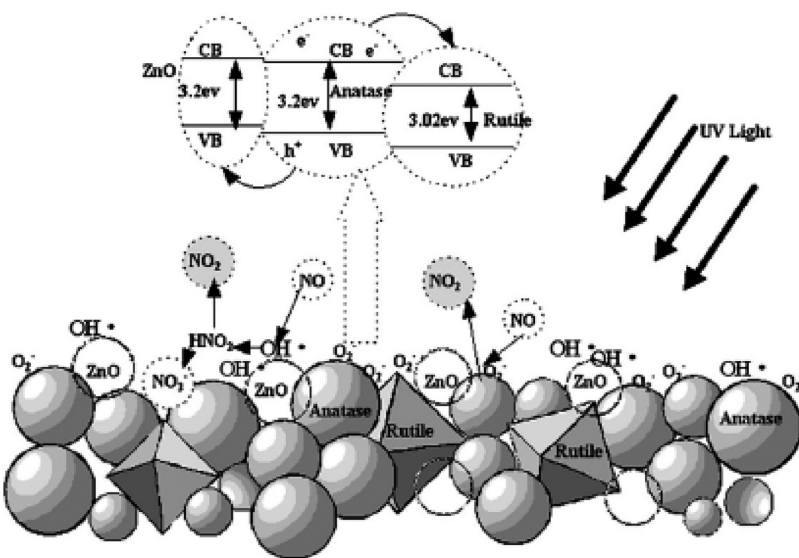


**Figure 2.** Interfacial charge transfer process in the tricomponent  $\text{ZnO}$ –anatase–rutile system responsible for NO degradation. Reprinted with permission from Wang, H.; Wu, Z.; Liu, Y.; Sheng, Z. *J. Mol. Catal. A: Chem.* 2008, 287, 176–181. Copyright Elsevier, 2008.

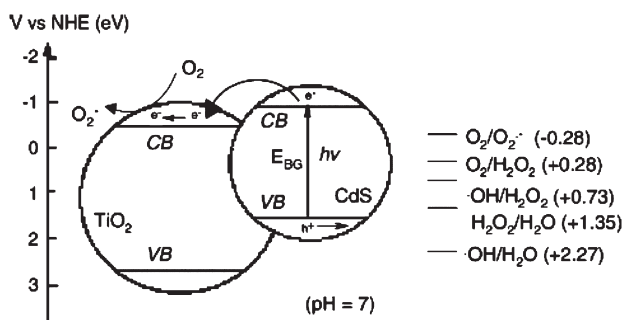


**Figure 3.** Redox potentials of the VB and CB of CdS sensitized  $\text{TiO}_2$  nanoparticles and various redox processes occurring on their surface at pH 7. Reprinted with permission from Wu, L.; Yu, J. C.; Fu, X. *J. Mol. Catal. A: Chem.* 2006, 244, 25–32. Copyright Elsevier, 2006.

milling (Table 1).<sup>37</sup> The ball milling increased the specific surface area of the composite and also shifted the absorption edge to longer wavelength ( $\sim 20 \text{ nm}$ ) compared to pure  $\text{TiO}_2$ . In fact, the activity of  $\text{SnO}_2\text{--TiO}_2$  prepared without ball milling showed a lower activity compared to pure  $\text{TiO}_2$  itself. The stress and strains induced during the ball milling process result in lattice deformation of  $\text{TiO}_2$  and  $\text{SnO}_2$  with many defects possessing high lattice and surface energy. This lowers the activation energy for diffusion of elements allowing the atomic or ionic diffusion at room temperature. When the activation of the powder system is sufficiently high during the ball milling process, the collision between balls and grains of the powder will produce a rise in interface temperature which induces a strong coupling reaction and hence the better photocatalytic activity.<sup>37</sup>

The coupled system of the type  $\text{ZnO}\text{--TiO}_2$  showed lower activity for the degradation of amaranth and procion red MX-5B compared to  $\text{ZnO}$ .<sup>38</sup> This insignificant interparticle electron transfer effect could be due to: (i) close proximity of the CB edge of both  $\text{TiO}_2$  and  $\text{ZnO}$ ; (ii) both  $\text{ZnO}$  and  $\text{TiO}_2$  are being photoactivated by UV illumination resulting in perfunctory separation of charge carriers. In contrast, coupling of  $\text{ZnO}$  (0.5 atom % of  $\text{Zn}^{2+}$ ) with Degussa P-25 (bicrystal of anatase and rutile)

by a wet impregnation method showed enhanced activity for the oxidation of  $\text{NO}_x$  under UV light due to the dense hydroxyl groups on the catalyst surface and efficient interfacial charge transfer in the tricomponent  $\text{ZnO}$ –anatase–rutile system.<sup>39</sup> The VB edge of  $\text{ZnO}$  lies above the anatase  $\text{TiO}_2$  VB, and the CB edge of rutile  $\text{TiO}_2$  lies below the anatase  $\text{TiO}_2$  CB. Under UV light excitation, vectorial hole transfer takes place from the VB of anatase  $\text{TiO}_2$  to  $\text{ZnO}$  (VB), while electron transfer takes place from the CB of anatase  $\text{TiO}_2$  to the rutile  $\text{TiO}_2$  CB (Figure 2). However, a high dosage of  $\text{ZnO}$  (0.5 atom %) was not beneficial to photocatalytic activity because the abundant  $\text{ZnO}$  particles on the  $\text{TiO}_2$  surface act as recombination centers.<sup>39</sup>

The formation of heterojunction structure between a narrow band gap semiconductor and  $\text{TiO}_2$  with matching band potentials provides an effective way to extend the photosensitivity of  $\text{TiO}_2$  to the visible portion of the solar spectrum. The ability of a small band gap semiconductor to photosensitize a large band gap semiconductor with no absorption in the visible region has many important applications from the viewpoint of solar energy conversion to photochemical reactions and photocatalysis. There are two prerequisite conditions for such a heterogeneous semiconductor to function efficiently: (i) the sensitizer should have a strong absorption threshold in the visible region and (ii) the CB edge potential of the sensitizer should be higher than the  $\text{TiO}_2$  CB to facilitate the smooth electron transfer. Wu et al.<sup>40</sup> reported that the direct formation of nanocrystalline  $\text{TiO}_2$  coupled with highly dispersed CdS nanocrystal at low temperature by a combined microemulsion and solvothermal method resulted in the faster degradation of methylene blue (MB) under visible light irradiation. ESR results revealed that the electrons from the excited CdS were injected into the titania CB and then were scavenged by molecular oxygen to yield a superoxide radical anion in oxygen-equilibrated media (Figure 3). CdS (bulk)– $\text{TiO}_2$  showed higher activity for  $\text{H}_2$  production compared to CdS– $\text{TiO}_2$  (bulk) and nanoCdS–nano $\text{TiO}_2$  under visible light irradiation (Figure 4 and Table 2). Here, CdS (bulk)– $\text{TiO}_2$  refers to the preparation of  $\text{TiO}_2$  on the bulk CdS surface, and CdS– $\text{TiO}_2$  (bulk) refers to preparation of CdS on the  $\text{TiO}_2$

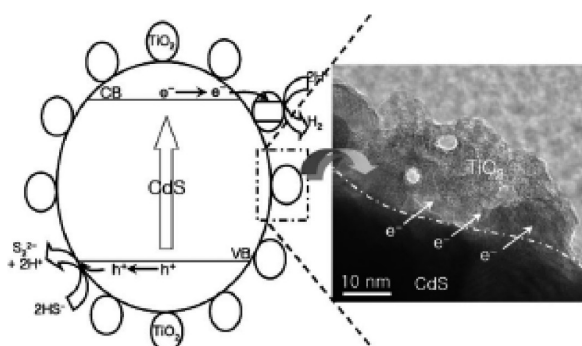


**Figure 4.** New configuration model consisting of bulky CdS decorated with nanosized TiO<sub>2</sub> particles. Reprinted with permission from Jang, J. S.; Li, W.; Oh, S. H.; Lee, J. S. *Chem. Phys. Lett.* **2006**, *425*, 278–282. Copyright Elsevier, 2006.

**Table 2. H<sub>2</sub> Evolution Using Different Photocatalysts<sup>a</sup>**

photocatalyst	H <sub>2</sub> evolution (μmol/h)	photocatalyst	H <sub>2</sub> evolution (μmol/h)
CdS-673 K	6.9	CdS (bulk)-TiO <sub>2</sub>	422.4
CdS-1073 K	96.4	CdS-TiO <sub>2</sub> (bulk)	1.3

<sup>a</sup> Reprinted with permission from Jang, J. S.; Li, W.; Oh, S. H.; Lee, J. S. *Chem. Phys. Lett.* **2006**, *425*, 278–282. Copyright Elsevier, 2006.

surface.<sup>41</sup> It is remarkable that the fabrication method of the composite had such a dramatic effect despite that the compositions were almost the same. According to Jang and co-workers, the rate of H<sub>2</sub> production for CdS (bulk)-TiO<sub>2</sub> represents one of the highest values ever reported under similar reaction conditions for any visible light active photocatalysts. The crystal structure of CdS in CdS (bulk)-TiO<sub>2</sub> was of hexagonal wurtzite, while a cubic zinc blende was observed in CdS-TiO<sub>2</sub> (bulk). It should be noted that the hexagonal wurtzite phase is known to be a more active phase than the cubic zinc blende phase.<sup>41</sup> Photoplatinization of CdS/TiO<sub>2</sub> [Pt/CdS-TiO<sub>2</sub>] showed lower activity compared to Pt-deposited TiO<sub>2</sub> which was followed by CdS deposition [CdS/TiO<sub>2</sub>-Pt], indicating that changing the hybridization order in the preparative step significantly altered the efficiency of H<sub>2</sub> production and photocurrent generation under visible light excitation.<sup>42</sup> The vectorial electron transfer takes place from CdS to TiO<sub>2</sub> and then to Pt which is well-defined in CdS/TiO<sub>2</sub>-Pt, favoring effective charge separation, while such unidirectional electron transfer is not favored in Pt/CdS-TiO<sub>2</sub> because Pt active sites coexist on the surfaces of both CdS and TiO<sub>2</sub>. Moreover, the physical mixture of CdS and Pt-TiO<sub>2</sub> shows higher activity compared to physical mixtures of Pt-CdS and TiO<sub>2</sub>, suggesting that the platinization of CdS was not beneficial and that the H<sub>2</sub> formation on the Pt surface was favorable only when deposited on TiO<sub>2</sub> (Figure 5).<sup>42</sup> The heterojunction prepared by the precipitation of CdS on TiO<sub>2</sub> or Bi<sub>2</sub>S<sub>3</sub> on TiO<sub>2</sub> showed a lower activity for the degradation of Orange II and 4-hydroxy benzoic acid than those prepared by direct mixing, which highlights that the intimate contact between the coupled semiconductors is critical for achieving maximum charge separation.<sup>43</sup> Bi<sub>2</sub>S<sub>3</sub>-TiO<sub>2</sub> showed higher efficiency compared to CdS-TiO<sub>2</sub>, despite the existence of a large difference in CB edge potential between TiO<sub>2</sub> and CdS which possess a higher thermodynamic driving force for electron transfer. It should be noted that the suitable

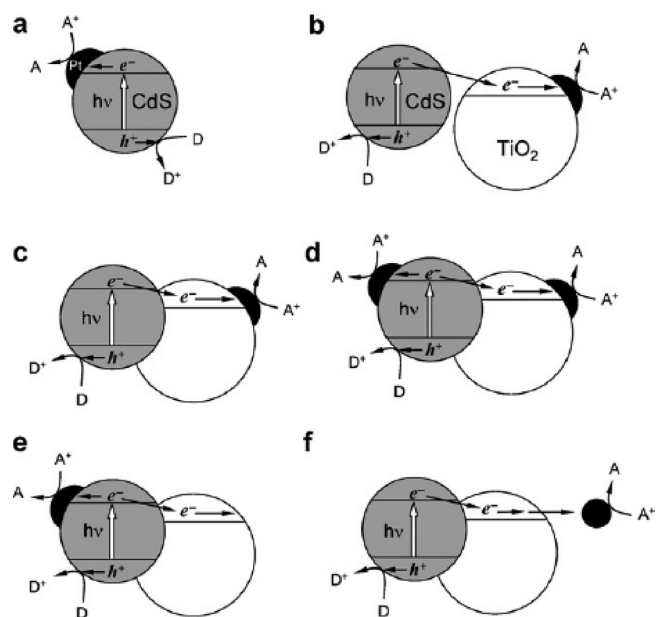


**Figure 5.** Schematic representation of electron transfer in hybrid photocatalysts. (a) Pt-CdS; (b) CdS + Pt-TiO<sub>2</sub> (physically mixed); (c) CdS/(Pt-TiO<sub>2</sub>); (d) Pt-(CdS/TiO<sub>2</sub>); (e) sg TiO<sub>2</sub>/(Pt-CdS); (f) CdS/TiO<sub>2</sub> + Pt sol. Reprinted with permission from Park, H.; Choi, W.; Hoffmann, M. R. *J. Mater. Chem.* **2008**, *18*, 2379–2385. Copyright Royal Society of Chemistry, 2008.

redox levels are not the only factor affecting interparticle electron transfer, but also coupling aspects between acceptor and donor electronic states of both the semiconductors, morphology of the particles, the surface texture, and the extent of surface contact between the particles play a crucial role. Such an interparticle electron transfer between the heterojunction is found to be dependent on the adsorption of pollutant on the sensitizer. Accordingly, the Bi<sub>2</sub>S<sub>3</sub>-TiO<sub>2</sub> and CdS-TiO<sub>2</sub> showed higher activity for the degradation of Orange II and 4-hydroxy benzoic acid and lower activity for benzamide degradation compared to bare TiO<sub>2</sub>.<sup>43</sup>

The hole generated on the VB of the sensitizer cannot oxidize the surface hydroxyls to hydroxyl radicals and hence can corrode the sensitizer itself. The addition of sulfite/sulfide as sacrificial electron donors prevents the corrosion of CdS in the CdS-TiO<sub>2</sub> system by reacting with the hole residing in the VB of the CdS.<sup>44</sup> This is an extra exciton dissociation mechanism in addition to the depletion layer from the single semiconductor dispersed in solution. The higher probability of exciton dissociation would reduce electron-hole recombination and can enhance photocatalytic activity of the heterojunction photocatalyst. Serving as a sacrificial reagent, S<sup>2-</sup> reacts with holes to form S. The aqueous SO<sub>3</sub><sup>2-</sup> added can dissolve S into S<sub>2</sub>O<sub>3</sub><sup>2-</sup> to prevent any detrimental deposition of S on CdS. Since the electron donors or sacrificial reagents are consumed in the photocatalytic reactions, continuous addition is required to sustain redox reactions.<sup>44</sup>

Yu et al. reported the deposition of quantum-sized semiconductors like WS<sub>2</sub>, MoS<sub>2</sub>, and CdSe semiconductors on the surface of TiO<sub>2</sub> for the first time.<sup>45,46</sup> Although the bulk WS<sub>2</sub> has a CB edge potential lower than that of TiO<sub>2</sub>, the strong quantum dot confinement effects for nanosized WS<sub>2</sub> make it possible for efficient electron transfer from WS<sub>2</sub> to TiO<sub>2</sub> (Figure 6), and the catalyst modified with 0.3 mol % of WS<sub>2</sub> showed high activity for the degradation of 4-chlorophenol (4-CP). However,

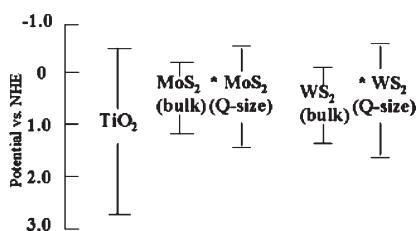


**Figure 6.** Energy levels of the CB and VB edges versus (NHE) for pure TiO<sub>2</sub>, WS<sub>2</sub>, and MoS<sub>2</sub> with various sizes at pH 7. (Asterisk indicates band gap increase due to the quantum-sized effect.) Reprinted with permission from Ho, W.; Yu, J. C.; Lin, J.; Yu, J.; Li, P. *Langmuir* 2004, 20, 5865–5869.

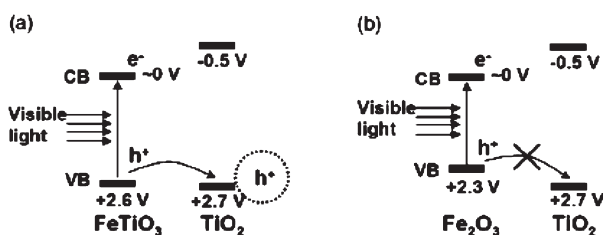


**Figure 7.** Proposed mechanism for the charge transfer: (a) Fe-TiO<sub>3</sub>-TiO<sub>2</sub> and (b) Fe<sub>2</sub>O<sub>3</sub>-TiO<sub>2</sub> under visible light. Reprinted with permission from Gao, B.; Kim, Y. J.; Chakraborty, A. K.; Lee, W. I. *Appl. Catal. B: Environ.* 2008, 83, 202–207. Copyright Elsevier, 2008.

the electron thus transferred from the sensitizer to TiO<sub>2</sub> induces photoreduction reactions that can only lead to partial decomposition of pollutants and are difficult to induce CO<sub>2</sub> evolution. For achieving complete mineralization of the contaminants, a new strategy utilizing the photogenerated hole is crucial, which was achieved by designing the electronic band structure of the sensitizer in the TiO<sub>2</sub>-based composite. The concept of such a heterojunction-type photocatalyst, utilizing the hole transfer from sensitizer to TiO<sub>2</sub>, was first realized by Lee and co-workers in the FeTiO<sub>3</sub>-TiO<sub>2</sub> system which showed superior activity for the degradation of 2-propanol and 4-CP compared to Fe<sub>2</sub>O<sub>3</sub>-TiO<sub>2</sub> and TiO<sub>2</sub> under visible light irradiation.<sup>47,48</sup> Although VB edge potentials of both FeTiO<sub>3</sub> and TiO<sub>2</sub> are almost the same, V<sub>fb</sub> of FeTiO<sub>3</sub> was lower than that of TiO<sub>2</sub> by 0.53 V as estimated by an electrochemical method. According to the proposed mechanism, hole transfers from the VB of FeTiO<sub>3</sub> to the TiO<sub>2</sub> VB leave behind electrons in the FeTiO<sub>3</sub> CB under visible light excitation (Figure 7). By this intersemiconductor hole transfer mechanism, the photogenerated charge carriers can be separated efficiently so that the composite semiconductors can utilize visible light to degrade the pollutants. Such a hole transfer mechanism was not observed for the Fe<sub>2</sub>O<sub>3</sub>-TiO<sub>2</sub> composite due to nonfavorable band edge positions.<sup>47</sup>

### 3.0. SENSITIZATION OF TITANIA WITH ORGANIC COMPOUNDS/INORGANIC METAL COMPLEXES

The mechanism of photoassisted degradation of organic dyes in aqueous TiO<sub>2</sub> dispersions under visible light irradiation is different from the pathway implicated under UV light illumination, except the fate of the injected electron under visible irradiation is no different from that of CB electrons photogenerated under UV illumination. The dye sensitization process is usually referred to as indirect electron injection which involves multiexponential

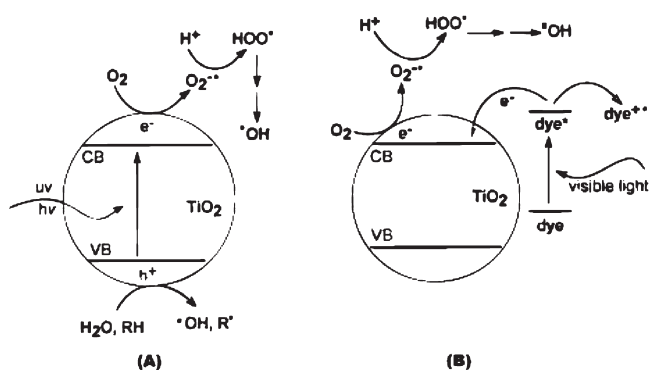
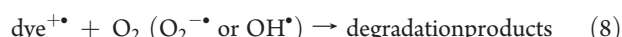
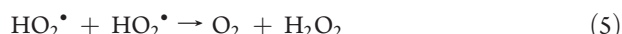
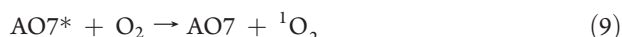


**Figure 8.** Comparison of the photocatalytic mechanism: (A) for UV irradiation of TiO<sub>2</sub> with the self-photosensitized pathway and (B) under visible light illumination. Reprinted with permission from Wu, T.; Liu, G.; Zhao, J.; Hidaka, H.; Serpone, N. *J. Phys. Chem. B* 1998, 102, 5845–5851.

kinetics with fast components of tens of femtoseconds (from the singlet excited state of the dye to the TiO<sub>2</sub> CB) and slow components of several picoseconds (from the triplet excited state of the dye to the TiO<sub>2</sub> CB).<sup>49</sup> In the sensitization process, dye gets excited rather than the TiO<sub>2</sub> particles to appropriate singlet and triplet states, and the dyes are subsequently converted to cationic dye radicals. The electrons are thus injected to the TiO<sub>2</sub> CB and react with the preadsorbed O<sub>2</sub> to form oxidizing species (super-oxide, hydroperoxyl, and hydroxyl radicals) resulting in photo-oxidation reactions (Figure 8).<sup>50</sup> Thus, TiO<sub>2</sub> plays an important role in electron-transfer mediation, even though TiO<sub>2</sub> itself is not excited. The photodegradation mechanism of dyes under visible irradiation is proposed as follows<sup>50–55</sup>



The formation of singlet oxygen in the TiO<sub>2</sub>-Acid Orange 7 (AO7)-visible light system is also reported wherein the excited dye molecule transfers an electron to preadsorbed O<sub>2</sub><sup>56</sup>



Molecular oxygen has two low-lying singlet excited states, <sup>1</sup>Δ<sub>g</sub> and <sup>1</sup>Σ<sub>g</sub><sup>+</sup>, having energies of 95 and 158 kJ/mol above the <sup>3</sup>Σ<sub>g</sub> triplet ground state, respectively.<sup>57,58</sup> Oxygen in its singlet excited state is about a 1 V more powerful oxidant compared to its ground state, and therefore it is more electrophilic. Hence, it reacts with the organic compound and also with the dye sensitizer itself, thus destroying its ability to absorb visible light

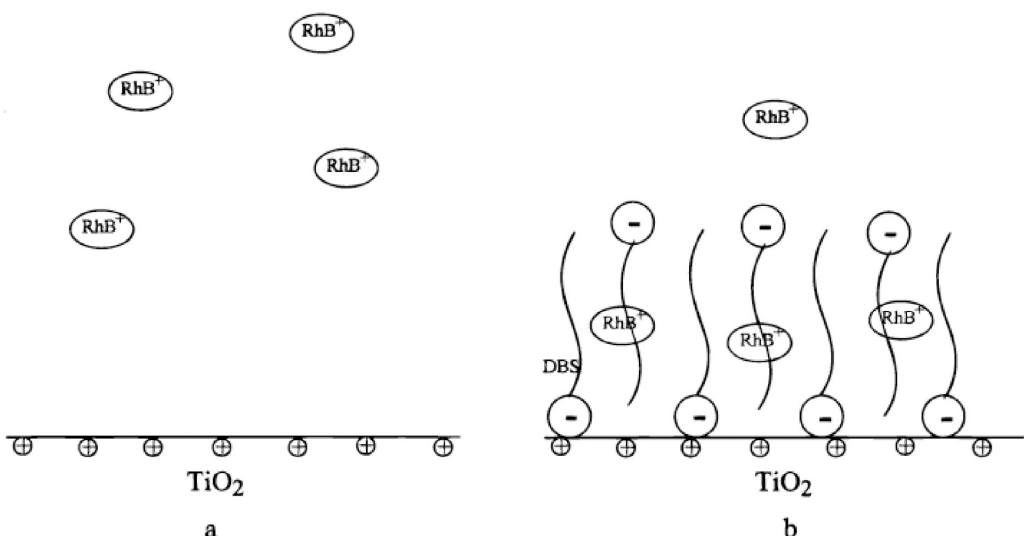


**Figure 9.** Adsorption model illustrating the coadsorption of RhB and DBS on the  $\text{TiO}_2$  particle surface: (a) RhB only and (b) coadsorption of RhB and DBS. Reprinted with permission from Zhao, J.; Wu, T.; Wu, K.; Oikawa, K.; Hidaka, H.; Serpone, N. *Environ. Sci. Technol.* 1998, 32, 2394–2400.

and to photosensitize the formation of singlet oxygen. The dye sensitization process can also be deeply suppressed by the competitive adsorption of other organic pollutants coexisting in the solution. The quantity of the dye preadsorbed on the catalyst surface is of paramount importance since only these adsorbed molecules contribute to the photocatalytic process and not the one which is in the bulk of the solution.<sup>23a</sup> To enhance the adsorption of dyes, anionic surfactant dodecylbenzene sulfonate (DBS) was added to  $\text{TiO}_2$  dispersion which rendered stronger adsorption of the cationic dye RhB even at acidic pH and resulted in faster degradation mainly attributed to the change in surface charge density from positive to negative due to adsorption of DBS (Figure 9).<sup>59</sup> The complete decomposition of RhB was observed in the presence of surfactant, while ~45% degradation was observed in the absence of DBS. Although the basic process for dye-sensitized photodegradation of organic pollutants was extensively reported, the synergistic mechanism of two dye pollutants coexisting in  $\text{TiO}_2$  suspension was first reported by Yin and co-workers.<sup>60</sup> The concentration of RhB or Methyl Orange (MO) was fixed (4 mg/L), while the concentration of Eosin Orange (EO) was varied from 10 to 25 mg/L. The degradation of RhB (or MO) increased with an increase in EO and decreased for higher EO concentration. The adsorption experiments revealed that the adsorption amount of EO decreased, while that of RhB increased with an increase in the concentration of EO.<sup>60</sup> Superoxide radicals were not detected by ESR studies which revealed that for the system P25–EO–RhB EO is more active than 5,5-dimethyl-1-pyrroline-N-oxide (DMPO) for oxygen active species. The acceleration of RhB degradation in the presence of EO can be attributed to the mutual interaction between two dyes and the generation of more active species by the effective electron transfer from EO to the  $\text{TiO}_2$  CB. Furthermore, RhB serves as the role of stabilizer, acting as a sacrificial electron donor of EO during the degradation course. Further improvement in the dye sensitization of titania was achieved by linking one –NCO group of tolylene-2, 4-diisocyanatae (TDI) with  $\text{Ti}(\text{IV})-\text{OH}$  and the other with the –NH<sub>2</sub> group of chrysoidine G (CG) dye which degraded MB under visible light. TDI was used as a bridging molecule whose two –NCO groups bond

with surface  $\text{Ti}-\text{OH}$  and –NH<sub>2</sub> groups of CG, respectively (Figure 10).<sup>61</sup> This resulted in the formation of a donor–acceptor-type extended  $\pi$ -conjugated surface complex on the surface of titania leading to the visible light response. The extent of substrate degradation depends on the adsorption capacity of the generated surface complex (Figure 10). However, the surface complex undergoes self-degradation during the photocatalytic reaction, lowering the visible light activity of the photocatalyst.<sup>61</sup>

If the dye modification enhances  $\text{TiO}_2$  photocatalytic activity in the UV or near UV region, the process may not be a trivial sensitization process. Therefore, sensitization formalism cannot be claimed in all the cases and should be limited to the instances where real sensitization occurs. Hilal et al. studied the sensitization of the  $\text{TiO}_2$  surface with 2,4,6-triphenylpyriliun hydrogen sulfate (TPPHS) and modified it with activated carbon ( $\text{TiO}_2$ –TPPHS–AC) for the degradation of phenol.<sup>62</sup> Two distinct mechanisms were proposed under different excitation sources: under UV light, the band gap excitation of  $\text{TiO}_2$  takes place, and the TPPHS molecule adsorbed on the  $\text{TiO}_2$  surface may facilitate charge transfer between the  $\text{TiO}_2$  VB and the contaminant molecule. The dye molecules may thus facilitate adsorption of phenol molecules and promote the interfacial charge transfer process. Thus, the role of the dye molecule in  $\text{TiO}_2$  catalytic enhancement is therefore understandable as a charge transfer formalism, while the trivial sensitization process was accounted for under visible light irradiation.<sup>62</sup> One of the major problems involved in the dye-sensitized photocatalysis is the difficulty in separating the sensitized dye fraction from the wastewater due to its high solubility.

The degradation of salicylic acid in the presence of both  $\text{TiO}_2$  and  $\text{H}_2\text{O}_2$  under visible light was attributed to the surface complexation of  $\text{H}_2\text{O}_2$  with the  $\text{TiO}_2$  surface which shows visible light response, although neither  $\text{TiO}_2$  nor  $\text{H}_2\text{O}_2$  absorb visible light (Figure 11).<sup>63</sup> In the presence of  $\text{H}_2\text{O}_2$ , the –OOH groups of  $\text{H}_2\text{O}_2$  substitute for the surface basic –OH groups of titania ( $\equiv\text{Ti}-\text{OH}$ ), forming a yellow colored surface complex of the type  $\equiv\text{Ti}(\text{IV})-\text{OOH}$ . The magnitude of visible light response increased with an increase in the number of  $\text{H}_2\text{O}_2$  molecules adsorbed on the  $\text{TiO}_2$  surface.<sup>64</sup> The adsorption and decomposition

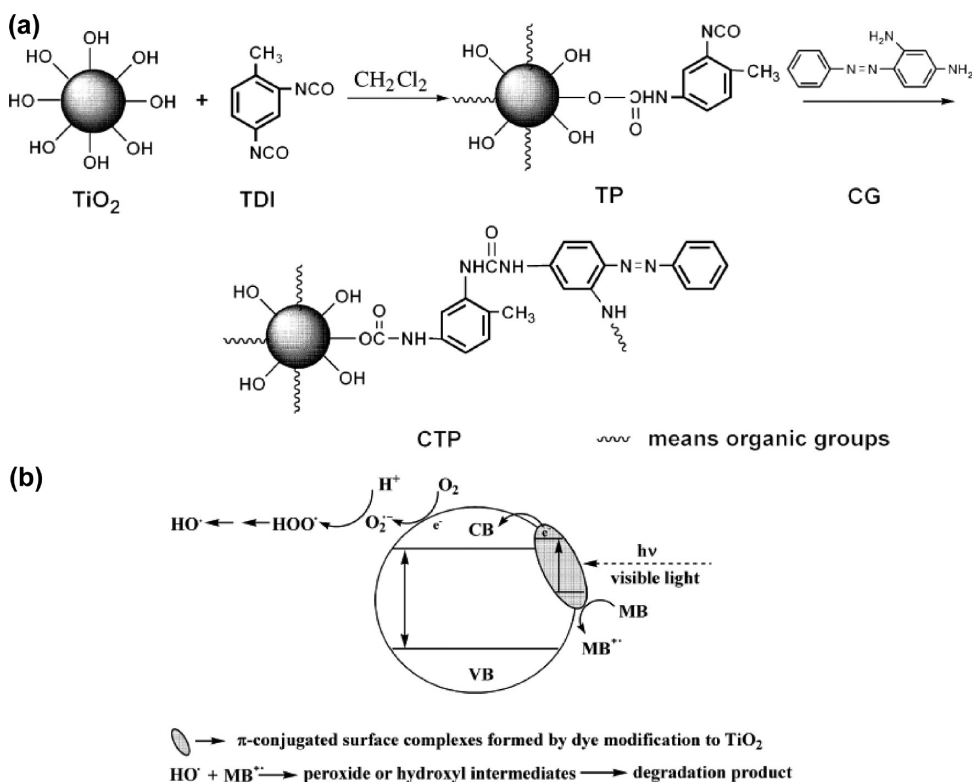


**Figure 10.** (a) Schematic illustration of CTP. (b) The mechanism of photocatalytic decomposition of MB over dye-modified  $\text{TiO}_2$  under visible light. Reprinted with permission from Jiang, D.; Xu, Y.; Wu, D.; Sun, Y. *J. Solid State Chem.* **2008**, *181*, 593–602. Copyright Elsevier, 2008.

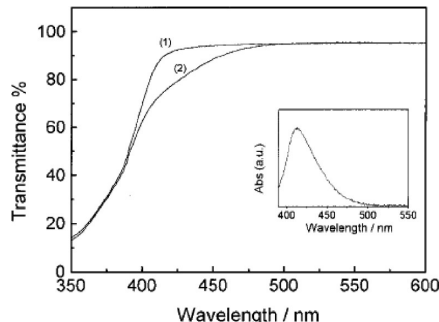


**Figure 11.** Diffuse reflectance absorption spectra of  $\text{TiO}_2$  powder in the absence (spectrum 1) or presence (spectrum 2) of  $\text{H}_2\text{O}_2$  ( $5 \times 10^{-3}$  mol/L). Inset: differential diffuse reflectance spectrum of the surface  $\text{Ti(IV)}-\text{H}_2\text{O}_2$  complex. Reprinted with permission from Li, X.; Chen, C.; Zhao, J. *Langmuir* **2001**, *17*, 4118–4122.

of  $\text{H}_2\text{O}_2$  on the  $\text{TiO}_2$  surface were higher in the pH range 2.0–5.4 and were reduced at higher pH values. The degradation of salicylic acid on this surface complex was attributed to the transfer of electrons from the excited surface complex ( $\equiv\text{Ti}-\text{OOH}^*$ ) to the CB of  $\text{TiO}_2$  to generate  $\equiv\text{Ti(IV)}-\text{OOH}^*$  which then gives rise to  $\equiv\text{Ti(IV)}-\text{OH}$  and  $1/2 \text{ O}_2$  (Figure 12).<sup>63</sup>

Kim and Choi reported that the charge transfer (CT) complex sensitization between  $\text{TiO}_2$  and 4-CP operates in a different way from the trivial sensitization process. In this case of CT sensitization, the electron is photoexcited from the ground state adsorbate to the  $\text{TiO}_2$  CB without involving the excited state of the adsorbate. Thus, the electrons excited through a ligand to metal charge transfer transition (LMCT) mechanism can be transferred

to electron acceptors and subsequently initiate redox reactions, which is also clearly distinguished from classical band gap excited photocatalysis (Figure 13).<sup>65,66</sup> The degradation of 4-CP under visible light was rapid, while dichloroacetate was not susceptible to oxidation, suggesting that CT complex formation is essential for degradation of an organic compound under visible light.<sup>65</sup> The degradation was not affected by the addition of *t*-butyl alcohol (TBA), suggesting that the hole-mediated oxidative mechanism was operative under visible light, while the degradation rate was quenched by TBA under UV light, indicating the role of hydroxyl radicals in the degradation process under UV light. The surface complexation was inhibited by the surface fluorination, by platinization, and at alkaline conditions, thereby inhibiting the degradation rate under these conditions. Wang et al. reported that an electron-donating substituent in the benzene ring raises the highest occupied molecular orbital and lowers the vertical ionization potential of organic compounds favoring the CT complex mediated photodegradation of pollutant, but an electron-withdrawing substituent showed an opposite effect (Table 3).<sup>66</sup> The order of degradation for various organic compounds followed the sequence: 8-hydroxyquinoline > salicylic acid > phenol > *p*-amino benzoic acid > *p*-hydroxy benzoic acid > aniline > benzoic acid ~ terephthalic acid, indicating that the chemical structure of the pollutant plays a crucial role in the degradation rate. Aniline showed a lower degradation rate compared to phenol due to protonation, which resists the surface complexation at pH 3 on the catalyst surface. 8-Hydroxy quinoline is more favorable to form a five-membered ring with the titanium orbital, and the electron donors (both N and O atoms) can supply their non-bonded electron pair to the pyridine and benzene ring, thereby stabilizing CT complex formation.<sup>66</sup>

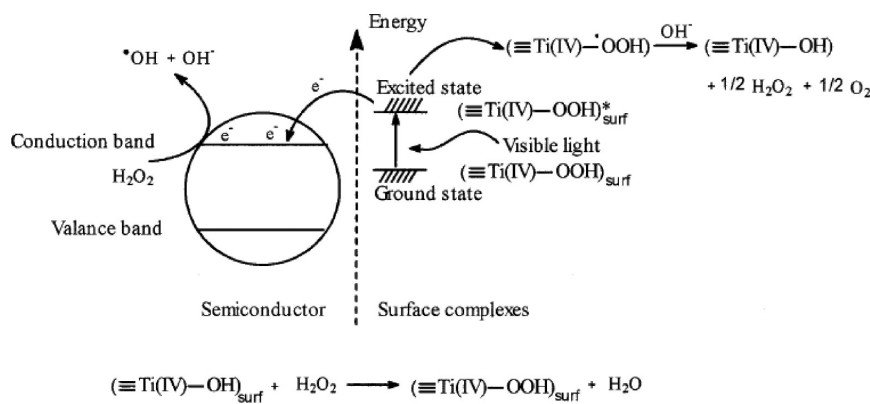


**Figure 12.** Mechanism for photoinduced electron transfer and interface photoreaction of the  $\text{H}_2\text{O}_2$ - $\text{TiO}_2$  complex. Reprinted with permission from Li, X.; Chen, C.; Zhao, J. *Langmuir* 2001, 17, 4118–4122.

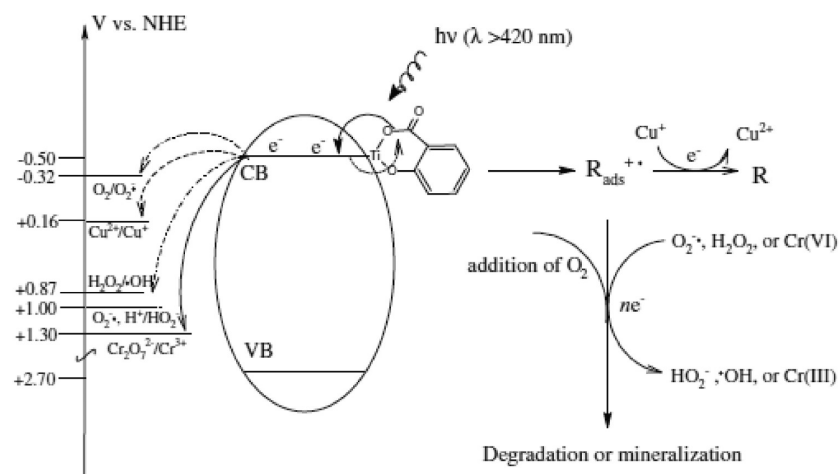


**Figure 13.** CTC-mediated mechanism for  $\text{TiO}_2$ -assisted photodegradation of colorless aromatic pollutants under visible light illumination. Reprinted with permission from Wang, N.; Zhu, L.; Huang, Y.; She, Y.; Yu, Y.; Tang, H. *J. Catal.* 2009, 266, 199–206. Copyright Elsevier, 2009.

**Table 3. Rate Constant ( $k$ ), Energy of the Highest Occupied Molecular Orbital ( $E_{\text{HOMO}}$ ), and Vertical Ionization Potential (VIP) of Different Organic Compounds<sup>a</sup>**

pollutant	$k (10^{-3} \text{ min}^{-1})$	$E_{\text{HOMO}} (\text{eV})$	VIP (eV)
benzoic acid	0.0	-6.313	9.130
phenol	0.46	-6.014	9.054
aniline	0.18	-5.959	8.973
terephthalic acid	0.0	-6.449	8.941
<i>p</i> -hydroxy benzoic acid	0.36	-6.204	8.910
<i>p</i> -amino benzoic acid	0.38	-6.177	8.786
salicylic acid	1.4	-5.769	8.550
8-hydroxyquinoline	5.7	-5.306	7.940

<sup>a</sup> Reprinted with permission from Wang, N.; Zhu, L.; Huang, Y.; She, Y.; Yu, Y.; Tang, H. *J. Catal.* 2009, 266, 199–206. Copyright Elsevier, 2009. Note: The influence of Cr(VI) on the degradation rate of organic compounds is not considered for clarity, as it was beyond the scope of this review.

A novel version of sensitized electron transfer was reported by Kisch and co-workers for titania containing Pt(IV), Rh(III), and Pd(III) chlorides either in the bulk or only at the surface (Figure 14).<sup>67–71</sup> In the aqueous suspension of common pollutant

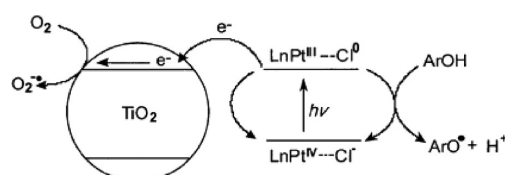


**Figure 14.** Primary steps of the postulated mechanism for titania modified with  $\text{PtCl}_4$  or  $[\text{PtCl}_6]^{2-}$  in the bulk/surface. Reprinted with permission from Kisch, H.; Macyk, W. *ChemPhysChem* 2002, 3, 399–400. Copyright Wiley-VCH, 2002.

4-CP, these hybrid materials sustain visible light photocatalytic activity for several days. This visible light activated  $\text{TiO}_2$  modified with metal ion doped titania system is quite different from the trivial metal ion doped titania system. In these systems, the surface complex of metal chloride serves as visible light absorbing sensitizers and centers of charge separation, while the titania matrix serves as a charge trap. The excited platinum complex first undergoes homolytic metal–chloride bond cleavage to afford the metal ion in a reduced oxidation state and an adsorbed chlorine atom. Subsequent electron transfer from the former to titania and 4-CP to the chlorine atom regenerates the sensitizer.<sup>67–71</sup>

Photoelectrochemical measurements indicate that the flat band potential of this novel n-type semiconductor is shifted to  $-0.30$  V (vs NHE, pH 7) as compared to  $-0.53$  V for an unmodified titania sample which increases the thermodynamic driving force of electron injection from the platinum (III) intermediate and shows increased photocatalytic activity.<sup>71</sup>

Zn(II) or Co(II) tetracarboxy phthalocyanine (TcPcM) anchored on the titania surface via ester linkage showed photocatalytic activity for phenol degradation in the visible spectral region. The photonic efficiencies were 0.043 for TcPcCo-TiO<sub>2</sub> and 0.033 for TcPcZn-TiO<sub>2</sub> which enhanced to 0.1 upon platinization.<sup>72</sup> The Ru(II) sensitizer, [RuII(py-pzH)<sub>3</sub>]<sup>2+</sup> (where py-pzH = 3-(2<sup>1</sup>-pyridyl) pyrazole), anchored on the TiO<sub>2</sub> surface via in situ silylation exhibited outstanding properties for the degradation of CCl<sub>4</sub> under visible light irradiation with iodide as the sacrificial electron donor compared to the Ru(II) sensitizer that was anchored on the titania surface via phosphonic linkage.<sup>73</sup> The sensitized Pt-TiO<sub>2</sub> photocatalyst on which the ruthenium complex was anchored through the carboxylic group (Pt-TiO<sub>2</sub>-Ru<sup>II</sup> (4,4<sup>1</sup> (COOH)<sub>2</sub> bpy)) was found to be photocatalytically less active for CCl<sub>4</sub> reduction/H<sub>2</sub> production in the entire pH range compared to the ruthenium bipyridyl complex which was anchored through a phosphonic linkage (Pt-TiO<sub>2</sub>-Ru<sup>II</sup> (bpy)<sub>2</sub> (4,4<sup>1</sup>-PO<sub>3</sub>H<sub>2</sub> bpy)), despite the fact that the former had higher molar absorptivity compared to the latter.<sup>74</sup> The IR spectral analysis revealed that the carboxyl group was anchored through the bidentate mode, while the phosphonic linkage via the bidentate or tridentate mode rendered stronger adsorption compared to the carboxylic linkage. This indicates that chemical bond formation between phosphonic acid (-PO<sub>3</sub>H<sub>2</sub>) and the TiO<sub>2</sub> surface hydroxyl group ( $\equiv$ Ti-OH) was highly favored over ester linkage ( $\equiv$ Ti-OCO-R) formation.<sup>74</sup>

#### 4.0. METAL ION DOPED TITANIA

Selective doping of metal ions into the crystalline titania matrix has been proven to be an efficient route for improving visible light photocatalytic activity with hindered charge carrier recombination.<sup>75-90</sup> Doping with a transition metal ion increases the formation of Ti<sup>3+</sup> ions, leading to the enhancement in the photocatalytic activity, as more Ti<sup>3+</sup> states may cause more oxygen defects which facilitate the efficient adsorption of oxygen on the titania surface. The formation of O<sub>2</sub><sup>-</sup> upon chemisorption of oxygen requires the presence of a surface defect site which can be enhanced by transition metal ion doping.<sup>91</sup> Since the redox energy states of many transition metal ions lie within the band gap states of TiO<sub>2</sub>, the substitution of metal ions into the TiO<sub>2</sub> introduces an intraband state close to the CB or VB edge, inducing visible light absorption at sub-band gap energies. The red shift in the band gap absorption is attributed to the charge transfer transition between the d electrons of the dopant and the CB (or VB) of TiO<sub>2</sub>.

Photoreduction of dinitrogen in a gas-solid regime using Fe<sup>3+</sup> and Cr<sup>3+</sup> doped TiO<sub>2</sub> had a favorable effect on setting a permanent space charge layer, enhancing the activity, while the displacement of the Fermi level at the TiO<sub>2</sub>-electrolyte interface due to the presence of donor ions did not favor the charge separation with respect to pure TiO<sub>2</sub>.<sup>92</sup> Choi et al. reported the systematic study on doping of Q-sized TiO<sub>2</sub> with 21 different metal ions and evaluated their photocatalytic activity for the CCl<sub>4</sub> reduction and CHCl<sub>3</sub> oxidation. It was reported that the

photoreactivity of metal ion doped TiO<sub>2</sub> appears to be a complex function of multiple factors like dopant concentration, the dopant energy levels within the TiO<sub>2</sub> lattice, their d electronic configuration, the distribution of dopants, the electron donor concentration, and also the light intensity. The dopants with closed shell electronic configuration like Li<sup>+</sup>, Mg<sup>2+</sup>, Al<sup>3+</sup>, Zn<sup>2+</sup>, Ga<sup>3+</sup>, Zr<sup>4+</sup>, Sn<sup>4+</sup>, Sb<sup>5+</sup>, and Ta<sup>5+</sup> had little effect on photoreactivity; however, Co<sup>3+</sup> with a partially filled electronic configuration showed lower activity, and the Fe<sup>3+</sup> dopant with unique half-filled electronic structure resulted in enhanced activity compared to pure TiO<sub>2</sub>.<sup>93</sup> When Fe<sup>3+</sup> traps electron and hole, it changes its oxidation state to Fe<sup>2+</sup> and Fe<sup>4+</sup>, respectively. According to crystal field theory, Fe<sup>4+</sup> and Fe<sup>2+</sup> ions are relatively unstable compared to Fe<sup>3+</sup> ions and hence detrap the electron and hole to adsorbed oxygen and surface hydroxyl groups, respectively, to restore its half-filled electronic configuration and thereby suppress the electron-hole recombination.<sup>77a</sup>

The Th<sup>4+</sup> doped TiO<sub>2</sub> photocatalyst at an optimum dopant concentration of 0.06 atom % showed superior activity for the degradation of imidachloprid<sup>83</sup> and chlorpyrifas<sup>87</sup> under UV/solar light compared to V<sup>5+</sup>-TiO<sub>2</sub> and Mo<sup>6+</sup>-TiO<sub>2</sub> which was attributed to (i) the large surface area of the photocatalyst; (ii) the presence of two absorption edges (460 and 482 nm) in the visible region which enabled the catalyst to absorb more visible light; (iii) strong adsorption of the pollutant due to the complex formation between the vacant "f" orbital of Th<sup>4+</sup> and the functional group of the pollutant; and (iv) induced defects like oxygen vacancies which served as shallow traps for the CB electrons. In another study, Zn<sup>2+</sup>-TiO<sub>2</sub> showed higher activity for the degradation of congo red (CR) compared to V<sup>5+</sup>-TiO<sub>2</sub>, although both the doped samples showed identical band gap absorption.<sup>82</sup> The smaller crystallite size of Zn<sup>2+</sup>-TiO<sub>2</sub> and the stable filled electronic configuration of the Zn<sup>2+</sup> ion served as a shallow trap for the charge carriers contributing to the overall activity, while bulk recombination of charge carriers prevailed in the larger crystallites of V<sup>5+</sup>-TiO<sub>2</sub>. The degradation of cationic dyes (RhB and MB) and anionic dyes (MO and CR) was found to be efficient at alkaline and acidic pH, respectively, due to the adsorption tendency of these dyes on the Mo<sup>6+</sup>-TiO<sub>2</sub> surface at different pH conditions.<sup>86</sup> The surface acidity of the titania was increased due to Mo<sup>6+</sup> doping which resulted in efficient adsorption of the pollutant on the catalyst surface and accelerated the interfacial charge transfer process.<sup>86</sup> The enhanced activity of Mn<sup>2+</sup>-TiO<sub>2</sub> (0.06 atom %) compared to other transition metal ion doped TiO<sub>2</sub> (V<sup>5+</sup>, Fe<sup>3+</sup>, Ni<sup>2+</sup>, Zn<sup>2+</sup>, Os<sup>3+</sup>, and Ru<sup>3+</sup>) for the degradation of indigo carmine and 4-CP was attributed to: (i) high redox potential of Mn<sup>2+</sup>/Mn<sup>3+</sup> pairs; (ii) synergistic effects in the bicrystalline framework of anatase and rutile; (iii) unique half-filled electronic structure of Mn<sup>2+</sup>, which served as a shallow trap for the charge carriers; (iv) smaller crystallite size with high intimate contact between the mixed phase; and (v) favorable surface structure of the photocatalyst. This study further highlighted that the existence of dopant with half-filled electronic structure in the metal ion doped titania in enhancing the photocatalytic activity is not universal; rather, it is the complex function of several physicochemical and electronic properties.<sup>80</sup> TiO<sub>2</sub> nanoparticles doped with an array of metal ions (V<sup>5+</sup>, Mn<sup>2+</sup>, Fe<sup>3+</sup>, Cr<sup>3+</sup>, Co<sup>2+</sup>, Ni<sup>2+</sup>, Cu<sup>2+</sup>, Zn<sup>2+</sup>) showed higher photocatalytic activity for the degradation of MO, only when the dopant ionic radius is close to 80 pm and the anatase crystallite size is  $\sim$ 18 nm in the concentration range of 0.00002 to 0.2 atom %.<sup>94</sup>

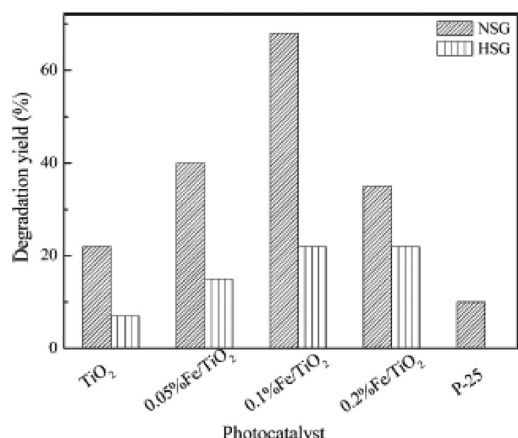
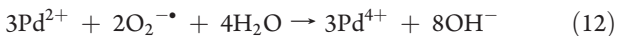


**Figure 15.** Photocatalytic degradation yield of MB over different photocatalysts calcined at 573 K (NSG = nonhydrolytic sol–gel; HSG = hydrolytic Sol–gel). Reprinted with permission from Zhu, J.; Ren, J.; Huo, Y.; Bian, Z.; Li, H. *J. Phys. Chem. C* 2007, 111, 18965–18969.

The change in the valence state of Pd had an important effect on the behavior of photocatalytic oxidation of nitrogen monoxide (NO) over Pd-modified TiO<sub>2</sub> prepared by the thermal impregnation method. During the initial state of the reaction, photogenerated electrons were transferred from the TiO<sub>2</sub> CB to the Pd<sup>2+</sup> ions or PdO particles, and a portion of Pd<sup>2+</sup> ions would be reduced to Pd<sup>0</sup> and a portion of Pd<sup>2+</sup> ions oxidized to Pd<sup>4+</sup> by hydroxyl or superoxide radicals with a simultaneous increase in the hydroxyl group density on the Pd modified TiO<sub>2</sub> surface. When the photogenerated electrons migrate to Pd<sup>4+</sup>, electrons and holes were spatially separated, leading to the improvement in photocatalytic activity. When the equilibrium between Pd<sup>2+</sup> and Pd<sup>4+</sup> was established, the highest conversion of NO was observed. In addition, Pd<sup>2+</sup> on the catalyst surface enhanced the NO adsorption.<sup>95,96</sup>



Furthermore, Pd<sup>4+</sup> can also trap the electron, hindering the recombination, thereby increasing the availability of holes for the degradation reaction. Fe<sup>3+</sup>–TiO<sub>2</sub> with mesoporous structure prepared via a facile nonhydrolytic sol–gel route showed superior activity for the degradation of MB under visible light irradiation compared to the samples obtained via a traditional hydrolytic sol–gel route which was attributed to the controlled reaction rate, lack of surface tension that ensures the formation of mesopores, and well-crystallized anatase phase with more surface oxygen vacancies (Figure 15).<sup>97</sup> Furthermore, the nonhydrolytic sol–gel process could strengthen the incorporation of the Fe<sup>3+</sup> dopant in the TiO<sub>2</sub> network, enhancing the photocatalytic activity.<sup>97</sup> When the dopant having higher ionic size (like Sn<sup>4+</sup>, Mn<sup>2+</sup>, Ag<sup>+</sup>, Zr<sup>4+</sup>, and Ln<sup>3+</sup>) substitutes the Ti<sup>4+</sup> ion in the TiO<sub>2</sub> lattice, the solid will exist in strained form with high lattice energy, due to the size difference between the host–guest ions. In such a situation, some structural defects such as vacancies particularly on the surface are expected to partially offset the

lattice strain. Therefore, it is suggested that more oxygen might escape from the lattice to trap the photogenerated holes to form hydroxyl radicals, preventing electron–hole recombination.<sup>98–102</sup> Murakami et al.<sup>103</sup> studied the photocatalytic activity of TiO<sub>2</sub> modified with Fe<sup>3+</sup>, Cu<sup>2+</sup>, Ni<sup>2+</sup>, and Cr<sup>3+</sup> ions by calcining the samples at 120 °C for CH<sub>3</sub>CHO oxidation. The order of activity for these metal ions in the modified titania followed the sequence Fe<sup>3+</sup> > Cu<sup>2+</sup> > Ni<sup>2+</sup> > Cr<sup>3+</sup> which was well in agreement with their reduction potentials. The standard electrode potentials of Fe<sup>3+</sup>/Fe<sup>2+</sup>, Cu<sup>2+</sup>/Cu<sup>+</sup>, Ni<sup>2+</sup>/Ni, and Cr<sup>3+</sup>/Cr<sup>2+</sup> are +0.771, +0.159, –0.257, and –0.424 V, respectively. Accordingly, Fe<sup>3+</sup> served as a better electron acceptor owing to its higher positive reduction potential. The mechanism of photocatalytic reactions investigated by double-beam photoacoustic spectroscopy suggested that metal ions on the semiconductor surface behave differently under different illumination conditions: as an electron acceptor under UV irradiation and as an electron injector under visible light illumination.<sup>103</sup>

Doping with a rare earth cation into TiO<sub>2</sub> was found to increase the photocatalytic activity for the degradation of organic contaminants by stabilizing the reactive anatase phase. Lanthanide ions are well-known for their ability to form complexes with various Lewis bases (acids, amines, aldehydes, alcohols, thiols, etc.) by the interaction of the functional group of the pollutant with the f-orbital of lanthanides. It is expected that lanthanide incorporation into the TiO<sub>2</sub> matrix could provide a means to concentrate the organic pollutants at the semiconductor surface, and therefore the photocatalytic degradation is thus promoted.<sup>104–110</sup> Liqiang et al. have found that the photocatalytic activity of the La<sup>3+</sup>–TiO<sub>2</sub> for phenol degradation with respect to the dopant concentration followed the order 1 > 1.5 > 3.0 > 0.5 > 5 > 0 mol %, which was in a trend similar to the photoluminescence intensity of the corresponding samples.<sup>107</sup> During the process of photocatalytic reactions, oxygen vacancies and dopant-induced defects could become the centers to capture the photoinduced electrons so that recombination could be effectively inhibited. Moreover, oxygen vacancies could promote the adsorption of O<sub>2</sub>, and there was a strong interaction between photoinduced electrons bound by oxygen vacancies and adsorbed O<sub>2</sub>. Thus, oxygen vacancies and defects were in favor of photocatalytic reactions in which O<sub>2</sub> was effective to promote the oxidation of organic substances.<sup>107</sup> RE doped TiO<sub>2</sub> (where RE = La<sup>3+</sup>, Ce<sup>3+</sup>, Er<sup>3+</sup>, Pr<sup>3+</sup>, Gd<sup>3+</sup>, Nd<sup>3+</sup>, Sm<sup>3+</sup>) prepared by the sol–gel technique was found to be beneficial for the degradation of nitrite. The degradation reaction over Gd<sup>3+</sup>–TiO<sub>2</sub> followed first-order kinetics, while zero-order kinetics prevailed over other RE-TiO<sub>2</sub> photocatalysts, indicating that the charge carrier recombination was dominated by the latter catalysts.<sup>109</sup> Ranjit et al. reported the enhanced degradation of salicylic acid compared to cinnamic acid due to the favorable stereoconfiguration which can coordinate to the catalyst surface through –COOH and –OH groups, resulting in efficient adsorption and interfacial charge transfer process, while the low adsorption of cinnamic acid on the catalyst surface resulted in a lower degradation rate.<sup>111</sup> Lanthanide oxide doped TiO<sub>2</sub> prepared by a coprecipitation method exhibited higher photocatalytic activity for RhB degradation under UV light irradiation (50 W medium pressure mercury lamp) compared to the samples prepared by the sol–gel method, although catalysts prepared by both the methods had almost the same dopant concentration and were biphasic of anatase and rutile.<sup>112</sup> The photocatalysts prepared by coprecipitation methods had a macro-/mesoporous structure with more

regular anatase crystal structure, while some carbon residues were found on the surface of sol–gel-prepared samples which lowered their activity. The carbon residues might occupy the surface active sites, thereby inhibiting the adsorption of molecular oxygen and charge transfer at the solid–liquid interface.<sup>112</sup>

Irrespective of metal ion doped titania, there exists an optimum dopant concentration within the TiO<sub>2</sub> matrix for the effective separation of charge carriers. Pleskov reported that the value of the space charge region potential for the effective separation of charge carriers must not be lower than 0.2 eV.<sup>113</sup> On the other hand, the thickness of the space charge layer is influenced by the dopant concentration according to the following equation.

$$W = \left( \frac{2\epsilon\epsilon_0 V_s}{eN_d} \right)^{1/2} \quad (13)$$

where  $W$  is the thickness of the space charge layer;  $\epsilon$  and  $\epsilon_0$  are the static dielectric constants of the semiconductor and of the vacuum;  $V_s$  is the surface potential;  $N_d$  is the number of dopant donor atoms; and  $e$  is the electronic charge. This clearly shows that  $W$  is inversely proportional to the concentration of the dopant. In addition, the penetration depth  $l$ , of the light into the solid is given by  $l = 1/a$ , in which  $a$  is the light absorption coefficient at a given wavelength. When the value of  $W$  approximates to that of  $l$ , all the absorbed photons generate electron–hole pairs that are efficiently separated. Consequently, the existence of an optimum value of  $N_d$  is understandable, for which a space charge region exists whose potential is not less than 0.2 eV and thickness is more or less equal to light penetration depth. The space charge region becomes very narrow for higher dopant concentration, and the penetration depth of light into TiO<sub>2</sub> greatly exceeds the thickness of the space charge layer, increasing the recombination rate of electrons and holes. The adverse effects of dopants are: (i) forming effective charge carrier recombination centers; (ii) causing a decrease in the mobility and lifetime of minority carriers; and (iii) causing a decrease of the hole diffusion length. There are conflicting results on the effects of doping on the visible light photoactivity of TiO<sub>2</sub>. The wide variability of reports on the visible light activity of metal ion doped titania is due to the specific preparation methods, experimental conditions used to quantify activity, and the broad array of chemical reactions used to verify photoactivity over a range of wavelengths  $\lambda > 400$  nm. Fundamentally, these issues can be understood in terms of: (i) lack of surface structure facilitating surface transfer and reactivity of carriers and (ii) the distribution of dopant-induced localized states not being optimal to facilitate the photo-oxidation reactions.<sup>11</sup> Therefore, it is difficult to compare the net effects of metal ion dopants in the photocatalytic activities of doped titania.<sup>80,114</sup>

## 5.0. NONMETAL ION DOPED TITANIA

Nonmetal ion doping is a promising way to avoid the deteriorating thermal stability of the TiO<sub>2</sub> lattice. For instance, TiO<sub>2-x</sub>N<sub>x</sub> samples prepared by the solvothermal route showed violet color, which on calcination in air at 200–800 °C for 1 h changes to weak violet, bright yellow, weak yellow, and gray. However, the sample did not change to white color, indicating the thermal stability of Ti–N bonding in TiO<sub>2-x</sub>N<sub>x</sub> powders.<sup>115</sup> Khan et al. for the first time reported the water splitting reaction using rutile TiO<sub>2</sub> doped with carbon as

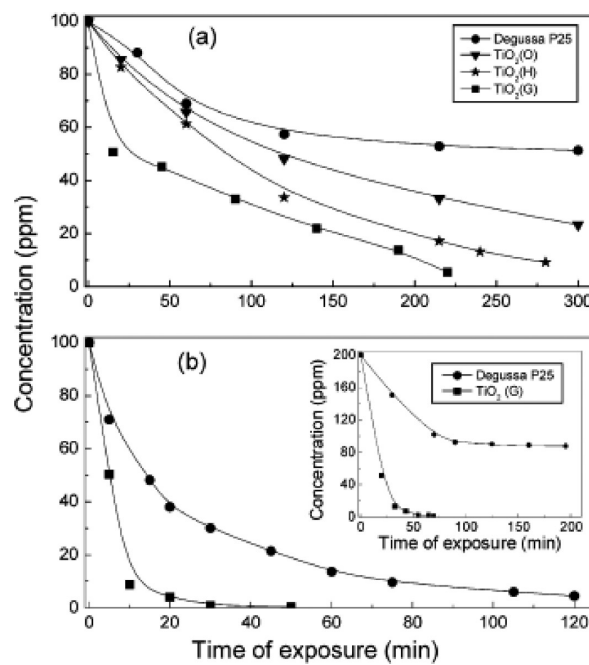


**Figure 16.** Degradation profiles of MB with an initial concentration of 100 ppm and a catalyst loading of 1 kg/m<sup>3</sup> with combustion-synthesized and Degussa P-25 TiO<sub>2</sub> under (a) solar and (b) UV conditions. Reprinted with permission from Nagaveni, K.; Hegde, M. S.; Ravishankar, N.; Subbanna, G. N.; Madras, G. *Langmuir* 2004, 20, 2900–2907.

substitutional impurity, and the band gap was reduced from 3.0 to 2.32 eV upon carbon incorporation.<sup>116</sup> Rutile TiO<sub>2</sub> was fabricated by flame pyrolysis of Ti metal, and carbon was incorporated during the pyrolysis process that was carried out in the presence of combustion products (CO<sub>2</sub> and H<sub>2</sub>O). Measurements of the photocurrent at various applied voltages indicated a high activity for the carbon-doped films compared to undoped materials.<sup>116</sup> TiO<sub>2</sub> prepared by the solution combustion route using glycine (G), hexamethylene tetramine (H), and oxalyldihydrazide (O) as fuel resulted in the visible light response due to the carbide ion substitution for oxygen, which forms an isolated electronic state above the O 2p level and also serves as effective sites for water adsorption.<sup>117</sup> TiO<sub>2</sub>-G showed a large shift in the band gap absorption (2.1 and 2.85 eV) compared to TiO<sub>2</sub>-H (2.85 eV) and TiO<sub>2</sub>-O (2.98 eV), probably due to the lower extent of incorporation of carbide ions in these samples. TiO<sub>2</sub>-G showed superior activity for the degradation of MB compared to other photocatalysts under solar irradiation which was attributed to the dense surface hydroxyl groups, high crystallinity, very high surface area, and greater amounts of surface acidic sites (Figure 16).<sup>117</sup> In addition to its higher photocatalytic activity, combustion-synthesized titania settles at a faster rate in the aqueous suspension and is easy to separate from the reaction mixture by centrifugation. The feasibility of carbon doping was found to depend on the carbon precursor in the preparation of carbon-modified titania (C-TiO<sub>2</sub>) by hydrothermal treatment. TiO<sub>2</sub> can be more readily doped by carbon in the presence of glucose compared with tetrabutylammonium hydroxide (TBAH), which is attributed to carrier diffusion of glucose due to its smaller size.<sup>118</sup> The charge and high molecular weight of C<sub>16</sub>H<sub>36</sub>N<sup>+</sup> hinder the diffusion into the bulk TiO<sub>2</sub>. Thus, C-TiO<sub>2</sub> with glucose showed 13-fold enhancements in the degradation rate of 4-CP compared

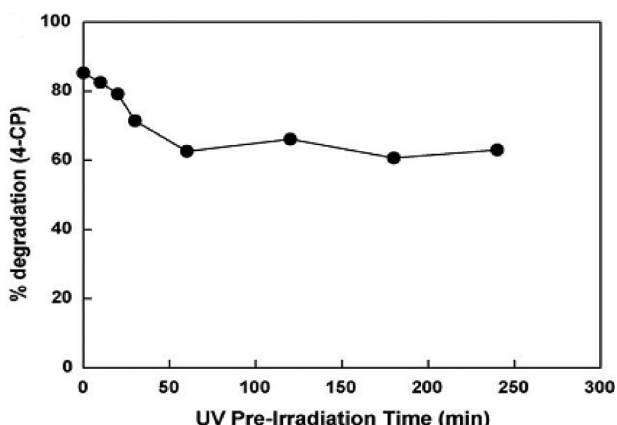


**Figure 17.** Effects of UV preirradiation ( $\lambda > 300$  nm) time on the degradation of 4-CP under visible light illumination using  $\text{TiO}_2$  prepared by sol–gel hydrolysis of titanium butoxide and calcined at  $250^\circ\text{C}$ . Reprinted with permission from Park, Y.; Kim, W.; Park, H.; Tachikawa, T.; Majima, T.; Choi, W. *Appl. Catal. B: Environ.* **2009**, *91*, 355–361. Copyright Elsevier, 2009.

to unmodified titania and 8-fold superiority compared to C- $\text{TiO}_2$  with TBAH. Furthermore, C- $\text{TiO}_2$  modified with glucose had two visible absorption edges at 2.78 and 1.45 eV, enabling the catalyst to absorb solar light more efficiently compared to C- $\text{TiO}_2$  modified with TBAH which had a single absorption threshold at 2.76 eV.<sup>118</sup> Kisch and co-workers reported that pyrolysis of alcohols employed in the sol–gel process of titanium alkoxides led to highly condensed coke-like carbonaceous species embedded in the  $\text{TiO}_2$  matrix during calcination at  $250^\circ\text{C}$  and was responsible for visible light sensitization. C- $\text{TiO}_2$  prepared from a titanium tetrabutoxide precursor showed maximum activity for the degradation of 4-CP under visible light irradiation. When the carbon-doped  $\text{TiO}_2$  samples were heated to  $400^\circ\text{C}$ , the carbon content was totally eliminated from the catalyst, and the photocatalysts were found to be completely inactive under visible light.<sup>119</sup> Choi et al. reported for the first time that the carbon was doped into  $\text{TiO}_2$  without the aid of an external carbon precursor through sol–gel hydrolysis of titanium tetrabutoxide, while the hydrolysis of titanium ethoxide and titanium isopropoxide did not lead to efficient carbon doping which highlights the sensitivity of carbon incorporation on the initial precursor used.<sup>120</sup> The extent of carbon doping was strongly influenced by the calcination temperature and reached maximum at  $\sim 250^\circ\text{C}$ . The preirradiation of C- $\text{TiO}_2$  reduced the visible light activity, while the activity under UV irradiation did not decrease (Figure 17). This suggests that surface carbon species acting as a sensitizer were removed photocatalytically during 1 h of preirradiation, and the remaining visible light activity was largely ascribed to carbon in the bulk. The calcined sample at  $\sim 250^\circ\text{C}$  showed enhanced activity for the 4-CP degradation even after three subsequent runs.<sup>120</sup> The enhanced activity of B- $\text{TiO}_2$  (with a molar ratio of B to Ti of 5) for nicotinamide adenine dinucleotide regeneration was due to the large band gap due to quantization, smaller crystallite size, and enhanced absorption of B- $\text{TiO}_2$  in the UV region compared to undoped  $\text{TiO}_2$ . The increased band gap energy of B- $\text{TiO}_2$  results in larger thermodynamic driving force and faster charge carrier transfer rates in the normal Marcus region than in its bulk phase counterparts.<sup>121a</sup>

Asahi et al. reported the  $\text{TiO}_{2-x}\text{N}_x$  prepared by sputtering the  $\text{TiO}_2$  target in a  $\text{N}_2$  (40%)/Ar gas mixture for the degradation of

MB and gaseous  $\text{CH}_3\text{CHO}$  under UV/visible light.<sup>121b</sup> N-doped layered titanates ( $\text{Cs}_{0.68}\text{Ti}_{1.83}\text{O}_{4-x}\text{N}_x$  and  $\text{H}_{0.68}\text{Ti}_{1.83}\text{O}_{4-x}\text{N}_x$ ) with a lepicrocite structure resulted in faster Rhodamine G degradation under visible light illumination.<sup>121c</sup> This was attributed to the unique layered structure and homogeneous distribution of N dopant in the layered titanates which significantly contributed to enhanced visible light absorption and high mobility of charge carriers. The interlayer galleries of the layered titanate precursors provided excellent channels for the diffusion of N dopant and resulted in uniform distribution of dopant over the whole layered titanate structure. The upward shift of the valence band maximum (VBM) by N 2p states was concluded for the cause of band to band visible light excitation. These layered titanates retained their activity even after four subsequent runs without undergoing any change in the crystal structure, chemical change, and content of N dopant.<sup>121c</sup> The multitype N- $\text{TiO}_2$  containing both substitutional (N-Ti-O and Ti-O-N) and interstitial (characteristic NO) states resulted in the intraband states at 0.14 and 0.73 eV above the top of the VB, resulting in visible light response and faster degradation of gaseous toluene.<sup>121d</sup> Mrowetz et al.<sup>122</sup> reported that N- $\text{TiO}_2$  failed to oxidize formate and  $\text{NH}_3-\text{OH}^+$  under visible light illumination, although band gap narrowing due to N-doping was observed. The oxidizing species formed in photoactivation of such states by the visible wavelength was both thermodynamically and kinetically unfavorable to oxidize such weak donors (formate anion) despite the creation of oxygen vacancies. Hence, the decomposition of organic compounds by N- $\text{TiO}_2$  may be carried out by the reactive oxygen species produced by the reduction and not via the trapped holes localized on the N atom at the mid-band-gap potential. It should be noted that the oxidation power and mobility of photogenerated hole in the isolated nitrogen electronic state is lower than that of the VB edge of  $\text{TiO}_2$ . Hirowaka and Nosaka quantitatively estimated the formation of a superoxide radical on N- $\text{TiO}_2$  using a luminal chemiluminescence probe.<sup>123</sup> The amount of superoxide radical reached a steady state for S- $\text{TiO}_2$  and gradually increased for N- $\text{TiO}_2$ . In other words, S- $\text{TiO}_2$  surpassed N- $\text{TiO}_2$  in the production of superoxide radicals, while N- $\text{TiO}_2$  surpassed S- $\text{TiO}_2$  in the production of  $\text{H}_2\text{O}_2$ , preferably attributed to the multivariance oxidation state of S in the  $\text{TiO}_2$  lattice. N- $\text{TiO}_2$  prepared by a solvothermal route using the  $\text{TiCl}_3$ -urea-methanol system showed enhanced activity under UV/visible light for the degradation of NO compared to other photocatalysts prepared in other solvents like ethanol, *n*-propanol, and *n*-butanol. The high dielectric constant of methanol ( $\epsilon = 33.1$ ) compared to ethanol ( $\epsilon = 23.8$ ), *n*-propanol ( $\epsilon = 20.1$ ), and *n*-butanol ( $\epsilon = 17.1$ ) induces high crystallinity in the samples with fine crystallite size, which obviously resulted in higher activity.<sup>115</sup> Sano et al. reported the formation of N- $\text{TiO}_2$  by thermal decomposition of the  $\text{Ti}^{4+}$ -bipyridine complex and its photocatalytic activity for the removal of  $\text{NO}_x$  under visible light.<sup>124</sup> N- $\text{TiO}_2$  prepared from the Ti–melamine complex showed higher activity than the Ti–salen complex for the decomposition of MB which can be attributed to the lower amount of N doping and smaller number of Ti–N bonds in the Ti–salen complex.<sup>125</sup>

F doped  $\text{TiO}_2$  prepared by spray pyrolysis from an aqueous solution of  $\text{H}_2\text{TiF}_6$  showed visible light activity for the degradation of  $\text{CH}_3\text{CHO}$  and  $\text{C}_2\text{HCl}_3$ , although F doping did not change the absorption properties of titania. The high photocatalytic activity of F doped  $\text{TiO}_2$  originated from the extrinsic absorption through the creation of oxygen vacancies rather than the intrinsic

absorption of bulk  $\text{TiO}_2$ .<sup>126</sup> The extrinsic absorption originates from the photoionization of original and newly formed defects and the excitation of surface states. Such extrinsic absorption requires less energy to activate, and hence it is possible to induce surface charge carriers by visible light.<sup>126</sup>

Phosphorus was incorporated into the mesoporous framework of titania using  $\text{H}_3\text{PO}_4$  as a phosphorus source.<sup>127</sup> The complete condensation between surface  $\text{Ti}-\text{OH}$  and the inhibition of crystalline growth of the embedded anatase  $\text{TiO}_2$  during the heat treatment lead to the stabilization of a phosphated mesoporous  $\text{TiO}_2$  framework which showed enhanced activity for the oxidation of *n*-pentane in air. The higher photocatalytic activity was due to the existence of Ti ions in a tetrahedral coordination. These tetrahedrally coordinated Ti ions can adsorb water and oxygen in air to produce more hydroxyl groups on the surface of  $\text{TiO}_2$ . Moreover, the adsorbed water and oxygen by the Ti ions in tetrahedral coordination can stabilize the photoexcited electron–hole pairs, which would hinder recombination.  $\text{P}-\text{TiO}_2$  prepared by the sol–gel method and calcined at two different temperatures (400 and 800 °C) showed higher activity for MB degradation compared to P25 under UV illumination, suggesting that  $\text{P}^{5+}$  restrained catalytic activity even at higher sintering temperature. For higher  $\text{P}^{5+}$  concentration ( $\text{P}/\text{Ti} > 0.1$ ), the activity decreased due to the formation of secondary oxides such as  $\text{TiP}_2\text{O}_7$  and  $(\text{TiO})_2\text{P}_2\text{O}_7$ .<sup>128</sup>

Iodine cation doped titania prepared by anodization at 20 V, using titanium nanotubes as the cathode and the Ni sheet as the anode, showed superior activity for photocurrent generation and MO degradation under visible light due to the presence of iodine in its multivalency state ( $\text{I}^{7+}$ ,  $\text{I}^{5+}$ , and  $\text{I}^-$ ).<sup>129a</sup> However, only iodine anion doped  $\text{TiO}_2$  was prepared by anodization, wherein titania nanotubes served as an anode and the Ni sheet as cathode showed lower activity. The electrolytic solution was  $\text{HIO}_4$  in the former and KI in the latter case with identical concentration. The first-principle calculation revealed that four I 5p bands (shallow acceptor and donor states) appeared within the band gap states for I (cation)– $\text{TiO}_2$ , while only two I 5p states (deeply trapped) were present close to the CB for I (anion)– $\text{TiO}_2$ . Furthermore, band potentials of I (cation)– $\text{TiO}_2$  shift downward to a larger extent due to the interaction between I 5p orbitals and Ti 3d electronic levels, indicating that the VB has a stronger oxidation potential than I (anion)– $\text{TiO}_2$ .<sup>129a</sup> The surface iodine doped titania with coexisting atomic configuration of iodine dopant I–O–I (unoccupied states) and I–O–Ti (occupied states) within the band gap states showed visible light photocatalytic activity even beyond 660 nm for RhB degradation.<sup>129b</sup> The coexistence of I–O–I and I–O–Ti states changed the surface structure of titania due to the release of local strain energies. The low-energy photon excitation from I–O–Ti to I–O–I states is directly responsible for the greatly extended band gap absorption edge up to ~800 nm. Furthermore, the occupied states close to the VB result in strong oxidative power for photogenerated holes, which together with favorable surface structure for the surface transfer of carriers contributes for robust activity of I– $\text{TiO}_2$ . This work has shown that controlling surface atomic configuration of dopant is vital to tune favorable surface-electronic properties and consequent photocatalytic activity of the photocatalyst.<sup>129b</sup>

## 6.0. HETEROSTRUCTURING OF TITANIA BY CODOPING

Heterostructuring the  $\text{TiO}_2$  by codoping with two or more dopants is reported to achieve significant synergistic effects

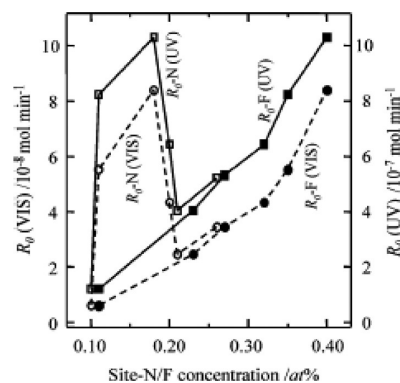


**Figure 18.** Dependence of the photocatalytic activity on the site-N/F concentration. Reprinted with permission from Li, D.; Haneda, H.; Hishita, S.; Ohashi, N. *Chem. Mater.* 2005, 17, 2596–2602.

compared to their single ion doped or undoped  $\text{TiO}_2$  counterparts.<sup>130–140</sup> The strong interaction between these dopants within the  $\text{TiO}_2$  matrix alters the charge carrier transfer–recombination dynamics and also shifts the band gap absorption to the visible region. The coupling of one dopant with second has been proposed to enable a reduction in the number of carrier recombination centers by the proposed charge equilibrium mechanism as well as enhance the visible light absorbance by increasing the solubility limit of dopants.<sup>130–140</sup> In the case of  $\text{Fe}^{3+}$ – $\text{Ho}^{3+}$ – $\text{TiO}_2$ ,  $\text{Fe}^{3+}$  broadens the absorption profile, improving the photoutilization of  $\text{TiO}_2$ , and generates more electron–hole pairs, while  $\text{Ho}^{3+}$  doping restrains the increase of grain growth and leads to crystal expansion retarding the recombination of charge carriers resulting in the faster degradation of MO compared with single ion doping or undoped  $\text{TiO}_2$  under UV light.<sup>130</sup> In an another study,  $\text{Fe}^{3+}$ – $\text{Ho}^{3+}$ – $\text{TiO}_2$  film loaded on activated carbon fibers (ACFs) prepared by the sol–gel method showed superior activity for the degradation of MO under UV illumination.<sup>131</sup> SEM analyses revealed that codoping restrained the thin film from cracking when calcined at 600 °C, while undoped titania showed enormous flakes due to shrinkage of  $\text{TiO}_2$  sol during the thermal treatment step. These cracks are disadvantageous for repeated application in photocatalysis because the flakes will break away from the surface of ACF in the process of repeated usage. The codoped film loaded ACF exhibited better and stable photocatalytic degradation for MO up to four cycles compared to undoped samples.<sup>131</sup> N–F– $\text{TiO}_2$  prepared by spray pyrolysis showed higher activity for the degradation of  $\text{CH}_3\text{CHO}$ ,  $\text{CCl}_3\text{CHO}$ , and  $\text{C}_6\text{H}_5\text{—CH}_3$  due to enhanced surface acidity and a large red shift in the band gap absorption of N–F– $\text{TiO}_2$ .<sup>132</sup> The presence of different electronic energy states like F center,  $\text{F}^+$  center, an unidentified energy state, and an impurity energy level within the band gap states (as revealed by PL studies) enhanced the interfacial charge transfer process. The increase in surface acidity due to F doping enhanced the adsorption of organic pollutants and also served as trap sites for electrons, thereby increasing the charge carrier mobility in  $\text{TiO}_2$ . Therefore, photogenerated electron diffuses from the bulk to the surface of the particles to take part in surface photochemical reactions. However, no correlation was obtained between site N concentration and initial rates for the degradation of organic pollutants due to the dual function of N (including both positive and detrimental effects). In contrast, the initial rate monotonically increased with an increase in site F concentration

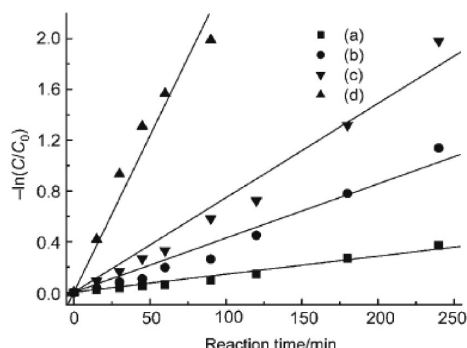


**Figure 19.** Kinetic photodegradation curves for RhB in the presence of B-doped titania (a), undoped titania (b), N-doped titania (c), and B–N codoped titania (d) upon irradiation with UV/vis irradiation. Reprinted with permission from Liu, G.; Zhao, Y.; Sun, C.; Lu, G. Q.; Cheng, H. M. *Angew. Chem., Int. Ed.* 2008, 47, 4516–4520. Copyright Wiley, 2008.

in UV/vis light, confirming that induced surface structure due to F doping was favorable for higher activity in N–F–TiO<sub>2</sub> (Figure 18).<sup>132</sup> The twist-like unique morphology of N–S–TiO<sub>2</sub> with a mesoporous microstructure obtained by simple hydrolysis of TiCl<sub>4</sub> using NH<sub>3</sub> in the presence of glacial acetic acid and ammonium sulfate followed by thermal treatment at 723 K for 3 h exhibited high thermal phase stability and efficiency for the degradation of phenol under UV/visible light illumination. The combined effect of large surface area, red shift in the band gap, and reduced recombination resulted in the enhanced quantum yield for N–S–TiO<sub>2</sub>.<sup>133</sup>

A substantial enhancement in UV/visible light activity of B–N–TiO<sub>2</sub> were observed for RhB degradation, while single ion doped titania (B–TiO<sub>2</sub> and N–TiO<sub>2</sub>) showed lower activity compared to undoped TiO<sub>2</sub> (Figure 19). The quantum mechanical calculation revealed that the surface electronic states around the Fermi level of pure TiO<sub>2</sub> were dramatically changed due to B–N codoping and at the same time introduced new states around the upper VB close to the Fermi level. The presence of O–Ti–B surface structure contributed to the visible light absorption, and O–Ti–B–N surface states served as active sites for the separation and transfer of visible light induced charge carriers. Thus, the synergistic effects of visible light absorption and separation of charge carriers are responsible for the higher activity of B–N–TiO<sub>2</sub>.<sup>134</sup> However, In et al. reported that the visible light photoactivities of B–N–TiO<sub>2</sub> are similar to B–TiO<sub>2</sub> for the degradation of methyl tertiary butyl ether, which indicates the absence of synergy.<sup>135</sup> The surface-terminating structure Ti–O–B–N in B–N–TiO<sub>2</sub> exhibited significant activity for the degradation of RhB, suggesting that the B–N bond can still be active in promoting the photocatalytic activity even when it ends on the exposed surface O atoms of TiO<sub>2</sub>.<sup>136</sup> It was proposed that Ti–O–B–N surface structure exhibits bifunctionality in promoting photocatalysis: (i) creation of partially occupied localized state attributed to B–N coupling with spectral distribution advantageous for enhancing the visible light absorption; (ii) acting as “hot spots” to support the localization and separation of charge carriers at the surface; (iii) occupied localized states of the B atom were very close to the conduction band minimum (CBM), while the occupied localized states from the coupled B–N atoms were located more close to the VBM indicating high oxidative power of holes in these states upon photon excitation (Figure 20).<sup>136</sup> B–N–TiO<sub>2</sub>

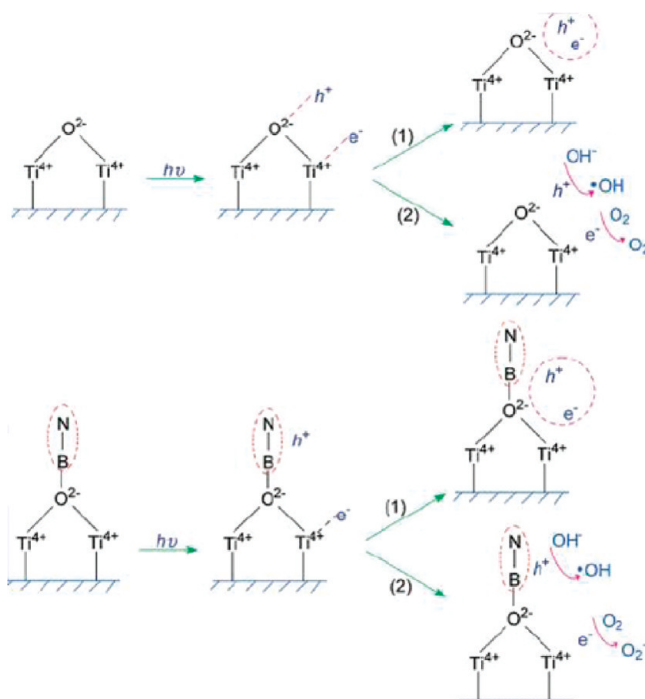


**Figure 20.** Schematic representation of photoexcitation, surface recombination process of photoinduced electrons and holes (Step 1), and surface transfer process (Step 2) of carriers by trapping with an electron donor and acceptor on anatase TiO<sub>2</sub> and B–N codoped anatase TiO<sub>2</sub>. Reprinted with permission from Liu, G.; Sun, C.; Cheng, L.; Jin, Y.; Lu, H.; Wang, L.; Smith, S. C.; Lu, G. Q.; Cheng, H. M. *J. Phys. Chem. C* 2009, 113, 12317–12324.

calcined at 600 °C showed superior activity for phenol degradation under visible light with nitrogen content (0.02 mol %) being twice than that of B content (0.01 mol %). Either an increase in B content or a decrease in N content resulted in the lower activity for B–N–TiO<sub>2</sub>.<sup>137</sup> La–I–TiO<sub>2</sub> showed enhanced activity for the degradation of oxalic acid compared to I–TiO<sub>2</sub>. The synergistic effect of dispersed La<sub>2</sub>O<sub>3</sub> in suppressing charge carrier recombination and the optical shift of the absorption edge to the visible region by the iodine dopant resulted in the enhanced activity. The photocatalytic oxidation of oxalic acid using La–I–TiO<sub>2</sub> was strongly quenched by the addition of KI and was not affected by the addition of TBA. This suggests that the predominant degradation pathway was mediated by VB holes and adsorbed hydroxyl radicals and not by free hydroxyl radicals that are present in the bulk of the solution.<sup>138</sup> Song et al. also reported that Ce–I–TiO<sub>2</sub> showed an identical degradation pathway for oxalic acid.<sup>139</sup> In this case, cerium ions served as an electron trap during the photocatalytic reaction due to its varied valencies and special 4f level. In addition, the existence of surface states of Ce<sup>4+</sup>/Ce<sup>3+</sup> can form labile oxygen vacancies and highly active bulk oxygen vacancies. The substitution of I<sup>5+</sup> into the crystal lattice produces some localized charge perturbation which results in deformation energy. Also, the reduction of titanium to a lower valence state may be provoked by a charge imbalance when I<sup>5+</sup> substitutes Ti<sup>4+</sup> during the heat treatment. These Ti<sup>3+</sup> ions can form a defect level which can act as the hole traps to promote the charge transfer, eventually suppressing the recombination. The decrease in the reaction rate under nitrogen purging conditions indicated that hydroxyl radicals and excited

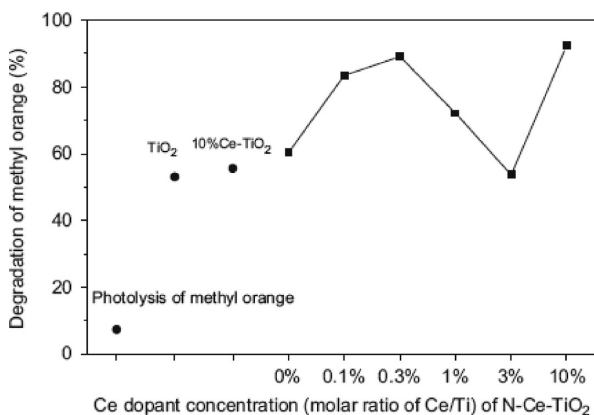


**Figure 21.** Degradation of MO with different cerium dopant concentrations in Ce–N–TiO<sub>2</sub> photocatalysts under visible light irradiation. Reprinted with permission from Liu, C.; Tang, X.; Mo, C.; Qiang, Z. *J. Solid State Chem.* 2008, 181, 913–919. Copyright Elsevier, 2008.

atomic oxygen were minor oxidants for oxalic acid degradation. The degradation of oxalic acid was inhibited by the addition of 50 mM NaF, indicating that oxalic acid needs to be first adsorbed on the catalyst surface rather than directly reacting with free radicals in the bulk solution.<sup>139</sup> N–TiO<sub>2</sub> showed superior activity for the MB degradation under visible light compared to Mo–N–TiO<sub>2</sub>, while Mo–TiO<sub>2</sub> showed lower activity compared to TiO<sub>2</sub>, suggesting that Mo serves as recombination centers in the codoped system.<sup>140</sup> The absence of synergy was explained based on the changes in oxygen vacancy concentration due to codoping. The lower valent N (−3) substitutes lattice O (−2), inducing oxygen vacancies for charge equilibrium in TiO<sub>2</sub>. These oxygen vacancies induce a visible light absorption edge, serve as trap centers for photoinduced electron, and act as reactive centers for the photocatalytic process. On doping with Mo<sup>6+</sup> at the lattice sites of Ti<sup>4+</sup>, the oxygen vacancy concentration decreases for charge compensation which reduces the activity of Mo–N–TiO<sub>2</sub>. This might probably account for the lower activity of Mo–TiO<sub>2</sub> compared to pure TiO<sub>2</sub> itself.<sup>140</sup> The degradation efficiency of MO increased up to 0.3 atom % of Ce<sup>3+</sup> doping, and a decrease in activity was observed beyond this optimum concentration for Ce–N–TiO<sub>2</sub>. However, when the concentration of Ce<sup>3+</sup> was 10 atom %, the activity was increased drastically due to the formation of cubic phase CeO<sub>2</sub> along with anatase structure (Figure 21).<sup>141</sup> The ternary oxides CeTiO<sub>4</sub> or CeTi<sub>2</sub>O<sub>6</sub> crystallite formed, along with TiO<sub>2</sub> and CeO<sub>2</sub> which enhanced the visible light absorption and thus improved the photocatalytic activity.<sup>142</sup> Furthermore, Ce–N codoping narrowed the band gap of titania and shifted the optical response to the visible region compared to their single doped counterparts.<sup>141</sup> The codoping of Fe–N introduced dopant states just below the CB and above the VB titania resulting in visible light photoresponse for the degradation of RhB. Under visible light, multiple transitions can take place: (i) from the N impurity level to the Fe<sup>3+</sup> impurity level; (ii) from the N impurity level to CB; (iii) from the VB to Fe<sup>3+</sup> impurity level. Therefore, the quantity of photoinduced charge carriers was much higher leading to better photocatalytic activity compared to pure titania or single ion doped titania. Under UV light, the trap sites of these dopants might serve as recombination centers, and also an unsuitable extent of nitrogen doping (which may not be of optimal value) renders the codoped titania to be very less effective.<sup>143</sup> In contrast,

Fe–N–TiO<sub>2</sub> titania prepared by the hydrothermal method showed lower activity compared to single ion doped titania for the degradation of MB under visible light. The concentration of the Ti<sup>3+</sup>/Ti<sup>4+</sup> ratio in the codoped titania was low compared to single ion doped samples as revealed by XPS analysis which indicates the interaction between dopant levels. The first-principle calculations suggested that in the case of codoped titania 3d orbitals of Fe overlap to a large extent with the O 2p level, arriving at a complete overlap of Density of States (DOS) between Fe 3d and O 2p at the VBM along with the reformation of VB and CB edges. For N–TiO<sub>2</sub>, a hybrid energy level is formed at the VBM due to the substitution of N<sup>3−</sup> for O<sup>2−</sup> with a continuum state at the VBM. However, for Fe–TiO<sub>2</sub>, there were only few DOS overlaps between Fe 3d and O 2p at the VBM, where the detached energy level is formed by Fe 3d. Hence, for Fe–N–TiO<sub>2</sub>, a majority of the charge carriers recombine in the deep traps resulting in lower activity.<sup>144</sup> Nitrided Pt<sup>4+</sup>–TiO<sub>2</sub> showed superior activity for 4-CP degradation compared to the nitrided TiO<sub>2</sub> and Pt<sup>4+</sup>–TiO<sub>2</sub> under UV/visible illumination, while the synergy of multiple modifications was observed for dichloroacetate degradation only under UV illumination but was absent under visible light.<sup>145</sup> Although interstitial B doping into the TiO<sub>2</sub> structure (Ti–O–B) resulted in the blue shift of the band gap due to the quantization, the subsequent codoping with Ni<sup>2+</sup> resulted in a red shift in the band gap absorption of B–Ni–TiO<sub>2</sub> prepared by the aerosol-assisted flow method. B doping increased the redox power of charge carriers and induced high crystallinity for the hollow structure, facilitating the diffusion of NO into the interior space. On the other hand, a large shift in the band gap due to Ni doping and the presence of NiO species on the surface acting as trap sites results in the highest photocatalytic activity for NO decomposition under visible light compared to their single ion doped counterparts.<sup>146</sup>

## 7.0. MIXED-PHASE TITANIA

Contrasting results are reported about the influence of phase composition on the photocatalytic degradation of organic pollutants in both air and water. Indeed, different authors reported that anatase works better than rutile,<sup>147</sup> while few authors reported the best results for rutile.<sup>148–156</sup> Much experimental evidence supports the existence of a synergistic effect in the bicrystalline titania containing anatase–rutile,<sup>157–196</sup> anatase–brookite,<sup>197–208</sup> rutile–brookite,<sup>209</sup> or tricrystalline anatase–rutile–brookite<sup>210–212</sup> in enhancing the photocatalytic activity. Although the coupling of two different semiconductors for better charge separation has received a great deal of attention for the development of highly active photocatalysts, bicrystals and tricrystals of heterogeneous titania nanostructure are intriguing since they involves only a change in the crystal structure of the same material. However, it is critical to note that the stabilization of charge separation in bicrystals or tricrystals of titania does not necessarily involve either sensitization or energy transfer (antenna effect) as electron–hole pairs are produced in the polymorphs involved owing to the small difference in their band gap excitation energies.

The different behavior shown by rutile and anatase was initially attributed to a difference in the position of the CB (more positive for rutile with respect to NHE). Anatase has inherent surface band bending that is spontaneously formed in the deeper region with a steeper potential in comparison with rutile. In anatase, surface hole trapping dominates because the spatial charge separation is achieved by the migration of

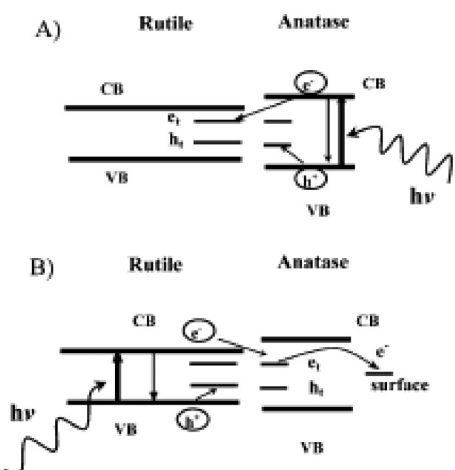


**Figure 22.** (A) Previously speculated model of P25 activity where charge separation occurs on anatase and rutile acts as an electron sink. (B) Proposed model of a rutile antenna and subsequent charge separation. Reprinted with permission from Hurum, D. C.; Agrios, A. G.; Gray, K. A.; Rajh, T.; Thurnauer, M. C. *J. Phys. Chem. B* 2003, 107, 4545–4549.

photogenerated holes toward the particle surface due to strong upward band bending. In rutile, a bulk generated charge carrier prevails since only the holes sufficiently close to the surface migrate before recombination.<sup>163</sup> However, in the mixed phase, one of the crystal phases sensitizes the transfer of a photoinduced electron to the other phase depending on the relative positions of band edges. Thus, the solid–solid interface between the two phases is a key structural feature that facilitates charge separation to suppress recombination which may be due to the locus of defect sites acting as “catalytic hot spots”. Compared to pure phases, the mixed-phase TiO<sub>2</sub> materials have unique charge transfer and recombination dynamics, fast diffusion of charge carriers to the surface, or an interface that enhances the interfacial charge transfer processes.<sup>163</sup>

Two distinct mechanisms on the interfacial charge transfer pathways in the bicrystal of anatase and rutile were proposed by Bickley et al.<sup>164</sup> and Hurum et al.<sup>187</sup> According to Bickley et al.<sup>164</sup> the high activity of Degussa P25 originated from an unusual microstructure consisting of the anatase phase which is in intimate contact with the rutile overlayer. According to their speculative model, the rutile phase serves as a passive sink, hindering the recombination in the anatase phase, and this mode of electron transfer is thermodynamically favored as the rutile CB lies 0.2 eV below the CB edge of anatase titania (Figure 22 A). The authors initially proposed that the enhancement in the photocatalytic properties of P25 stemmed from a space charge region formed at the rutile–anatase interface where band bending occurred due to the energy differences in the band gap of the two phases. Bickley also noted that the actual mechanism remains unclear and might be more complex. This explanation however did not consider the energies of the lattice or surface trapping sites or the effects of interfacial distortion leading to the band bending.<sup>164</sup> Hurum et al.<sup>187</sup> explained the direction of electron transfer based on EPR technique and proposed that electron transfer under visible light illumination takes place from the rutile CB edge to electron trapping sites of anatase and subsequent transfer to lattice trapping sites favors effective charge separation.<sup>187</sup> This process is energetically favored since the

anatase lattice trapping site is 0.8 eV lower in energy than the anatase CB which is even lower than the rutile CB itself (Figure 22 B).<sup>213</sup> The photocatalytic oxidation of naphthalene using mixed-phase titania prepared by mixing rutile particles with small size anatase particles exhibited superior activity, while pure anatase was inactive for naphthalene oxidation. The electrons were transferred from rutile to anatase particles via thermal activation which was supported from electrochemical properties of the TiO<sub>2</sub> electrode for oxygen reduction. It was proposed that naphthalene was mainly oxidized on rutile particles, while oxygen was reduced on anatase particles.<sup>171</sup>

Action spectral studies revealed that the active crystalline phase in the bicrystal titania was found to differ with the kind of photocatalytic reactions, even if the mixed phase TiO<sub>2</sub> powders were used as photocatalysts.<sup>214</sup> For H<sub>2</sub> evolution, the action spectra of mixed powders (anatase + rutile) were intermediate between those of pure anatase and rutile and shifted to the rutile phase with a decrease in the anatase fraction in the mixed-phase powders. For a Ag deposition reaction, action spectra of mixed powders were similar to that of the rutile phase even when anatase was the major content in the TiO<sub>2</sub> samples. Conversely, for the decomposition of acetic acid, all the action spectra of the mixed powders were similar and blue-shifted from that of pure anatase. These results suggested that anatase and rutile were the active components for the decomposition of acetic acid and Ag deposition, respectively, even when these phases were in lower content. However, for the H<sub>2</sub> evolution, both the phases were found to be very active in the case of a Pt-loaded bicrystalline sample. It is interesting to note that pure anatase and pure rutile displayed almost similar spectral behavior irrespective of the probe reaction.<sup>214</sup>

Kawahara et al.<sup>215</sup> devised a model system to mimic the mixed particle system by patterning a photocatalyst film consisting of the anatase and rutile region with varying widths and depths. They evidenced the electron transfer from the anatase CB to the rutile CB edge in the patterned anatase/rutile bilayer type photocatalyst, and consequently much higher efficiency for CH<sub>3</sub>CHO photodecomposition (for the thickness of the anatase layer of about 70 ± 5 nm) was observed compared to pure anatase and pure rutile. In another study, buried anatase–rutile heterojunction thin films showed superior activity for the degradation of MO for the thickness of an anatase layer of about ~130 nm. The enhanced activity was explained by assuming a higher slope for the Schottky potential barrier formed at the external anatase layer.<sup>216</sup>

Rosseler et al.<sup>217</sup> reported that high rutile content in the mixed phase of anatase and rutile will be detrimental on photocatalytic activity, while Choi et al.<sup>114</sup> reported that an increase in the fraction of rutile in the bicrystal of anatase and rutile increased the photocatalytic activity for the degradation of MB using Pt<sup>2+</sup>–TiO<sub>2</sub> under visible light irradiation. A new insight was proposed taking into account the theories of previous models and also the localized electronic states of dopant in Mn<sup>2+</sup>–TiO<sub>2</sub> with the bicrystalline framework of anatase and rutile.<sup>88</sup> Although the bicrystalline framework in metal ion doped titanates showed superior activity,<sup>190–193</sup> the mechanism was not clear as previous reports did not focus on the localized electronic state of the dopant influencing the charge transfer. It is proposed that the electronic state of the dopant mediates the electron transfer under UV/solar light irradiation (Figure 23).<sup>88</sup> Mn<sup>2+</sup>–TiO<sub>2</sub> with an anatase to rutile ratio of 90:10 exhibited enhanced activity for the degradation of an oxo-fused polycyclic aromatic

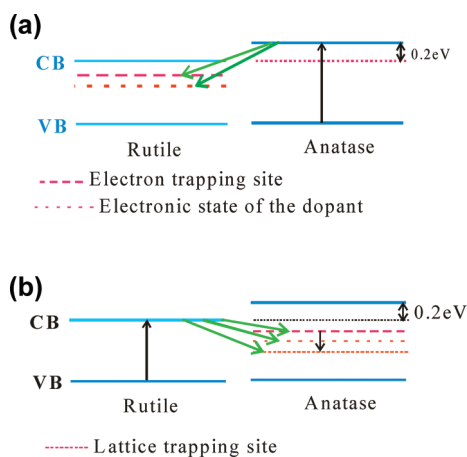


**Figure 23.** (a) Vectorial interparticle electron transfer in the  $\text{Mn}^{2+}$ – $\text{TiO}_2$  mixed phase under UV light. (b) Vectorial interparticle electron transfer in the  $\text{Mn}^{2+}$ – $\text{TiO}_2$  mixed phase under solar light. Reprinted with permission from Devi, L. G.; Kottam, N.; Kumar, S. G. *J. Phys. Chem. C* 2009, 113, 15593–15601.

dye compared to Degussa P25 with an anatase to rutile ratio of 80:20. Furthermore, the P25 possesses rutile crystallite slightly larger than anatase. However, in  $\text{Mn}^{2+}$ – $\text{TiO}_2$ , the crystallite sizes of anatase and rutile being almost same results in higher intimate contact between the two phases. In the mixed phase of anatase and rutile,  $\text{h}^+$  and  $\text{e}^-$  were preferentially trapped on  $\text{O}^-$  and  $\text{Ti}^{3+}$  centers of the rutile phase, even when anatase is the main component.<sup>218</sup> For such an interparticle electron transfer to be possible, the two crystalline polymorphs must be in close contact. The intimate contact between the two polymorphs critically depends on their crystallite size. Hong et al.<sup>219</sup> prepared iodine-doped titania with mixed phases of anatase and rutile by calcining the sample at 500 °C, which showed lower activity for phenol degradation compared to iodine-doped anatase titania. The observed lower activity may be due to the large rutile crystal size which resulted in poor intimate contact between these two phases which fails to demonstrate its structure advantage. Hence in the case of bicrystalline titania, it is important to obtain smaller rutile crystallite size since the charge carrier generated will have high redox potential compared to those generated in the bulk rutile.

I– $\text{TiO}_2$ , core shell structured titania, and N– $\text{TiO}_2$  with bicrystal of anatase–rutile showed enhanced activity for the degradation of organic pollutants due to the presence of abundant surface states as evidenced by PL spectral studies.<sup>193,194,220,221</sup> Most of the samples prepared by Liu et al. contained a higher concentration of surface-adsorbed water molecules and hydroxyl groups on the catalyst surface yet resulted in lower activity. This indicates that these surface hydroxyl groups cannot always trap holes to generate hydroxyl radicals. In any photocatalytic reactions, surface adsorbed water and hydroxyl groups can only be potential sites to trap the holes on the surface, but the final hole transfer requires favorable surface structure. The surface structure with dense surface states detraps the adsorbed hole, favoring efficient charge separation.<sup>193,194,220,221</sup>

The existence of an optimum rutile fraction to enhance the activity of a mixed phase was recently explained using a new model based on band gap configuration in the connected nanocrystallite as a function of size distribution and phases involved.<sup>183</sup> It is assumed that the anatase  $\text{TiO}_2$  is made up of

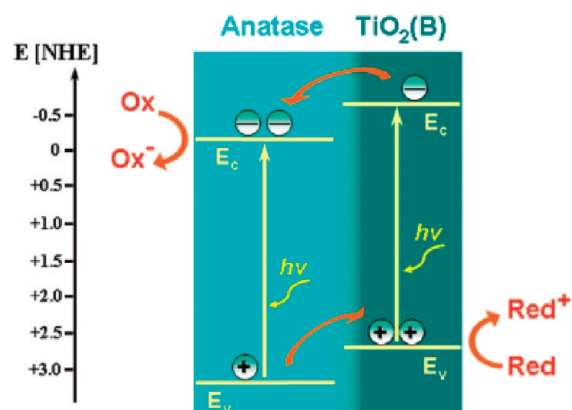


**Figure 24.** Illustration of energy band and diffusion of photogenerated charge carriers for the anatase  $\text{TiO}_2$  and monoclinic  $\text{TiO}_2$  (B). Reprinted with permission from Li, W.; Liu, C.; Zhou, Y.; Bai, Y.; Feng, X.; Yang, Z.; Lu, L.; Lu, X.; Chan, K. Y. *J. Phys. Chem. C* 2008, 112, 20539–20545.

broad size distribution, and the band gap of anatase  $\text{TiO}_2$  increases below the critical size. The mixed phase of anatase and rutile synthesized via solvent mixing and calcination contained a mixture of band gap configurations depending on their crystallite size. If the nanocrystallite size distribution is below the critical size, then the band gap of connected nanocrystallite would be different depending on their size. As a result, a hole photogenerated in one nanocrystallite migrates to the neighbor, leading to the charge separation. On the other hand, if the nanocrystallite size distribution lies above the critical size, then size distribution would not exhibit any variation in the band gap as a function of crystallite size. Since anatase-to-rutile transformation is accompanied by the growth of rutile crystallite size, the mixed phase possesses a mixture of band gap configurations. In such a situation, nanocrystallite located at the center performs a dual function by serving as an electron sink and hole source in these band gap configurations. Thus, a change in the band gap configuration due to the presence of rutile crystallite with anatase enhanced the charge separation with respect to pure anatase. This model suggests that photocatalytic activity of the mixed phase increases with an increase in the rutile fraction up to the optimum content in the mixed-phase sample. With a large fraction of rutile in the mixed-phase powder, a larger number of rutile–rutile nanocrystallites having an identical band gap will be established, resulting in the recombination.<sup>183</sup>

The core–shell anatase  $\text{TiO}_2$ /monoclinic  $\text{TiO}_2$  (B) nanofibers showed enhanced activity for the oxidation of iodide compared to either  $\text{TiO}_2$  anatase or  $\text{TiO}_2$  (B) phase nanofibers.<sup>222</sup> Although the anatase  $\text{TiO}_2$  and  $\text{TiO}_2$  (B) have the same band gap of 3.2 eV, the theoretical calculations showed that the CB and VB energies in anatase are slightly lower than the corresponding CB and VB level of  $\text{TiO}_2$  (B). Accordingly, holes migrate from anatase  $\text{TiO}_2$  to  $\text{TiO}_2$  (B) and electrons from  $\text{TiO}_2$  (B) to  $\text{TiO}_2$  anatase (Figure 24).<sup>222</sup> This mechanism was later supported by Zheng et al. based on EPR results.<sup>223</sup> Such an interfacial charge transfer process results in increased population of holes in  $\text{TiO}_2$  (B) and thus increase the hole density that reaches the surface and initiates redox reactions. It is interesting to note that the bicrystal of anatase and rutile facilitates only the transfer of electron without the promotion of hole movement and distribution since VB energy is the same in both anatase and rutile. This difference in the band energy structure may explain the better

photocatalytic activity of core–shell  $\text{TiO}_2$  anatase/ $\text{TiO}_2$  (B) compared to P2S.<sup>222,223</sup> The orientation relationship between anatase and  $\text{TiO}_2$  (B) is such that the [010] vector in anatase is parallel to [010] in  $\text{TiO}_2$  (B) and the [001] vector in anatase is parallel to the [100] vector in  $\text{TiO}_2$  (B) (Figure 25).<sup>222</sup> Furthermore, the (202) diffraction crystal planes in both anatase and  $\text{TiO}_2$  (B) have similar *d*-spacings of  $\sim 0.18$  nm which join together to form a stable interface. Thus, the interface between  $\text{TiO}_2$  anatase and  $\text{TiO}_2$  (B) was not an aggregate of randomly oriented crystals of two polymorphs; rather, both the phases join at the atomic level with the minimum mismatching lattice planes (Figure 26).<sup>223</sup> This well-matched structure minimizes the large crystallographic discrepancies, number of dangling bonds, and voids in the interface regions. The smallest effective mass of holes ( $0.8 m_e = m_h^*$ ) is consistent with its high mobility and reaches very quickly the VB of  $\text{TiO}_2$  (B), while in the mixed phase of anatase and rutile, the time required for the electrons ( $m_e^* > 10 m_e$ ,  $m_e$  is the free electron mass) to reach the same distance will be considerably longer than those for holes.<sup>223</sup>

## 8.0. METAL-DEPOSITED TITANIA

Apart from introducing various bulk irregularities via doping to provide shallow trap states for CB electrons, another effective method for increasing the lifetime of electron–hole pairs and to extend the band gap absorption of titania to the visible region is to deposit the noble metal on the surface of titania.<sup>224</sup> Earlier investigations revealed that semiconductor–metal composites enhance the efficiency of the photocatalytic process, wherein metal deposits serve as a passive sink for electrons, hindering the

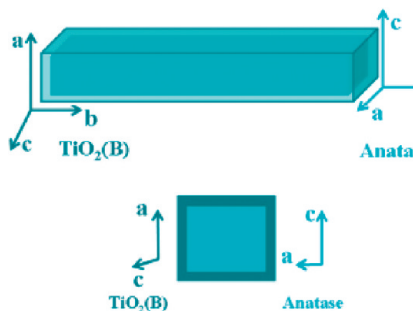


**Figure 25.** Schematic illustration of crystallographic orientation for the anatase  $\text{TiO}_2$  and monoclinic  $\text{TiO}_2$  (B) phase. Reprinted with permission from Li, W.; Liu, C.; Zhou, Y.; Bai, Y.; Feng, X.; Yang, Z.; Lu, L.; Lu, X.; Chan, K. Y. *J. Phys. Chem. C* 2008, 112, 20539–20545.

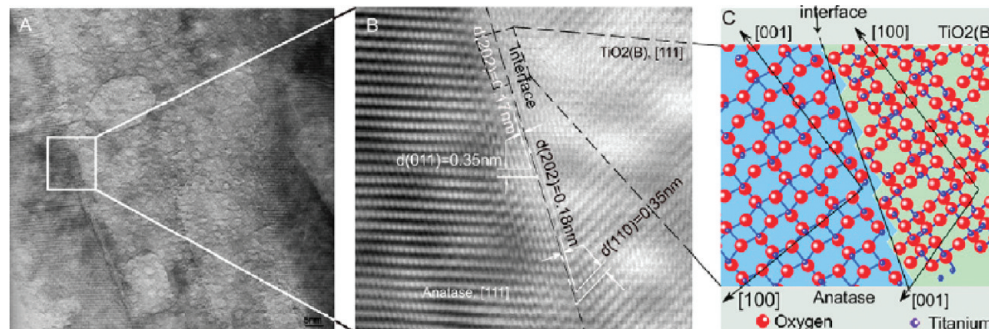


**Figure 26.** HRTEM image and the atomic arrangement of an interface between monoclinic  $\text{TiO}_2$  (B) and anatase  $\text{TiO}_2$  phases. Reprinted with permission from Zheng, Z.; Liu, H.; Ye, J.; Zhao, J.; Waclawik, E. R.; Zhu, H. *J. Mol. Catal. A: Chem.* 2010, 316, 75–82. Copyright Elsevier, 2010.

recombination. When the semiconductor and metal nanoparticles are in contact, the photogenerated electrons are distributed between  $\text{TiO}_2$  and metal nanoparticles. The transfer of electrons from semiconductor to metal composites continues until the semiconductor–metal composite system attains equilibration. The electron accumulation on the metal deposits shifts the Fermi level of metal to more negative potentials, and the resultant Fermi level of the composite shifts closer to the CB of the semiconductor (Figure 27). The negative shift in the Fermi level is an indication of better charge separation and more reductive power of the composite system.<sup>225</sup> The photocatalytic performance of the metal–semiconductor heterojunction is strongly influenced by the size and shape of metal nanoclusters.

Photoluminescence spectral studies revealed that the Pt deposition on the anatase surface favored hydrogen generation from the  $\text{H}_2\text{O}-\text{CH}_3\text{OH}$  mixture, while Pt deposition on the rutile surface was detrimental on the photocatalytic activity.<sup>226</sup> Anatase  $\text{TiO}_2$  displayed a visible luminescence band centered at about 505 nm, while rutile  $\text{TiO}_2$  mainly shows a near-infrared luminescence band centered at about 835 nm, ascribed to the oxygen vacancies in anatase and intrinsic defect in rutile, respectively. When Pt is deposited, the intensity of the visible luminescence band of anatase decreases due to the transfer of excited electrons from the trapped oxygen vacancies to the Pt deposits. A negligible change in the intensity of the near-infrared luminescence band indicated that the charge carrier recombination dynamics at the intrinsic defects of rutile was not influenced by Pt deposition.<sup>226</sup> Pt–rutile showed superior activity for CO conversion; while only 75% CO conversion was achieved with Pt–P2S; and Pt–anatase showed no activity at all under visible light irradiation. In this case, Pt–rutile was considered as a multifunctional catalyst, wherein rutile was activated by visible light and Pt deposits enhanced the CO adsorption and charge

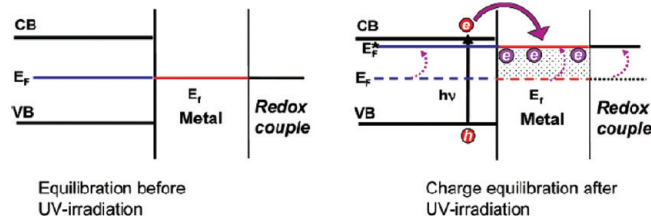


**Figure 27.** Equilibration of the semiconductor–metal nanocomposite with the redox couple before and after UV irradiation. Reprinted with permission from Subramanian, V.; Wolf, E. E.; Kamat, P. V. *J. Am. Chem. Soc.* 2004, 126, 4943–4950.

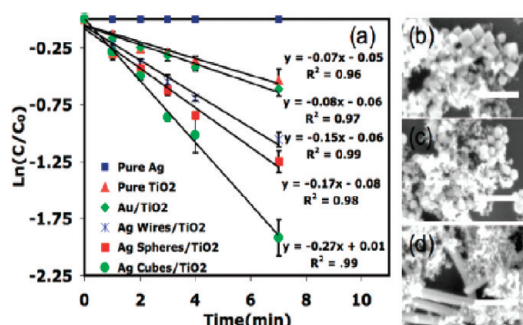


**Figure 28.** (a) Kinetic data for the decomposition of MB over pure TiO<sub>2</sub>, pure Ag nanocubes, 15 wt % composite Ag–TiO<sub>2</sub> systems containing Ag spheres, cubes, and wires, and the Au–TiO<sub>2</sub> composite system. SEM micrographs of the Ag nanocube–TiO<sub>2</sub> composite, Ag nanosphere–TiO<sub>2</sub> composite, and Ag nanowire–TiO<sub>2</sub> composite (b–d). Reprinted with permission from Christopher, P.; Ingram, D. V.; Linic, S. *J. Phys. Chem. C* 2010, 114, 9173–9177.

transfer process.<sup>227</sup> Hidalgo et al.<sup>228</sup> have also reported that Pt–rutile showed higher activity compared to Pt–anatase for phenol oxidation. Sclafani and Herrmann reported that Pt–rutile had beneficial effects for the photocatalytic oxidation of 2-propanol to acetone, while Pt deposits were found to be detrimental on anatase titania.<sup>229</sup> Pt–rutile was found to be a better photocatalyst compared to Pt–anatase for the degradation of trichloroacetate under nitrogen-saturated dispersion, while Pt–anatase was active in oxygen-saturated solutions.<sup>230a</sup> The probable speculation from all these results that can be made is that the drawback of lower electron mobility and inefficient electron transfer to the adsorbed oxygen in rutile titania due to insufficient concentration of active oxygen was overcome by the Pt deposition. However, such enhancement in anatase phase after Pt deposition can only be marginal. Pt-deposited (1 wt %) pure anatase enhanced the decomposition of phenol and TOC removal by a factor of 1.5 compared to unmodified titania, while Pt-deposited P25 (anatase + rutile) showed lower activity compared to unmodified P25, which suggested that platinization did not further increase the efficiency of charge separation in P25.<sup>230b</sup>

Christopler and co-workers<sup>231</sup> reported that by changing the size and shape of the Ag nanocluster it is possible to maximize photochemical activity of a semiconductor at a given excitation wavelength. There are a number of physical mechanisms previously observed that could potentially explain the enhanced activity of the Ag–TiO<sub>2</sub> composite compared to pure titania: (i) effective electron transfer from TiO<sub>2</sub> to Ag nanoparticles; (ii) electron transfer from Ag to TiO<sub>2</sub> mediated by Ag surface plasmons; (iii) the localized heating of Ag nanostructures due to nonirradiation decay of Ag surface plasmons into phonon modes in the Ag particles; and (iv) transfer of photons from Ag nanoparticles to TiO<sub>2</sub> via radiative decay of surface plasmon states to excite electrons in TiO<sub>2</sub> and increase the concentration of electron–hole pairs. However, the authors ruled out mechanisms (i)–(iii) and suggested that pathway (iv) is responsible for enhanced activity for the Ag nanocube ( $79 \pm 12$  nm diameter)–TiO<sub>2</sub> compared to Ag nanospheres ( $75 \pm 13$  nm diameter)–TiO<sub>2</sub> and Ag nanowire ( $70 \pm 12$  nm diameter)–TiO<sub>2</sub> systems for the degradation of MB (Figure 28).<sup>231</sup> The presence of Ag deposits on the TiO<sub>2</sub> surface enhanced the photo-oxidation of oxalic acid by a factor of 5 times. The accumulation of electrons in

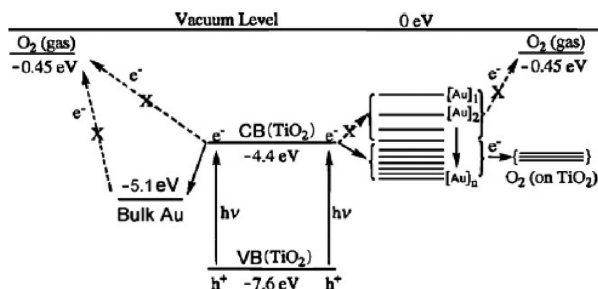


**Figure 29.** Electronic energy levels of gold particles, VB and CB of TiO<sub>2</sub>, and adsorbed O<sub>2</sub>. Reprinted with permission from Tian, B.; Zhang, J.; Tong, T.; Chen, F. *Appl. Catal. B: Environ.* 2008, 79, 394–401. Copyright Elsevier, 2008.

the nanosized silver particle increases the probability function of excited oxygen atoms via electron transfer from O<sub>2</sub><sup>–ads</sup> produced from O<sub>2</sub><sup>2–</sup> to the hole.<sup>232</sup>

Orlov et al.<sup>233</sup> reported the degradation of methyl *tert*-butyl ether using gold nanoparticles on TiO<sub>2</sub> and found that optimum loading corresponds to a Au particle size  $\leq 3$  nm, at which Au can behave as a semiconducting material, rather than as metallic. One can invoke a semiconductor–semiconductor heterojunction in which photoexcited electrons are injected from a Au deposit to the TiO<sub>2</sub> CB, indicating a distinct charge transfer mechanism. It is generally accepted that deposition of noble metal nanoparticles on the TiO<sub>2</sub> surface results in a substantial decrease in work function, and O<sub>2</sub> adsorbs between the Au and TiO<sub>2</sub> interface. Thus, lowering the local work function of titania in the vicinity of such an interfacial oxygen adsorption site obviously enhances the dioxygen reduction to yield superoxide radicals. However, in the absence of O<sub>2</sub>, the activity of Au–TiO<sub>2</sub> was almost similar to that of unmodified titania.<sup>233</sup> The size of gold deposited on the titania surface plays a major role in the interfacial electron transfer to adsorbed oxygen. When the size of gold particles is too large, the Fermi energy level of gold particles will be lower than that of adsorbed O<sub>2</sub>, and thus the photoelectrons cannot be transferred to the adsorbed O<sub>2</sub>. However, for very small gold particles, photoelectrons cannot be transferred from the bottom of the TiO<sub>2</sub> CB to the gold particles because the Fermi level of gold particles will be considerably higher due to quantum size effect (Figure 29). Therefore, the Au particle with an appropriate size possessing an energy level between the TiO<sub>2</sub> CB and adsorbed O<sub>2</sub> is most essential.<sup>234</sup> Wu et al.<sup>235</sup> reported the degradation of 2,4-dichlorophenol (DCP) via two distinct mechanisms operating under UV and visible light for Au-deposited Fe<sup>3+</sup>–TiO<sub>2</sub>; under visible light, the Fe<sup>3+</sup> dopant in the TiO<sub>2</sub> lattice enables the catalyst to absorb visible light, and the deposited Au serves as an electron trap, resulting in high activity. However, under UV light illumination, electrons and holes were effectively trapped on Au particles and Fe<sup>3+</sup> ions, respectively, which on subsequent transfer to the surface initiates the efficient photocatalytic process. A similar kind of mechanism was operative in Au-deposited N–TiO<sub>2</sub> which resulted in the enhanced degradation of MO under visible light. Furthermore, oxygen vacancies induced by N-doping were lowered after Au deposition on the surface of N–TiO<sub>2</sub> which hindered surface recombination and increased the dioxygen reduction.<sup>236</sup>

Simultaneous sulfation and platinization of TiO<sub>2</sub> had shown remarkable improvement in the photocatalytic activity for phenol degradation due to the synergistic effect between sulfation and platinization.<sup>237</sup> The enhancement in photocatalytic activity

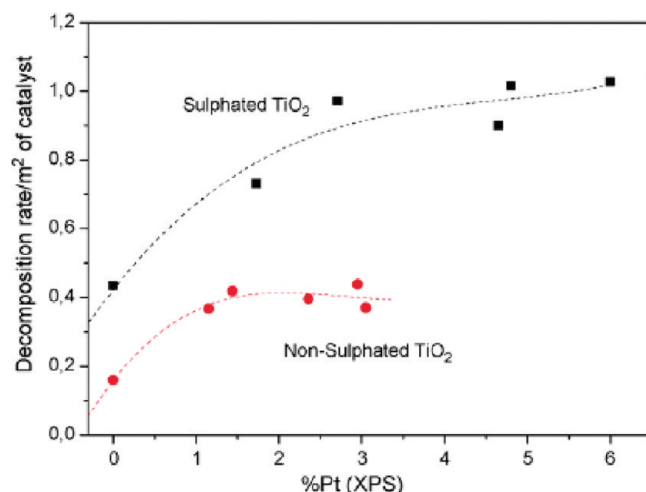


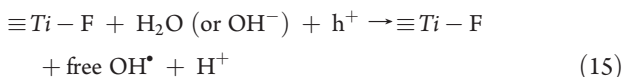
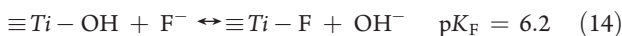
**Figure 30.** Initial reaction rate of phenol photo-oxidation for the catalysts with different surface platinum content measured by XPS. Reprinted with permission from Hidalgo, M. C.; Maicu, M.; Navio, J. A.; Colon, G. *Appl. Catal. B: Environ.* 2008, 81, 49–55. Copyright Elsevier, 2008.

of sulfated titania increased drastically with an increase in Pt content compared to nonsulfated titania (Figure 30). The relatively high dispersion of Pt particles on sulfated titania can be related with the features of the oxide surface and the interaction between the Pt precursor and the titania surface. Hidalgo et al.<sup>237</sup> suggested that sulfation could change the adsorption properties of TiO<sub>2</sub> for hexachloroplatinic acid, leading to a smaller degree of agglomeration between the titania particles and thus increasing the surface area available for adsorption and deposition of metal ions.

## 9.0. STRATEGIES TO IMPROVE THE INTERFACIAL CHARGE TRANSFER PROCESS

The photocatalytic efficiency of TiO<sub>2</sub> depends on the lifetime of charge carriers generated on its surface. Surface recombination of electron–hole in the absence of an electron donor or acceptor is extremely high and thus represents the major energy-wasting step, thereby inhibiting the achievable quantum yield. The surface recombination of charge carriers can be inhibited by modifying the TiO<sub>2</sub> surface with anions like fluoride, sulfate, and polyoxometallates (POM). The surface modification may have a marked influence on the photocatalytic process by altering the charge transfer pathways occurring at the water–TiO<sub>2</sub> interface.

The surface acidity of TiO<sub>2</sub> can be enhanced by surface fluorination which can be achieved by a simple ligand exchange reaction of surface titanols with fluoride anions<sup>238</sup>



The extent of surface fluorination on TiO<sub>2</sub> (F–TiO<sub>2</sub>) critically depends on pH and shows maximal adsorptive tendency at pH 3–4.<sup>239,240</sup> Minero et al.<sup>239</sup> for the first time reported the enhanced activity of F–TiO<sub>2</sub> for phenol oxidation compared to

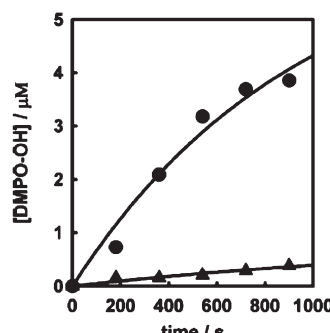


**Figure 31.** DMPO–OH concentration as a function of time during the irradiation at 330 nm of suspensions containing naked (triangles) and fluorinated (circles) TiO<sub>2</sub>. Reprinted with permission from Mrowetz, M.; Selli, E. *Phys. Chem. Chem. Phys.* 2005, 7, 1100–1102. Copyright Royal Society of Chemistry, 2005.

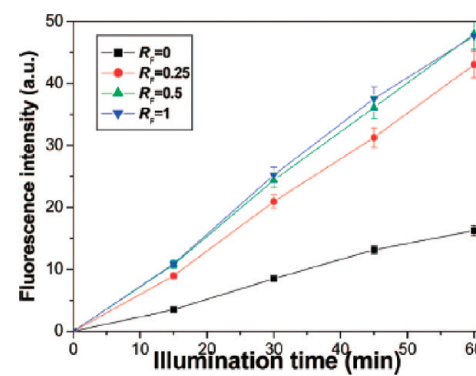


**Figure 32.** Plots of the induced PL intensity at 426 nm against illumination time for terephthalic acid on the naked and fluorinated TiO<sub>2</sub> samples prepared at R<sub>F</sub> = 0, 0.25, 0.5, and 1. R<sub>F</sub> refers to different atomic ratios of F to Ti. Reprinted with permission from Yu, J.; Wang, W.; Cheng, B.; Su, B. L. *J. Phys. Chem. C* 2009, 113, 6743–6750.

unmodified titania. They ascribed this positive effect to the replacement of surface hydroxyl groups by the isovalent fluoride ion, which forces the VB hole to oxidize solvent water molecules to generate free hydroxyl radicals. Furthermore, fluoride is highly stable toward oxidation by the VB hole owing to the high oxidation potential of the redox couple F<sup>•</sup>/F<sup>−</sup> = 3.6 V.<sup>239</sup> A kinetic analysis and competition experiments with different hydroxyl radical scavengers revealed that the degradation of phenol proceeds completely by free hydroxyl radicals on F–TiO<sub>2</sub>, while for bare titania, about 10% is due to direct hole oxidation and 90% to the adsorbed hydroxyl radicals.<sup>240</sup> The generation of surplus free hydroxyl radical on F–TiO<sub>2</sub> was later confirmed by Mrowetz and Selli<sup>241</sup> using a DMPO–spin trap ESR technique (Figure 31) and Yu et al.<sup>242</sup> using a photoluminescence technique through the hydroxylation of terephthalic acid as a probe reaction (Figure 32). Surface fluorination resulted in the efficient charge separation as it prevents the formation of deep traps which is otherwise possible on bare TiO<sub>2</sub>. Thus, the lower concentration of trapped holes reduces the probability of their ultrafast recombination with CB electrons. However, Macyk and co-workers<sup>243</sup> have recently claimed that the surface modification of TiO<sub>2</sub> with fluoride or silyl groups leads to the enhanced production of singlet oxygen instead of hydroxyl groups. Cyanuric acid was degraded by F–TiO<sub>2</sub> with singlet oxygen as the potential oxidant which is otherwise inert for the

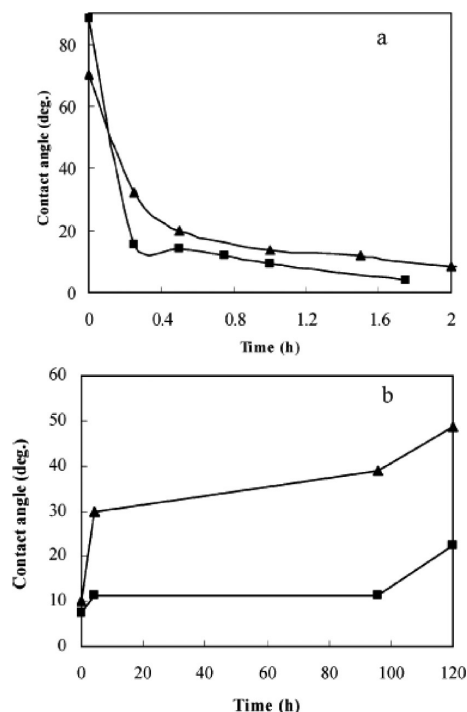


**Figure 33.** (a) Change of water contact angle under weak UV light irradiation on TiO<sub>2</sub> (▲) and F-TiO<sub>2</sub> (■) and (b) change of water contact angle versus time after turning off the black lamp on TiO<sub>2</sub> (▲) and F-TiO<sub>2</sub> (■). Reprinted with permission from Tang, J.; Quan, H.; Ye, J. *J. Chem. Mater.* 2007, 19, 116–122.

degradation with bare TiO<sub>2</sub>.<sup>243</sup> The photoinduced hydrophilicity (PH) was found to increase when rutile TiO<sub>2</sub> was fluorinated with anhydrous HF by vapor-phase fluorination.<sup>244</sup> F-TiO<sub>2</sub> being hydrophobic will always have a higher contact angle (CA) compared to naked TiO<sub>2</sub> without illumination. The highly electronegative fluorine deviates the electron density from the original position in titanium–oxygen polyhedral resulting in the weakening of bonds between Ti and O in F-TiO<sub>2</sub>. This results in surplus availability of oxygen vacancies under UV illumination in F-TiO<sub>2</sub>, which can significantly enhance the PH. Hence, CA decreases at a much faster rate for F-TiO<sub>2</sub> compared to TiO<sub>2</sub> under UV illumination. Since the F-TiO<sub>2</sub> renders the adsorption of polar molecules, the hydroxyl groups produced by fluorination can stabilize the dissociated water adsorption through the formation of a hydrogen bond, hindering the desorption of adsorbed water molecules on F-TiO<sub>2</sub>, and hence shows a slow increase in CA when UV light is turned off (Figure 33).<sup>244</sup> A new insight into the mechanism of surplus generation of free hydroxyl radicals on the F-TiO<sub>2</sub> for the enhanced degradation of phenol was proposed by Xu and co-workers.<sup>245</sup> They suggested that the fluoride ions present in the Helmholtz layer promote the desorption of surface-bound hydroxyl radicals in the solution from irradiated TiO<sub>2</sub>, through a fluorine hydrogen bond which is thermodynamically favorable (Figure 34). With an increase in the number of fluoride ions in the Helmholtz layer, desorption of surface hydroxyl radicals is favored. As the solution pH is increased, the amount of fluoride in the Helmholtz layer is decreased, resulting in the lower activity as observed by many researchers.<sup>245</sup> The mode of dye adsorption also altered the degradation pathway on F-TiO<sub>2</sub> compared to bare titania. The RhB dye anchors on the TiO<sub>2</sub> through the carboxylate group,

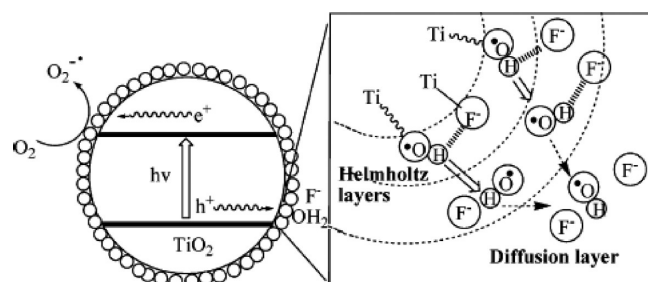


**Figure 34.** Possible mechanism for the fluoride-induced enhancement in the production of free hydroxyl radicals in bulk solution from irradiated TiO<sub>2</sub>. Reprinted with permission from Xu, Y.; Lv, K.; Xiong, Z.; Leng, W.; Du, W.; Liu, D.; Xue, X. *J. Phys. Chem. C* 2007, 111, 19024–19032.

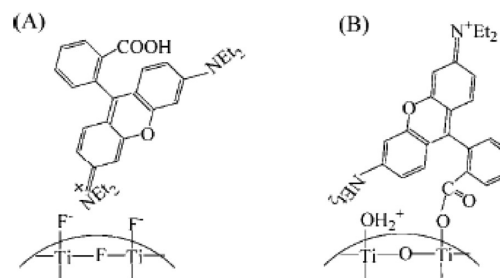
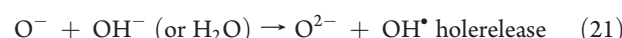
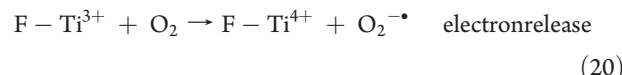
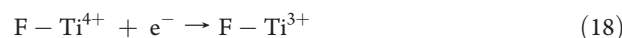
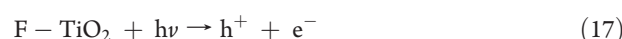


**Figure 35.** Proposed adsorption modes of RhB in aqueous F-TiO<sub>2</sub> (A) and pure TiO<sub>2</sub> (B) dispersions. Reprinted with permission from Wang, Q.; Chen, C.; Zhao, D.; Ma, W.; Zhao, J. *Langmuir* 2008, 24, 7338–7345.

while the cationic moiety (–N<sub>Et</sub><sub>2</sub> group) adsorbs on the F-TiO<sub>2</sub> under acidic conditions (Figure 35). Hence, direct cleavage of the chromophore structure and rapid N-dealkylation were observed for TiO<sub>2</sub> and F-TiO<sub>2</sub>, respectively, under visible light irradiation.<sup>246</sup> F-TiO<sub>2</sub> prepared by a hydrothermal route in a NH<sub>4</sub>HF<sub>2</sub>–H<sub>2</sub>O–C<sub>2</sub>H<sub>5</sub>OH mixed solution with tetrabutyl orthotitanate as a precursor showed enhanced activity for the decomposition of gaseous acetone.<sup>242</sup> According to the proposed mechanism, the surface  $\equiv$ Ti–F group served as an effective trapping site by tightly holding the trapped electrons due to strong electronegativity of the fluorine and then transferring to adsorbed O<sub>2</sub> on the TiO<sub>2</sub> surface. The detailed charge transfer mechanism is as follows



Mrowetz and Selli<sup>247a</sup> have observed that a decrease in the production of H<sub>2</sub>O<sub>2</sub> over irradiated TiO<sub>2</sub> upon surface fluorination is attributed to the decreased rate of interfacial electron transfer to O<sub>2</sub> during the degradation of Acid Red 1 and benzoic acid. These results suggest that surface fluorination tightly holds

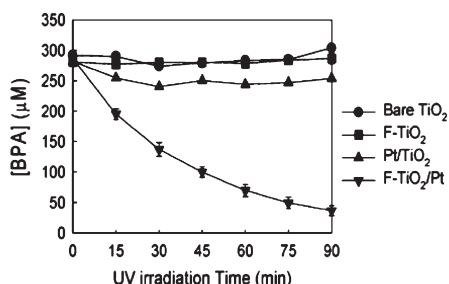


**Figure 36.** Anoxic degradation of BPA in aqueous suspensions of bare  $\text{TiO}_2$ ,  $\text{F}-\text{TiO}_2$ ,  $\text{Pt}/\text{TiO}_2$ , and  $\text{F}-\text{TiO}_2/\text{Pt}$ . Reprinted with permission from Kim, J.; Lee, J.; Choi, W. *Chem. Commun.* 2008, 756–758. Copyright Royal Society of Chemistry, 2008.

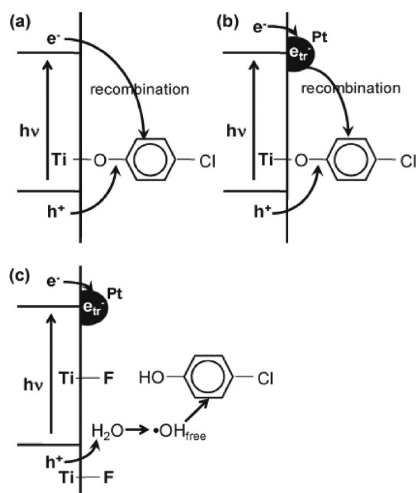


**Figure 37.** Photoinduced charge transfer/recombination processes occurring on (a) bare  $\text{TiO}_2$ , (b)  $\text{Pt}/\text{TiO}_2$ , and (c)  $\text{F}-\text{TiO}_2/\text{Pt}$  in the presence of 4-CP and in the absence of  $\text{O}_2$ . Reprinted with permission from Kim, J.; Lee, J.; Choi, W. *Chem. Commun.* 2008, 756–758. Copyright Royal Society of Chemistry, 2008.

the trapped CB electrons besides enhancing the generation of free hydroxyl radicals. On the other hand, the specific adsorption of fluoride ions on the  $\text{TiO}_2$  surface may act as a Lewis base, which is speculated to reduce the density of surface states (deep traps) and even possibly give rise to new surface states that can enhance the mobility and transfer the charge carriers from the catalyst surface to the bulk of the solution.<sup>247b</sup> Simultaneous surface fluorination and platinization of  $\text{TiO}_2$  increased the degradation rate of 4-CP, bisphenol A (BPA), and 2,4-dichlorophenoxy acetic acid even under anoxic conditions (Figure 36).<sup>248</sup> The enhanced activity of  $\text{F}-\text{TiO}_2/\text{Pt}$  compared to  $\text{Pt}/\text{TiO}_2$  and  $\text{F}-\text{TiO}_2$  indicates that the charge carrier recombination can be efficiently suppressed even in the absence of  $\text{O}_2$ , a dominant electron acceptor. The surface complexed 4-CP serves as an external hole trap, which recombines with an electron in the absence of  $\text{O}_2$  to make a null reaction in  $\text{TiO}_2$  dispersions. Pt serves as an electron sink in  $\text{Pt}/\text{TiO}_2$ , although trapped electrons slowly recombine with hole. In the case of  $\text{F}-\text{TiO}_2/\text{Pt}$ , a surface complex mediated degradation pathway is hindered due to the surface preoccupation by fluoride ions (Figure 37). Under this condition, free hydroxyl radicals generated on a fluorinated surface mediate the degradation of organic contaminants, while the electrons will be trapped by platinum favoring effective charge

separation. The accumulated electrons can subsequently react with water or protons in the solution.<sup>248</sup>

Sulfated  $\text{TiO}_2$  is also reported to enhance photocatalytic activity compared to the nonsulfated sample for phenol oxidation. The creation of bulk oxygen vacancies through a dehydroxylation process of the excess adsorbed protons during calcination generates a highly defective material that improves the separation of charge carriers and their diffusion to the surface in the photocatalytic process.<sup>249</sup> Pretreatment of  $\text{TiO}_2$  with sulfuric acid has been reported to stabilize the  $\text{TiO}_2$  surface area against sintering and anatase crystalline phase up to 700 °C probably due to the presence of sulfate groups anchored on the  $\text{TiO}_2$  surface before calcination.  $\text{H}_2\text{SO}_4$ -treated amorphous  $\text{TiO}_2$  exhibited higher durability against deactivation than pure  $\text{TiO}_2$  for repeated decomposition of gaseous toluene even at higher concentrations.<sup>250</sup> The higher quantum yield for this modified  $\text{TiO}_2$  was attributed to the faster decomposition of intermediates by a strong acid surface itself and also to suppressing recombination of photogenerated charge carriers. The strong acid property is related to sulfate ions, which can induce polarization of the neighboring hydroxyl group. This highly polarized state of surface acidity would serve as reactive electron trapping sites, resulting in improved quantum yield with production of oxidative hydroxyl radicals.

Many researchers have used POM as a cocatalyst to gain further insights into the underlying reaction mechanism and to estimate the feasibility of using POM– $\text{TiO}_2$  in the degradation of organic compounds. A typical homogeneous POM– $\text{PW}_{12}\text{O}_{40}^{3-}$  photocatalyst has a band gap energy of 3.5 eV, and it is very similar to the heterogeneous photocatalyst  $\text{TiO}_2$  in its light absorption properties and has an almost similar electrochemical band edge position.<sup>251</sup> Since the standard one-electron reduction potential of  $\text{O}_2$ ,  $\text{PW}_{12}\text{O}_{40}^{3-}$ , and  $\text{PW}_{12}\text{O}_{40}^{4-}$  is  $-0.33$ ,  $+0.22$ , and  $-0.025$  V (vs NHE), respectively, the POM is thermodynamically a better electron acceptor than  $\text{O}_2$ .<sup>252</sup> Zhao et al.<sup>253a</sup> reported that the hydroxylation of 2,4-dichlorophenol (DCP) was accelerated in  $\text{TiO}_2$ –POM suspension, and hence mineralization of DCP was suppressed in the presence of POM. The maximum yields of intermediates like 2,4-dichlorophenol-1,5-diol, 2,4-dichlorocatechol, 4-chlorocatechol, and chloroquinone were much higher on  $\text{TiO}_2$ –POM compared to  $\text{TiO}_2$  dispersion. Although the degradation kinetics of 2,4-DCP was faster in  $\text{TiO}_2$ –POM suspension, the mineralization was rather slower compared to pure  $\text{TiO}_2$  suspension.<sup>253a</sup> The addition of POM in  $\text{TiO}_2$  suspension altered the degradation pathway of X3B dye; the degradation proceeds via subsurface holes with naked  $\text{TiO}_2$ , while surface-bound hydroxyl radicals were found to be oxidative species responsible for degradation in  $\text{TiO}_2$ –POM suspension. The higher concentration of POM in  $\text{TiO}_2$  dispersions seems to be detrimental to photocatalytic activity. Since POM is the light-absorbing species, it might function as a screening filter, shunting the UV photons away from the catalyst surface. Furthermore, the strong competitive adsorption of POM compared to X3B due to its higher ionic charge covers all the reactive photoactive sites, leaving only nonactive sites for X3B dye adsorption. The number of such inactive sites is expected to increase with [POM] resulting in slower degradation of X3B dye.<sup>253b</sup>

## 10.0. EFFECTS OF OXIDANTS ON DEGRADATION RATE

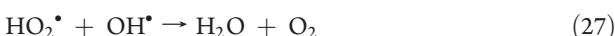
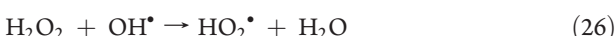
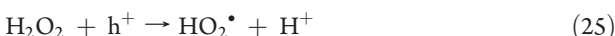
The addition of suitable electron acceptors or oxidizing agents in the titania suspension inhibits the charge carrier recombination.

These oxidizing agents can have several beneficial effects such as (i) to increase the number of trapped electrons which hinders its recombination with holes; (ii) to generate more free radicals and other oxidizing species; (iii) to increase the oxidation rate of intermediate compounds; and (iv) to avoid problems caused by low oxygen concentration as the solution phase may at times be oxygen starved because of either oxygen consumption or slow oxygen mass transfer.<sup>254–264</sup>

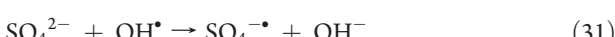
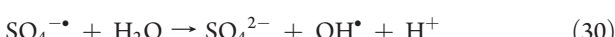
Oxygen atoms in H<sub>2</sub>O<sub>2</sub> are more electropositive than free O<sub>2</sub>, implying that H<sub>2</sub>O<sub>2</sub> is a stronger electron acceptor than O<sub>2</sub>. The reactions taking place when H<sub>2</sub>O<sub>2</sub> is present in the TiO<sub>2</sub> suspension are as follows<sup>22,265,266</sup>



However, at a very high concentration of H<sub>2</sub>O<sub>2</sub>, they can also act as a scavenger for VB holes or hydroxyl radicals, thereby reducing the degradation efficiency.



Furthermore, H<sub>2</sub>O<sub>2</sub> can be adsorbed onto TiO<sub>2</sub> particles to modify their surfaces and subsequently decrease their catalytic activity. Though voluminous literature is available for the application of H<sub>2</sub>O<sub>2</sub> as an effective oxidant, the least approach is made toward the application of peroxydisulfate, bromates, and iodates in the wastewater treatment. From the thermodynamic point of view, the persulfate anion should serve as a better electron acceptor than the molecular oxygen.<sup>254–264</sup> The reaction of ammonium persulfate (APS) with TiO<sub>2</sub> is as follows



In addition to their oxidizing strength, persulfate and sulfate radicals have several advantages over other oxidant systems. First, they are kinetically fast, and second, sulfate radicals are more stable than the hydroxyl radicals and thus are able to transport greater distances in the subsurface. In addition, they provide a better acidity to the catalyst surface which enhances the adsorption of pollutants thereby accelerating the degradation rate. The sulfate radical anion produced participates in the degradation reaction of the pollutants in the following ways: (i) by abstracting a hydrogen atom from the saturated carbon, (ii) by adding to an unsaturated or aromatic carbon, and (iii) by removing an electron from the carboxylate anions and also from certain neutral molecules.<sup>267–273</sup> These attributes makes peroxy disulfate

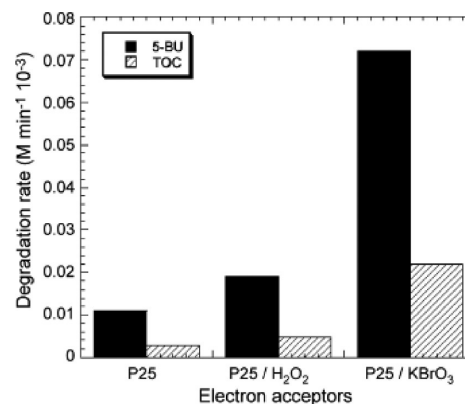


**Figure 38.** Degradation and mineralization of 5-bromouracil (5-BU) in the presence of electron acceptors. Reprinted with permission from Singh, H. K.; Saquib, M.; Haque, M. M.; Munneer, M. *J. Hazard. Mater.* 2007, 142, 425–430. Copyright Elsevier, 2007.

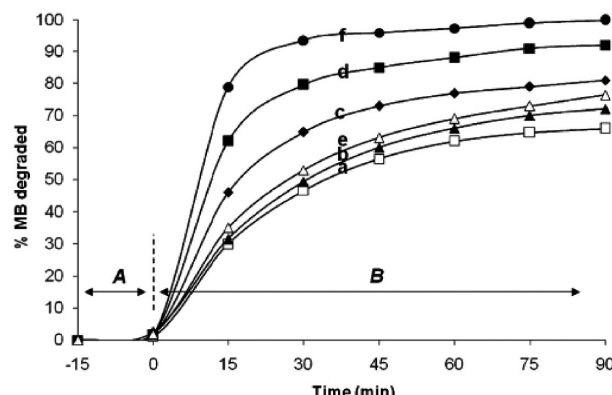
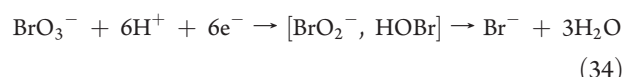


**Figure 39.** Decomposition of MB by titania hollow sphere photocatalysts in the presence of various electron scavengers: (b) 10 mM KCLO<sub>4</sub>, (c) 10 mM KBrO<sub>3</sub>, (d) 10 mM KIO<sub>4</sub>, (e) 10 mM H<sub>2</sub>O<sub>2</sub>, and (f) 10 mM K<sub>2</sub>S<sub>2</sub>O<sub>8</sub>. The plot (a) represents the decomposition of MB by titania hollow spheres in the absence of the electron scavengers. Reprinted with permission from Syoufian, A.; Nakashima, K. *J. Colloid Interface Sci.* 2008, 317, 507–512. Copyright Elsevier, 2008.

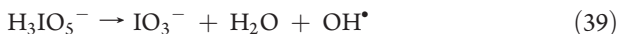
a viable option for the treatment of wastewater in advanced oxidation processes.

The addition of KBrO<sub>3</sub> in TiO<sub>2</sub> suspension is also reported to enhance the degradation of uracil and 5-bromouracil compared to pure TiO<sub>2</sub> which can be attributed to a large number of electrons involved in trapping (Figure 38).<sup>260</sup> Another plausible explanation is that there might be a change in the photocatalytic degradation reaction mechanism since the reduction of bromate anions by electrons does not lead directly to the formation of hydroxyl radicals but rather leads to the formation of other reactive radicals or oxidizing agents (BrO<sub>2</sub><sup>-</sup> or HOBr).<sup>260,264</sup>



Syoufian and Nakashima reported that the degradation of MB with various oxidants in titania dispersions showed the following order: S<sub>2</sub>O<sub>8</sub><sup>2-</sup> > IO<sub>4</sub><sup>-</sup> > BrO<sub>3</sub><sup>-</sup> > H<sub>2</sub>O<sub>2</sub> > ClO<sub>3</sub><sup>-</sup> (Figure 39).<sup>266</sup>

The degradation of 4-chloro-2-methyl phenol in the UV-TiO<sub>2</sub>-oxidant system was enhanced in the presence of various oxidants followed the order: IO<sub>4</sub><sup>-</sup> > BrO<sub>3</sub><sup>-</sup> > H<sub>2</sub>O<sub>2</sub> > O<sub>2</sub> > ClO<sub>3</sub><sup>-</sup>.<sup>274</sup> The effectiveness of oxyhalogens as electron scavengers in the TiO<sub>2</sub> system depends on the electronegativity and atomic radius of halogens. Electronegativity of the halogens is in the order Cl > Br > I, while the oxidation efficiency exhibited the reverse order. On the other hand, the atomic radius of the halogen in the oxyhalogens also plays an important role. Though BrO<sub>3</sub><sup>-</sup> and ClO<sub>3</sub><sup>-</sup> have the same number of oxygen atoms in the molecule, the smaller atomic radius of Cl makes it more sterically hindered by oxygens than Br for the approach of the CB electron. This is the reason why ClO<sub>3</sub><sup>-</sup> has a lower ability to trap electrons on the TiO<sub>2</sub> surface. Additionally, the oxidation rate may also depend on the number of radical and nonradical intermediates.<sup>266,274</sup>



The addition of the oxidants also enhanced the degradation rate of a few pesticides in both TiO<sub>2</sub> and BaTiO<sub>3</sub> suspension.<sup>275-277</sup> It is worthy to note that in highly toxic wastewater where the degradation of organic pollutants is of major concern the addition of electron acceptors or oxidizing agents to enhance the degradation rate may quite often be justified.<sup>265,266</sup>

## 11.0. ANATASE TITANIA WITH EXPOSED REACTIVE {001} FACETS

Toward the end of this century, exploring the photocatalytic application of the energetic {001} facet of titania was another recent venture in the area of TiO<sub>2</sub> photocatalysis. Since the recombination tends to occur on the grain boundaries and crystalline defects, the use of a single crystal with highly exposed reactive facets and low defect density is one possible strategy to prolong the separation of charge carriers. For anatase TiO<sub>2</sub>, the average surface energy of {001}, {100}, and {101} is 0.90, 0.53, and 0.44 J/m<sup>2</sup>, respectively.<sup>278</sup> Owing to the low atomic coordination numbers of exposed atoms and the wide bond angle of Ti—O—Ti, the anatase TiO<sub>2</sub> {001} facet is theoretically considered to be more reactive than the {101} facet in heterogeneous reactions.<sup>279</sup> According to the symmetries of anatase titania, two flat and square surfaces in the crystal structure of anatase titania can be ascribed to the {001} facet, and the eight isosceles trapezoidal surfaces are {101} facets (Figure 40). The high-quality truncated anatase bipyramids of isotropic anatase TiO<sub>2</sub> crystal with a large percentage (~47%) of reactive energetic {001} facets using TiF<sub>4</sub> as the precursor and HF as the capping agent under strong acidic hydrothermal conditions were first reported by Yang and co-workers.<sup>280</sup> They demonstrated that the order of surface free energy of the TiO<sub>2</sub> facet is {001} > {100} > {101} based on first-principle calculations. The calculations suggested that fluoride ions can significantly reduce the surface free energy of {001} to a level lower than that of {101},

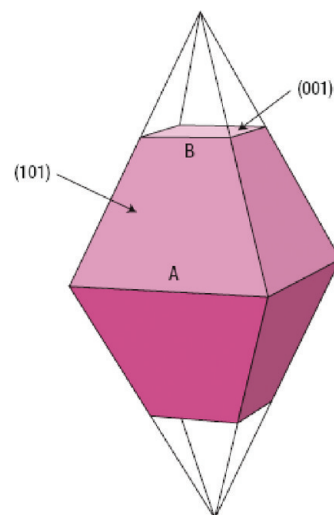


**Figure 40.** Facets of anatase TiO<sub>2</sub>. The truncated tetragonal bipyramidal crystal form, showing the {001} and {101} facets. A and B define the aspect ratio. Reprinted with permission from Selloni, A. *Nat. Mater.* 2008, 7, 613–615. Copyright Nature Publishing Group, 2008.

consequently resulting in the {001} surface being more stable than the {101} surface.<sup>280</sup> Amano et al.<sup>281</sup> prepared ~40% decahedral single crystalline anatase {001} facets ranging from 50 to 250 nm through gas-phase reaction of TiCl<sub>4</sub>.<sup>280</sup> The photocatalytic activity of {001} facets was higher or at least comparable to that of P25 for H<sub>2</sub> evolution and degradation of organic compounds in an aqueous solution.<sup>281</sup> The percentage of {001} facets was improved to 64%, when {001} facets were prepared by a solvothermal route using 2-propanol as a synergistic capping agent together with HF in the reaction medium.<sup>282</sup> The synergistic functionality of chemisorbed F to lower {001} surface energy and 2-propanol to enhance this stabilization and its role as a protective capping agent leads to the formation of {001} nanosheets. The normalized concentration of generated hydroxyl radicals (probed by the hydroxylation of terephthalic acid) was found to be five times higher than that of P25.<sup>282</sup> The TiO<sub>2</sub> nanosheet with ~80% {001} facet prepared by a hydrothermal route using titanium tetrabutoxide and 47% HF showed higher catalytic activity for the degradation of MO.<sup>283</sup> The percentage of reactive facets was tuned by changing the atomic ratio of F to Ti,<sup>284</sup> with a preparation method almost similar to that of Han and co-workers.<sup>283</sup> With an increase in the atomic ratio of F to Ti from 0 to 2.67, the percentage of {001} facets was increased from 10 to 78 ± 9%. When the F to Ti atomic ratio was 1, the optimal reactive {001} facets with 70% showed higher activity for the oxidation of acetone in air compared to TiO<sub>2</sub> with 78% {001} facets, suggesting the existence of optimum percentage of reactive facets to show enhanced activity (Figure 41).<sup>284</sup> Anatase polyhedra with an exposed ~20% {001} facet fluorinated hollow microsphere showed preferential decomposition for MO compared to MB in water, while the nonfluorinated surface that was obtained by calcination at 600 °C or with NaOH washing favored decomposition of MB over MO.<sup>285</sup> The preparation of {001} facets so far reported in the literature used the extremely corrosive and toxic HF which is against the principle of green chemistry. To overcome this task, Yu and co-workers<sup>286</sup> reported a microwave-assisted method using an aqueous solution of TiF<sub>4</sub> and a tetrafluoroborate-based ionic liquid which resulted in an

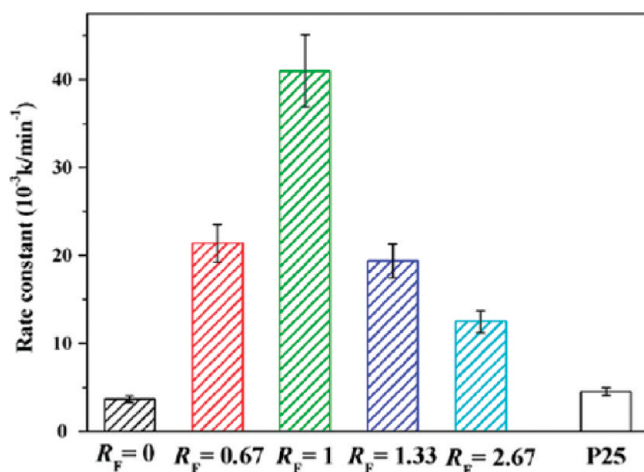


**Figure 41.** Comparison of photocatalytic activity of P25 and the  $\text{TiO}_2$  samples prepared with varying  $R_F$  for photocatalytic decomposition of acetone.  $R_F$  refers to atomic ratio of F to Ti in the preparation of the photocatalyst. Reprinted with permission from Xiang, Q.; Lv, K.; Yu, J. *J. Appl. Catal. B: Environ.* 2010, 96, 557–564. Copyright Elsevier, 2010.

anatase  $\text{TiO}_2$  single-crystal microsheet with as high as  $\sim 80\%$  {001} facets, which were easily recyclable for 4-CP degradation and thermally stable up to  $800\text{ }^\circ\text{C}$ . It should be noted that this temperature is high enough to induce the phase transformation to rutile in polycrystalline anatase titania. The anion of the ionic liquid is  $\text{BF}_4^-$  with four fluorine atoms that created a rich and dense fluorine environment on the crystal surface and promotes the growth along {001} facets compared to those systems in which HF was used as the fluorine source. In addition, improved anatase crystallinity by the ionic liquid was beneficial for exposing the {001} facets.

Doping with nonmetals is reported to shift the band gap response of {001} facets of anatase titania toward the visible region.<sup>287–292</sup> The nonmetal dopant forms an intraband state and serves as “stepping stones” for the absorption of low-energy photons via excitation of electrons at the top of the VB to intraband states, where they can be further excited to the bottom of the CB for effective photoresponse. Liu et al.<sup>287</sup> reported one-pot synthesis of a N– $\text{TiO}_2$  anatase nanosheet with dominant {001} facets ( $\sim 60\%$ ) by hydrothermal treatment of TiN and HF, which showed a visible absorption edge in the range 400–570 nm and also superior hydrogen evolution rate compared to N– $\text{TiO}_2$  without the {001} facet. N– $\text{TiO}_2$  with an exposed {001} facet ( $\sim 67\%$ ) synthesized by solvothermal synthesis of TiN in a  $\text{HNO}_3$ –HF ethanolic solution also exhibited much higher activity for the hydrogen evolution compared to the N– $\text{TiO}_2$  microcrystallite with an exposed {001} facet due to the larger surface area of the former compared to the latter. Ethanol in the synthesis process served as a capping agent, which hinders the growth of the anatase titania single crystal because of its specific bonding with the titania surface via the Ti–O–C bond.<sup>288</sup> Similarly, S– $\text{TiO}_2$  with an exposed {001} facet ( $\sim 41\%$ ) obtained by hydrothermal treatment of  $\text{TiS}_2$  and HF showed faster RhB degradation upon visible light irradiation,<sup>289</sup> but the activity was lower than N– $\text{TiO}_2$  with the {001} facet.<sup>287</sup> The amount of fluorine species in the S– $\text{TiO}_2$  {001} facet was  $\sim 5.6$  atom %,<sup>289</sup> while it was  $\sim 9.1$  atom % in the case of a N-doped nanosheet with 60% {001} facet.<sup>287</sup> This result suggests that more extensive surface-terminated Ti–F bonds

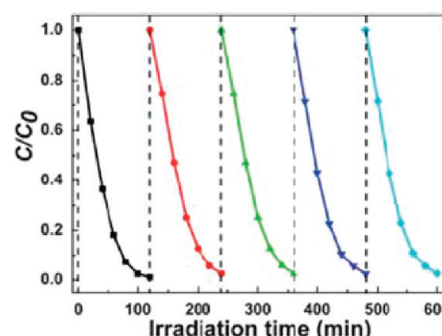


**Figure 42.** Cycling degradation curves of carbon doped titania {001} nanosheets for MB degradation under visible light irradiation. Reprinted with permission from Yu, J.; Dai, G.; Xiang, Q.; Jaroniec, M. *J. Mater. Chem.* 2011, 21, 1049–1057. Copyright Royal Society of Chemistry, 2011.

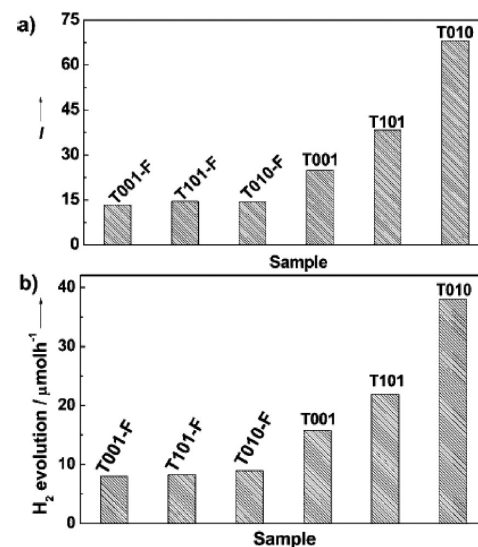


**Figure 43.** Comparison of photoreactivity of different facets: (a) fluorescence signal intensity of TAOH at 426 nm and (b) hydrogen evolution rate from water containing 10 vol % methanol for surface fluorine-terminated anatase  $\text{TiO}_2$  crystals T001-F, T101-F, and T010-F and clean anatase  $\text{TiO}_2$  crystals T001, T101, and T010. All samples for measurements of hydrogen evolution were deposited with 1 wt % Pt cocatalyst. Reprinted with permission from Pan, J.; Liu, G.; Lu, G. Q.; Cheng, H. M. *Angew. Chem., Int. Ed.* 2011, 50, 2133–2137. Copyright Wiley, 2011.

in anatase  $\text{TiO}_2$  play a significant role in tuning the percentage of {001} facets presumably by lowering the surface energy of {001} facets. C– $\text{TiO}_2$  with {001} facets ( $\sim 58\%$ ) prepared by hydrothermal treatment of TiC in a  $\text{HNO}_3$ –HF aqueous solution resulted in faster degradation of MB under visible irradiation compared to C– $\text{TiO}_2$  nanoparticles.<sup>290</sup> C– $\text{TiO}_2$  nanosheets retained their catalytic activity even after five subsequent runs (Figure 42), and it was easy to separate from slurry by natural settlement after the photocatalytic reaction, which was not possible for C– $\text{TiO}_2$  nanoparticles and Degussa P25. N–S– $\text{TiO}_2$  with  $\sim 54\%$  {001} facet showed higher activity for 4-CP degradation under visible light compared to the pure  $\text{TiO}_2$  nanosheet and N–S– $\text{TiO}_2$  nanoparticles.<sup>291</sup> The higher amount of pollutant adsorption on the 2D nanosheet was observed compared to their undoped counterparts. Furthermore, the enhanced generation of hydroxyl radicals by the nonmetal ion doped titania

with exposed {001} reactive facets under visible irradiation was also confirmed by photoluminescence technique using terephthalic acid as the probe molecule.<sup>286–291</sup> These nonmetal doped reactive facets are also of great interest for applications related to solar cells, optoelectronic devices, sensors, and catalysis.<sup>293</sup> Contrary to the above explanations, the photocatalytic activity of different clean facets for the generation of hydroxyl radicals and hydrogen evolution followed the order: {010} > {101} > {001} (Figure 43). However, these facets showed similar reactivity when partially terminated with fluorine which was attributed to a change in the surface structure imposed due to the presence of the Ti–F bond. It was proposed that {010} facets possess both favorable surface atomic-electronic structures, so that more CB electrons can be transferred via the surface Ti<sub>5c</sub> atoms as the active reaction sites. Thus, the efficient consumption of excited electrons in the photoreduction process promotes the holes in the photo-oxidation process.<sup>294</sup> Hence, more reliable theoretical and experimental evidence is needed to clarify the root cause of this inconsistency.

## 12.0. CONCLUSION

The search for visible light activated titania has been an increasing topic of interest worldwide because of its significance as a photocatalyst for environmental applications under solar irradiation. TiO<sub>2</sub> represents a new frontier material and has been the focal point of numerous investigations in recent years particularly because of its application in the quantitative destruction of undesirable pollutants. The significant number of voluminous literature on TiO<sub>2</sub> photocatalysis from the past four decades attests to the popularity of this remediation approach. Indeed, it is generally accepted that unmodified TiO<sub>2</sub> photocatalysis is only feasible for tackling low to medium concentration of pollutants because of relatively low efficiency and inability to utilize the visible portion of the solar spectrum. Hence, research aimed at enhancing its efficiency has intensified over the years. This review attempts to provide a comprehensive update and research focused on some fundamental issues besides highlighting the advancements made to improve the surface-electronic structure of titania with high efficiency. The tuning of physicochemical and optical electronic properties of TiO<sub>2</sub> by several methods like coupling with narrow band gap semiconductor, metal ion/nonmetal ion doping, codoping with two or more foreign ions, surface sensitization by organic dyes or metal complexes, and noble metal deposition, etc. have revealed a flexible line of action for wastewater treatment technologies. Rather than the generalization of the data, unique results so far developed have been highlighted. Tailoring the interface and bulk properties including surface band bending, surface and bulk recombination, surface state distribution, etc. mainly reflects the charge carrier separation and transfer behavior. We positively hope that this review article has provided some useful contribution for the future design, fabrication, and modification of semiconductor materials with nanoscale features for environmental and energy applications. The effective utilization of clean, safe, and abundant solar energy by the TiO<sub>2</sub> photocatalyst will lead to promising solutions not only for the solar energy crisis but also for serious environmental challenges. The applications of such photocatalytic systems not only convert inexhaustible light energy into chemical energy but also protect our environment, which is our greatest dream and hope. To this end, we are

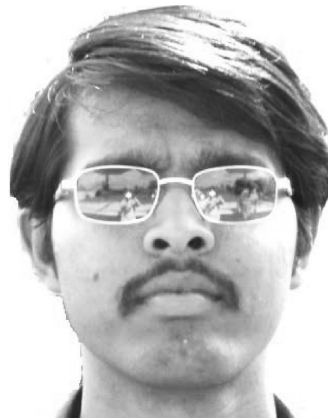
moving in a very positive direction with practical photocatalytic applications.

## ■ AUTHOR INFORMATION

### Corresponding Author

\*Tel.: + 91-080-22961336. E-mail: gomatidevi\_naik@yahoo.co.in.

## ■ BIOGRAPHIES



Shivashankar Girish Kumar, a native of Karnataka State, India, was born in 1983. He received his MSc in Physical Chemistry in 2005, and he is currently a PhD student of Prof. L. Gomathi Devi at Department of Chemistry, Bangalore University, India. His scientific research focuses on the application of titania-based photocatalysis and the photo Fenton process for wastewater treatment.



Professor Lakshmi Naik Gomathi Devi received her MSc degree (1981) from the University of Mysore and obtained her PhD in Chemistry from Indian Institute of Science (1988), Bangalore, India. She is currently working as a senior professor at Department of Chemistry, Bangalore University since 1992. Her research interest spans a broad spectrum of energy, environment, and materials chemistry problems.

## ■ REFERENCES

- (1) Fujishima, A.; Honda, K. *Nature* **1972**, *238*, 37–38.
- (2) Yang, Y.; Zhong, H.; Tian, C. *Res. Chem. Intermed.* **2011**, *37*, 91–102.
- (3) Friedmann, D.; Mendive, C.; Bahnemann, D. *Appl. Catal. B: Environ.* **2010**, *99*, 398–406.

- (4) Yu, J.; Yu, H.; Cheng, B.; Trapalis, C. *J. Mol. Catal. A: Chem.* **2006**, *249*, 135–142.
- (5) Yu, J.; Zhang, L.; Cheng, B.; Su, Y. *J. Phys. Chem. C* **2007**, *111*, 10582–10589.
- (6) (a) Yu, J.; Liu, W.; Yu, H. *Cryst. Growth Des.* **2008**, *8*, 930–934. (b) Yu, J.; Yu, H.; Cheng, B.; Zhao, X.; Yu, J. C.; Ho, W. *J. Phys. Chem. B* **2003**, *107*, 13871–13879. (c) Su, Y.; Yu, J.; Lin, J. *J. Solid State Chem.* **2007**, *180*, 2080–2087. (d) Yu, J.; Su, Y.; Cheng, B.; Zhou, M. *J. Mol. Catal. A: Chem.* **2006**, *258*, 104–112. (e) Yu, J.; Zhao, X.; Zhao, Q. *Mater. Chem. Phys.* **2001**, *69*, 25–29. (f) Yu, H.; Yu, J.; Cheng, B.; Lin, J. *J. Hazard. Mater.* **2007**, *147*, 581–587. (g) Yu, J.; Zhang, J. *Dalton Trans.* **2010**, *39*, 5860–5867.
- (7) (a) Yu, J.; Wang, G.; Cheng, B.; Zhou, M. *Appl. Catal. B: Environ.* **2007**, *69*, 171–180. (b) Houas, A.; Lachheb, H.; Ksibi, M.; Elaloui, E.; Guillard, C.; Herrmann, J. M. *Appl. Catal. B: Environ.* **2004**, *31*, 145–157. (c) Galindo, C.; Jacques, P.; Kalt, A. *J. Photochem. Photobiol. A: Chem.* **2000**, *130*, 35–47.
- (8) Yu, J.; Su, Y.; Cheng, B. *Adv. Funct. Mater.* **2007**, *17*, 1984–1990.
- (9) Yu, J.; Liu, S.; Yu, H. *J. Catal.* **2007**, *249*, 59–66.
- (10) Yu, J.; Wang, B. *Appl. Catal. B: Environ.* **2010**, *94*, 295–302.
- (11) Liu, G.; Wang, L.; Yang, H. G.; Cheng, H. M.; Lu, G. Q. *J. Mater. Chem.* **2010**, *20*, 831–843.
- (12) Hangfeldt, A.; Gratzel, M. *Chem. Rev.* **1995**, *95*, 49–68.
- (13) Kamat, P. V. *Chem. Rev.* **1993**, *93*, 267–300.
- (14) Legrini, O.; Oliveros, E.; Braun, A. M. *Chem. Rev.* **1993**, *93*, 671–698.
- (15) Linsebigler, A. L.; Lu, G.; Yates, J. T. *Chem. Rev.* **1995**, *95*, 735–758.
- (16) Hoffmann, M. R.; Martin, S. T.; Choi, W.; Bahnemann, D. W. *Chem. Rev.* **1995**, *95*, 69–96.
- (17) Thomson, T. L.; Yates, J. T. *Chem. Rev.* **2006**, *106*, 4428–4453.
- (18) Fox, M. A.; Dulay, M. T. *Chem. Rev.* **1993**, *93*, 341–357.
- (19) Chen, X. X.; Mao, S. S. *Chem. Rev.* **2007**, *107*, 2891–2959.
- (20) (a) Fujishima, A.; Rao, T. N.; Tryk, D. A. *J. Photochem. Photobiol. C: Photochem. Rev.* **2000**, *1*, 1–21. (b) Fujishima, A.; Zhang, X.; Tryk, D. A. *Surf. Sci. Rep.* **2008**, *63*, 515–582. (c) Henderson, M. A. *Surf. Sci. Rep.* **2011**, *66*, 185–297.
- (21) Mills, A.; Hunte, S. L. *J. Photochem. Photobiol. A: Chem.* **1997**, *108*, 1–35.
- (22) Carp, O.; Huisman, C. L.; Reller, A. *Prog. Solid State Chem.* **2004**, *32*, 33–177.
- (23) (a) Chatterjee, D.; Dasgupta, S. *J. Photochem. Photobiol. C: Photochem. Rev.* **2005**, *6*, 186–205. (b) Kudo, A.; Miseki, Y. *Chem. Soc. Rev.* **2009**, *38*, 253–278.
- (24) (a) Gaya, U. I.; Abdulla, A. H. *J. Photochem. Photobiol. C: Photochem. Rev.* **2008**, *9*, 1–12. (b) Akpan, U. G.; Hameed, B. H. *J. Hazard. Mater.* **2009**, *170*, 520–529. (c) Ahmed, S.; Rasul, M. G.; Brown, R.; Hashib, M. A. *J. Environ. Manage.* **2011**, *92*, 311–330.
- (25) Han, F.; Kambala, V. S. R.; Sirnivasan, M.; Rajarathnam, D.; Naidu, R. *Appl. Catal. A: Gen.* **2009**, *359*, 25–40.
- (26) Chen, X.; Shen, S.; Guo, L.; Mao, S. S. *Chem. Rev.* **2010**, *110*, 6503–6570.
- (27) Augliaro, V.; Litter, M.; Palmisano, L.; Soria, J. *J. Photochem. Photobiol. C: Photochem. Rev.* **2006**, *7*, 127–144.
- (28) Kitano, M.; Matsuoka, M.; Ueshima, M.; Anpo, M. *Appl. Catal. A: Gen.* **2007**, *325*, 1–14.
- (29) Hu, X.; Li, G.; Yu, J. C. *Langmuir* **2010**, *26*, 3031–3039.
- (30) Aprile, C.; Corma, A.; Garcia, H. *Phys. Chem. Chem. Phys.* **2008**, *10*, 769–783.
- (31) Serpone, N.; Borgarello, E.; Gratzel, M. *J. Chem. Soc., Chem. Commun.* **1984**, 342–344.
- (32) Serpone, N.; Maruthamuthu, P.; Pichat, P.; Pelizzetti, E.; Hidaka, H. *J. Photochem. Photobiol. A: Chem.* **1995**, *85*, 247–255.
- (33) Zhou, M.; Yu, J.; Liu, S.; Zhai, P.; Jiang, L. *J. Hazard. Mater.* **2008**, *154*, 1141–1148.
- (34) Hattori, A.; Yokihisa, Y.; Tada, H.; Ito, S. *J. Electrochem. Soc.* **2000**, *147*, 2279–2283.
- (35) Cao, Y.; Zhang, X.; Yang, W.; Du, H.; Bai, Y.; Li, T.; Yao, J. *Chem. Mater.* **2000**, *12*, 3445–3448.
- (36) Vinodgopal, K.; Kamat, P. V. *Environ. Sci. Technol.* **1995**, *29*, 841–845.
- (37) Shifu, C.; Lie, C.; Shen, G.; Gengyu, C. *Mater. Chem. Phys.* **2006**, *98*, 116–120.
- (38) Wu, C. H. *Chemosphere* **2004**, *57*, 601–608.
- (39) Wang, H.; Wu, Z.; Liu, Y.; Sheng, Z. *J. Mol. Catal. A: Chem.* **2008**, *287*, 176–181.
- (40) Wu, L.; Yu, J. C.; Fu, X. *J. Mol. Catal. A: Chem.* **2006**, *244*, 25–32.
- (41) Jang, J. S.; Li, W.; Oh, S. H.; Lee, J. S. *Chem. Phys. Lett.* **2006**, *425*, 278–282.
- (42) Park, H.; Choi, W.; Hoffmann, M. R. *J. Mater. Chem.* **2008**, *18*, 2379–2385.
- (43) Bessekhouad, Y.; Robert, D.; Weber, J. V. *J. Photochem. Photobiol. A: Chem.* **2004**, *163*, 569–580.
- (44) Sang, J. S.; Ji, S. M.; Bae, S. W.; Son, H. C.; Lee, J. S. *J. Photochem. Photobiol. A: Chem.* **2007**, *188*, 112–119.
- (45) Ho, W.; Yu, J. C.; Lin, J.; Yu, J.; Li, P. *Langmuir* **2004**, *20*, 5865–5869.
- (46) Ho, W.; Yu, J. C. *J. Mol. Catal. A: Chem.* **2006**, *247*, 268–274.
- (47) Gao, B.; Kim, Y. J.; Chakraborty, A. K.; Lee, W. I. *Appl. Catal. B: Environ.* **2008**, *83*, 202–207.
- (48) Kim, Y. J.; Gao, B.; Han, S. Y.; Jung, M. H.; Chakraborty, A. K.; Ko, T.; Lee, C.; Lee, W. I. *J. Phys. Chem. C* **2009**, *113*, 19179–19184.
- (49) Benko, G.; Kallioinen, J.; Tommola, J. E. I. K.; Yarstev, A. P.; Sundstrom, V. *J. Am. Chem. Soc.* **2002**, *124*, 489–493.
- (50) Wu, T.; Liu, G.; Zhao, J.; Hidaka, H.; Serpone, N. *J. Phys. Chem. B* **1998**, *102*, 5845–5851.
- (51) Vinodgopal, K.; Wynkoop, D. E.; Kamat, P. V. *Environ. Sci. Technol.* **1996**, *30*, 1660–1666.
- (52) Liu, G.; Wu, T.; Zhao, J.; Hidaka, H.; Serpone, N. *Environ. Sci. Technol.* **1999**, *33*, 2081–2087.
- (53) Qu, P.; Zhao, J.; Shen, T.; Hidaka, H. *J. Mol. Catal. A: Chem.* **1998**, *129*, 257–268.
- (54) Zhang, F.; Zhao, J.; Shen, T.; Hidaka, H.; Pelizzetti, E.; Serpone, N. *Appl. Catal. B: Environ.* **1998**, *15*, 147–156.
- (55) Zhang, F.; Zhao, J.; Zang, L.; Shen, T.; Hidaka, H.; Serpone, N.; Pelizzetti, E. *J. Mol. Catal. A: Chem.* **1997**, *120*, 173–178.
- (56) Stylidi, M.; Kondarides, D. I.; Verykios, X. E. *Appl. Catal. B: Environ.* **2004**, *47*, 189–201.
- (57) Schweitzer, C.; Schmidt, R. *Chem. Rev.* **2003**, *103*, 1685–1758.
- (58) DeRosa, M. C.; Crutchley, R. J. *Coord. Chem. Rev.* **2002**, *233*, 351–371.
- (59) Zhao, J.; Wu, T.; Wu, K.; Oikawa, K.; Hidaka, H.; Serpone, N. *Environ. Sci. Technol.* **1998**, *32*, 2394–2400.
- (60) Yin, M.; Li, Z.; Kou, J.; Zou, Z. *Environ. Sci. Technol.* **2009**, *43*, 8361–8366.
- (61) Jiang, D.; Xu, Y.; Wu, D.; Sun, Y. *J. Solid State Chem.* **2008**, *181*, 593–602.
- (62) Hilal, H. S.; Majjad, L. Z.; Zaatar, N.; Hamouz, A. E. *Solid State Sci.* **2007**, *9*, 9–15.
- (63) Li, X.; Chen, C.; Zhao, J. *Langmuir* **2001**, *17*, 4118–4122.
- (64) Boonstra, A. H.; Mutsaers, C. A. H. A. *J. Phys. Chem.* **1975**, *79*, 1940–1943.
- (65) Kim, S.; Choi, W. *J. Phys. Chem. B* **2005**, *109*, 5143–5149.
- (66) Wang, N.; Zhu, L.; Huang, Y.; She, Y.; Yu, Y.; Tang, H. *J. Catal.* **2009**, *266*, 199–206.
- (67) Kisch, H.; Macyk, W. *ChemPhysChem.* **2002**, *3*, 399–400.
- (68) Zhang, L.; Lange, C.; Abraham, I.; Storck, S.; Maier, W. F.; Kisch, H. *J. Phys. Chem. B* **1998**, *102*, 10765–10771.
- (69) Kisch, H.; Zang, L.; Lange, C.; Maier, W. F.; Antonius, C.; Meissner, D. *Angew. Chem., Int. Ed.* **1998**, *37*, 3034–3036.
- (70) Burgeth, G.; Kisch, H. *Coord. Chem. Rev.* **2002**, *230*, 41–47.
- (71) Macyk, H.; Kisch, H. *Chem.—Eur. J.* **2001**, *7*, 1862–1867.
- (72) Gilma, O. G.; Carlos, A. P. M.; Fernando, O. M.; Mozo, E. A. P. *Catal. Today* **2005**, *107*–108, 589–594.

- (73) Fung, A. K. M.; Chiu, B. K. W.; Lam, M. H. W. *Water Res.* **2003**, 37, 1939–1947.
- (74) Bae, E.; Choi, W.; Park, J.; Shin, H. S.; Kim, S. B.; Lee, J. S. *J. Phys. Chem. B* **2004**, 108, 14093–14101.
- (75) Wilke, K.; Breuer, H. D. *J. Photochem. Photobiol. A: Chem.* **1999**, 121, 49–53.
- (76) Zhiyong, Y.; Bensimon, M.; Sarria, V.; Stolichnov, I.; Jardin, W.; Laub, D.; Mielczarski, E.; Mielczarski, J.; Minsker, L. K.; Kiwi, J. *Appl. Catal. B: Environ.* **2007**, 76, 185–195.
- (77) (a) Zhou, M.; Yu, J.; Cheng, B. *J. Hazard. Mater.* **2006**, 137, 1838–1847. (b) Zhou, M. H.; Yu, J.; Cheng, B.; Yu, H. G. *Mater. Chem. Phys.* **2005**, 93, 159–163. (c) Yu, J.; Yu, H.; Ao, C. H.; Lee, S. C.; Yu, J. C.; Ho, W. *Thin Solid Films* **2006**, 496, 273–280. (d) Yu, J.; Xiang, Q.; Zhou, M. *Appl. Catal. B: Environ.* **2009**, 90, 595–602. (e) Bouras, P.; Stathatos, E.; Lianos, P. *Appl. Catal. B: Environ.* **2007**, 73, 51–59.
- (78) Kim, S.; Hwang, S. J.; Choi, W. *J. Phys. Chem. B* **2005**, 109, 24260–24267.
- (79) Colmenares, J. C.; Aramendia, M. A.; Marinas, A.; Marinas, J. M.; Urbano, F. J. *Appl. Catal. A: Gen.* **2006**, 306, 120–127.
- (80) Devi, L. G.; Kumar, S. G. *Appl. Surf. Sci.* **2011**, 257, 2779–2790.
- (81) Devi, L. G.; Kottam, N.; Murthy, B. N.; Kumar, S. G. *J. Mol. Catal. A: Chem.* **2010**, 328, 44–52.
- (82) Devi, L. G.; Murthy, B. N.; Kumar, S. G. *Mater. Sci. Eng., B* **2010**, 166, 1–6.
- (83) Devi, L. G.; Kottam, N.; Murthy, B. N.; Kumar, S. G. *Catal. Lett.* **2009**, 130, 496–503.
- (84) Devi, L. G.; Kumar, S. G.; Murthy, B. N.; Kottam, N. *Catal. Commun.* **2009**, 10, 794–798.
- (85) Devi, L. G.; Kottam, N.; Kumar, S. G.; Raju, K. S. A. *Catal. Lett.* **2009**, 131, 612–617.
- (86) Devi, L. G.; Murthy, B. N.; Kumar, S. G. *Chemosphere* **2009**, 76, 1163–1166.
- (87) Devi, L. G.; Murthy, B. N.; Kumar, S. G. *J. Mol. Catal. A: Chem.* **2009**, 308, 174–181.
- (88) Devi, L. G.; Kottam, N.; Kumar, S. G. *J. Phys. Chem. C* **2009**, 113, 15593–15601.
- (89) Devi, L. G.; Murthy, B. N. *Catal. Lett.* **2008**, 125, 320–330.
- (90) Devi, L. G.; Kottam, N.; Kumar, S. G.; Rajashekhar, K. E. *Cent. Eur. J. Chem.* **2010**, 8, 142–148.
- (91) Li, F. B.; Li, X. Z. *Appl. Catal. A: Gen.* **2002**, 228, 15–27.
- (92) Palmisano, L.; Augugliaro, V.; Sclafani, A.; Schiavello, M. *J. Phys. Chem.* **1988**, 92, 6710–6713.
- (93) Choi, W.; Termin, A.; Hoffmann, M. R. *J. Phys. Chem.* **1994**, 98, 13669–13679.
- (94) Chen, J.; Yao, M.; Wang, X. *J. Nanopart. Res.* **2008**, 10, 163–171.
- (95) Sheng, J.; Wu, Z.; Liu, Y.; Wang, H. *Catal. Commun.* **2008**, 9, 1941–1944.
- (96) Wu, Z.; Sheng, Z.; Liu, Y.; Wang, H.; Tang, N.; Wang, J. *J. Hazard. Mater.* **2009**, 164, 542–548.
- (97) Zhu, J.; Ren, J.; Huo, Y.; Bian, Z.; Li, H. *J. Phys. Chem. C* **2007**, 111, 18965–18969.
- (98) Lukac, J.; Klementova, M.; Bezdecik, P.; Bakardjieva, S.; Subrt, J.; Szatmary, L.; Bastl, Z.; Jirkovsky, J. *Appl. Catal. B: Environ.* **2007**, 74, 83–91.
- (99) Yu, J. C.; Lin, J.; Kwok, R. W. M. *J. Phys. Chem. B* **1998**, 102, 5094–5098.
- (100) Huang, Y.; Zheng, Z.; Ai, Z.; Zhang, L.; Fan, X.; Zou, Z. *J. Phys. Chem. B* **2006**, 110, 19323–19328.
- (101) Yu, J.; Liu, S.; Zhou, M. *J. Phys. Chem. C* **2008**, 112, 2050–2057.
- (102) Liu, H. J.; Liu, G. G.; Zhou, Q. X. *J. Solid State Chem.* **2009**, 182, 3238–3242.
- (103) Murakami, N.; Chiyo, T.; Tsubota, T.; Ohno, T. *Appl. Catal. A: Gen.* **2008**, 348, 148–152.
- (104) Zhang, Y.; Xu, H.; Xu, Y.; Zhang, H.; Wang, Y. *J. Photochem. Photobiol. A: Chem.* **2005**, 170, 279–285.
- (105) Lin, J.; Yu, J. C. *J. Photochem. Photobiol. A: Chem.* **1998**, 116, 63–67.
- (106) Ranjit, K. T.; Willner, I.; Bossmann, S. H.; Braun, A. M. *Environ. Sci. Technol.* **2001**, 35, 1544–1549.
- (107) Liqiang, J.; Xiaojun, S.; Baifu, X.; Baiqi, W.; Weimin, C.; Honggang, F. *J. Solid State Chem.* **2004**, 177, 3375–3382.
- (108) Li, F. B.; Li, X. Z.; Hou, M. F. *Appl. Catal. B: Environ.* **2004**, 48, 185–194.
- (109) Xu, A. W.; Gao, Y.; Liu, H. Q. *J. Catal.* **2002**, 207, 151–157.
- (110) Binham, S.; Daoud, W. A. *J. Mater. Chem.* **2011**, 21, 2041–2050.
- (111) Ranjit, K. T.; Wilner, I.; Bossmann, S. H.; Braun, A. M. *J. Catal.* **2001**, 204, 305–313.
- (112) Quan, X.; Zhao, Q.; Tan, H.; Sang, X.; Wang, F.; Dai, Y. *Mater. Chem. Phys.* **2009**, 114, 90–98.
- (113) Pleskov, Y. V. *Sov. Electrochem.* **1981**, 17, 1–25.
- (114) Choi, J.; Park, H.; Hoffmann, M. R. *J. Phys. Chem. C* **2010**, 114, 783–792.
- (115) Yin, S.; Aita, Y.; Komatsu, M.; Sato, T. *J. Eur. Ceram. Soc.* **2006**, 26, 2735–2742.
- (116) Khan, S. U. M.; Al-Shahry, M.; Ingler, W. B. *Science* **2002**, 297, 2243–2245.
- (117) Nagaveni, K.; Hegde, M. S.; Ravishankar, N.; Subbanna, G. N.; Madras, G. *Langmuir* **2004**, 20, 2900–2907.
- (118) Xu, C.; Killmeyer, R.; Gray, M. L.; Khan, S. U. M. *Appl. Catal. B: Environ.* **2006**, 64, 312–317.
- (119) Lettmann, C.; Hilderband, K.; Kisch, H.; Macyk, W.; Maier, W. E. *Appl. Catal. B: Environ.* **2001**, 32, 215–227.
- (120) Park, Y.; Kim, W.; Park, H.; Tachikawa, T.; Majima, T.; Choi, W. *Appl. Catal. B: Environ.* **2009**, 91, 355–361.
- (121) (a) Chen, D.; Yang, D.; Wang, Q.; Jiang, Z. *Ind. Eng. Chem. Res.* **2006**, 45, 4110–4116. (b) Asahi, R.; Morikawa, T.; Ohwaki, T.; Aoki, K.; Taga, Y. *Science* **2001**, 293, 269–271. (c) Liu, G.; Wang, L.; Sun, C.; Yan, X.; Wang, X.; Chen, Z.; Smith, S. C.; Cheng, H. M.; Lu, G. Q. *Chem. Mater.* **2009**, 21, 1266–1274. (d) Dong, F.; Zhao, W.; Wu, Z.; Guo, S. J. *Hazard. Mater.* **2009**, 162, 763–770.
- (122) Mrowetz, M.; Balcerski, W.; Colussi, A. J.; Hoffmann, M. R. *J. Phys. Chem. B* **2004**, 108, 17269–17273.
- (123) Hirakawa, T.; Nosaka, Y. *J. Phys. Chem. C* **2008**, 112, 15818–15823.
- (124) Sano, T.; Negishi, N.; Koike, K.; Takeuchi, T.; Matsuzawa, S. *J. Mater. Chem.* **2004**, 14, 380–384.
- (125) Satish, M.; Viswanathan, B.; Viswanath, R. P. *Appl. Catal. B: Environ.* **2007**, 74, 307–312.
- (126) Li, D.; Haneda, H.; Labhestwar, N. K.; Hishita, S.; Ohashi, N. *Chem. Phys. Lett.* **2005**, 401, 579–584.
- (127) Yu, J. C.; Zhang, L.; Zheng, Z.; Zhao, J. *Chem. Mater.* **2003**, 15, 2280–2286.
- (128) Yu, H. F. *J. Mater. Res.* **2007**, 22, 2565–2572.
- (129) (a) Su, Y.; Xiao, Y.; Fu, X.; Deng, Y.; Zhang, F. *Mater. Res. Bull.* **2009**, 44, 2169–2173. (b) Liu, G.; Sun, C.; Yan, X.; Cheng, L.; Chen, Z.; Wang, X.; Wang, L.; Smith, S. C.; Lu, G. Q.; Cheng, H. M. *J. Mater. Chem.* **2009**, 19, 2822–2829.
- (130) Shi, J. W.; Zheng, J. T.; Hu, Y.; Zhao, Y. C. *Mater. Chem. Phys.* **2007**, 106, 247–249.
- (131) Shi, J. W. *Chem. Eng. J.* **2009**, 151, 241–246.
- (132) Li, D.; Haneda, H.; Hishita, S.; Ohashi, N. *Chem. Mater.* **2005**, 17, 2596–2602.
- (133) Xu, J. H.; Li, J.; Dai, W.; Cao, Y.; Li, H.; Fan, K. *Appl. Catal. B: Environ.* **2008**, 79, 72–80.
- (134) Liu, G.; Zhao, Y.; Sun, C.; Lu, G. Q.; Cheng, H. M. *Angew. Chem., Int. Ed.* **2008**, 47, 4516–4520.
- (135) In, S.; Orlov, A.; Berg, R.; Garcia, F.; Jimenez, S. P.; Tikhov, M. S.; Wright, D. W.; Lambert, R. M. *J. Am. Chem. Soc.* **2007**, 129, 13790–13791.
- (136) Liu, G.; Sun, C.; Cheng, L.; Jin, Y.; Lu, H.; Wang, L.; Smith, S. C.; Lu, G. Q.; Cheng, H. M. *J. Phys. Chem. C* **2009**, 113, 12317–12324.
- (137) Ling, Q.; Sun, J.; Zhou, Q. *Appl. Surf. Sci.* **2008**, 254, 3236–3241.
- (138) He, Z.; Xu, X.; Song, S.; Xie, L.; Tu, J.; Chen, J.; Yan, B. *J. Phys. Chem. C* **2008**, 112, 16431–16437.

- (139) Song, S.; Tu, J.; Xu, L.; Xu, X.; He, Z.; Qiu, J.; Ni, J.; Chen, J. *Chemosphere* **2008**, *73*, 1401–1406.
- (140) Tan, K.; Zhang, H.; Xie, C.; Zheng, H.; Gu, Y.; Zhang, W. F. *Catal. Commun.* **2010**, *11*, 331–335.
- (141) Liu, C.; Tang, X.; Mo, C.; Qiang, Z. *J. Solid State Chem.* **2008**, *181*, 913–919.
- (142) Matsuo, S. O.; Omata, T.; Yoshimura, M. *J. Alloys Compd.* **2004**, *376*, 262–267.
- (143) Cong, Y.; Zhang, J.; Chen, F.; Anpo, M.; He, D. *J. Phys. Chem. C* **2007**, *111*, 10618–10623.
- (144) Liu, Z.; Wang, Y.; Chu, W.; Li, Z.; Ge, C. *J. Alloys Compd.* **2010**, *501*, 54–59.
- (145) Kim, S.; Lee, S. K. *J. Photochem. Photobiol. A: Chem.* **2009**, *203*, 145–150.
- (146) Huang, Y.; Ho, W.; Ai, Z.; Song, X.; Zhang, L.; Lee, S. *Appl. Catal. B: Environ.* **2009**, *89*, 398–405.
- (147) Sclafani, A.; Herrmann, J. M. *J. Phys. Chem.* **1996**, *100*, 13655–13661.
- (148) Sclafani, A.; Palmisano, L.; Davi, E. *New J. Chem.* **1990**, *14*, 265–268.
- (149) Testino, A.; Bellobono, I. R.; Buscaglia, V.; Canevali, C.; Arizeno, M. D.; Polizzi, S.; Scotti, R.; Morazzoni, F. *J. Am. Chem. Soc.* **2007**, *129*, 3564–3575.
- (150) Watson, S. S.; Beydoun, D.; Scott, J. A.; Amal, R. *Chem. Eng. J.* **2003**, *95*, 213–220.
- (151) Mills, A.; Lee, S. K.; Lepre, A. *J. Photochem. Photobiol. A: Chem.* **2003**, *155*, 199–205.
- (152) Habibi, M. H.; Vosooghiyan, H. *J. J. Photochem. Photobiol. A: Chem.* **2005**, *174*, 45–52.
- (153) Kim, S. J.; Lee, H. G.; Lee, J. K.; Lee, E. G.; Kim, S. J. *Appl. Catal. A: Gen.* **2003**, *242*, 89–99.
- (154) Li, Y.; Lee, N. H.; Lee, E. G.; Song, J. S.; Kim, S. J. *Chem. Phys. Lett.* **2004**, *389*, 124–128.
- (155) Nag, M.; Guin, D.; Basak, P.; Manorama, S. V. *Mater. Res. Bull.* **2008**, *43*, 3270–3285.
- (156) (a) Sun, B.; Smirniotis, P. G. *Catal. Today* **2003**, *88*, 49–59.  
(b) Wang, Sun, W.; Zhang, Z.; Zhang, X.; Li, R.; Ma, T.; Zhang, P.; Li, Y. *J. Mol. Catal. A: Chem.* **2007**, *272*, 84–90.
- (157) Jung, K. Y.; Park, S. B.; Jang, H. D. *Catal. Commun.* **2004**, *5*, 491–497.
- (158) Jongsomjit, B.; Wongsalee, T.; Praserthdam, P. *Catal. Commun.* **2005**, *6*, 705–710.
- (159) Baiju, K. V.; Zachariah, A.; Shukla, S.; Biju, S.; Reddy, M. L. P.; Warrier, K. G. K. *Catal. Lett.* **2009**, *130*, 130–136.
- (160) Sun, C.; Wang, N.; Zhou, S.; Hu, X.; Zhou, S.; Chen, P. *Chem. Commun.* **2008**, *3293*–3295.
- (161) Li, Z.; Zhang, X.; Nishimoto, S.; Jin, M.; Tryk, D. A.; Murakami, T.; Fujishima, A. *Langmuir* **2007**, *23*, 10916–10919.
- (162) Li, G.; Dimitrijevic, N. M.; Chen, L.; Nichols, J. M.; Rajh, T.; Gray, K. A. *J. Am. Chem. Soc.* **2008**, *130*, 5402–5403.
- (163) (a) Li, G.; Gray, K. A. *Chem. Phys.* **2007**, *339*, 173–187.  
(b) Hurum, D. C.; Gray, K. A.; Thurnauer, M. C. *J. Phys. Chem. B* **2005**, *109*, 977–980.
- (164) Bickley, R. I.; Carreno, T. G.; Lees, J. S.; Palmisano, L.; Tilley, R. J. D. *J. Solid State Chem.* **1991**, *92*, 178–190.
- (165) Yan, M.; Chen, F.; Zhang, J.; Anpo, M. *J. Phys. Chem. B* **2005**, *109*, 8673–8678.
- (166) Meulen, T. V. D.; Mattson, A.; Osterlund, L. *J. Catal.* **2007**, *251*, 131–144.
- (167) Bacsa, R. R.; Kiwi, J. *Appl. Catal. B: Environ.* **1998**, *16*, 19–29.
- (168) Jun, W.; Gang, Z.; Zhaozhong, Z.; Xiangdong, Z.; Guan, Z.; Teng, M.; Yuefeng, J.; Peng, Z.; Ying, L. *Dyes Pigm.* **2007**, *75*, 335–343.
- (169) Lei, S.; Duan, W. *J. Environ. Sci.* **2008**, *20*, 1263–1267.
- (170) Ohno, T.; Sarukawa, K.; Tokieda, K.; Matsumura, M. *J. Catal.* **2001**, *203*, 82–86.
- (171) Ohno, T.; Tokieda, K.; Higashida, S.; Matsumura, M. *Appl. Catal. A: Gen.* **2003**, *244*, 383–391.
- (172) Zhang, Q.; Gao, L.; Guo, J. *Appl. Catal. B: Environ.* **2000**, *26*, 207–215.
- (173) Zhao, L.; Han, M.; Lian, J. *Thin Solid Films* **2008**, *516*, 3394–3398.
- (174) Ambrus, Z.; Mogyorosi, K.; Szalai, A.; Alapi, T.; Demeter, K.; Dombi, A.; Sipos, P. *Appl. Catal. A: Gen.* **2008**, *340*, 153–161.
- (175) Bessekhouad, Y.; Robet, D.; Weber, J. V. *J. Photochem. Photobiol. A: Chem.* **2003**, *157*, 47–53.
- (176) Li, G.; Chen, L.; Graham, M. E.; Gray, K. A. *J. Mol. Catal. A: Chem.* **2007**, *275*, 30–35.
- (177) Li, G.; Ciston, S.; Saponjic, Z. V.; Chen, L.; Dimitrijevic, N. M.; Rajh, T.; Gray, K. A. *J. Catal.* **2008**, *253*, 105–110.
- (178) Chen, L.; Graham, M. E.; Li, G.; Gray, K. A. *Thin Solid Films* **2006**, *515*, 1176–1181.
- (179) Wu, C.; Yue, Y.; Deng, X.; Hua, W.; Gao, Z. *Catal. Today* **2004**, *93*–95, 863–869.
- (180) Bakardjieva, S.; Subrt, J.; Stengl, V.; Dianez, M. J.; Sayagues, M. *J. Appl. Catal. B: Environ.* **2005**, *58*, 193–202.
- (181) Chen, L.; Zhu, J.; Liu, Y. M.; Cao, Y.; Li, H. X.; He, H. Y.; Dai, W. L.; Fan, K. N. *J. Mol. Catal. A: Chem.* **2006**, *255*, 260–268.
- (182) Chan, C. K.; Porter, J. F.; Li, Y. G.; Guo, W.; Chan, C. M. *J. Am. Ceram. Soc.* **1999**, *82*, 566–572.
- (183) Zachariah, Z.; Baiju, K. V.; Shukla, S.; Deepa, K. S.; James, J.; Warrier, K. G. *J. Phys. Chem. C* **2008**, *112*, 11345–11356.
- (184) Chen, L.; Yao, B.; Cao, Y.; Fan, K. *J. Phys. Chem. C* **2007**, *111*, 11849–11853.
- (185) Panpranot, J.; Kontapakdee, K.; Praserthdam, P. *J. Phys. Chem. B* **2006**, *110*, 8019–8024.
- (186) Watson, S.; Beydoun, D.; Scott, J.; Amal, R. *J. Nanopart. Res.* **2004**, *6*, 193–207.
- (187) Hurum, D. C.; Agrios, A. G.; Gray, K. A.; Rajh, T.; Thurnauer, M. C. *J. Phys. Chem. B* **2003**, *107*, 4545–4549.
- (188) Emeline, A. V.; Smirnova, L. G.; Kuzmin, G. N.; Basov, L. L.; Serpone, N. *J. Photochem. Photobiol. A: Chem.* **2002**, *148*, 97–102.
- (189) Li, Y.; Li, H.; Li, T.; Li, G.; Cao, R. *Microporous Mesoporous Mater.* **2009**, *117*, 444–449.
- (190) Xiao, Q.; Si, Z.; Yu, Z.; Qiu, G. *Mater. Sci. Eng., B* **2007**, *137*, 189–194.
- (191) Xiao, Q.; Si, Z.; Zhang, J.; Xiao, C.; Tan, X. *J. Hazard. Mater.* **2008**, *150*, 62–67.
- (192) Xiao, Q.; Si, Z.; Yu, Z.; Qiu, G. *J. Alloys Compd.* **2008**, *450*, 426–431.
- (193) Liu, G.; Chen, Z.; Dong, C.; Zhao, Y.; Li, F.; Lu, G. Q.; Cheng, H. M. *J. Phys. Chem. B* **2006**, *110*, 20823–20828.
- (194) Liu, G.; Yan, X.; Chen, Z.; Wang, X.; Wang, L.; Lu, G. Q.; Cheng, H. M. *J. Mater. Chem.* **2009**, *19*, 6590–6596.
- (195) Jiang, D.; Zhang, S.; Zhao, H. *Environ. Sci. Technol.* **2007**, *41*, 303–308.
- (196) Yu, J.; Yu, J. C.; Ho, W.; Jiang, Z. *New J. Chem.* **2002**, *26*, 607–613.
- (197) Ardizzone, S.; Bianchi, C. L.; Cappelletti, G.; Gialanella, S.; Pirola, C.; Ragaini, V. *J. Phys. Chem. C* **2007**, *111*, 13222–13231.
- (198) Ozawa, T.; Iwasaki, M.; Tada, H.; Akita, T.; Tanaka, K.; Ito, S. *J. Colloid Interface Sci.* **2005**, *281*, 510–513.
- (199) Tian, B.; Fu, H.; Jing, L.; Tian, C. *J. Hazard. Mater.* **2009**, *161*, 1122–1130.
- (200) Yu, J. C.; Zhang, L.; Yu, J. *Chem. Mater.* **2002**, *14*, 4647–4653.
- (201) Yu, J.; Yu, J. C.; Ho, W.; Zhang, L. Z. *Chem. Commun.* **2001**, 1942–1943.
- (202) Li, L.; Liu, C. Y. *Eur. J. Inorg. Chem.* **2009**, 3727–3733.
- (203) Yu, J.; Yu, J. C.; Ho, W.; Jiang, Z.; Zhang, L. *Chem. Mater.* **2002**, *14*, 3808–3816.
- (204) Yu, J.; Zhou, M.; Cheng, B.; Yu, H.; Zhao, X. *J. Mol. Catal. A: Chem.* **2005**, *227*, 75–80.
- (205) Yu, J.; Yu, J. C.; Yu, J.; Kwok, Y. C.; Che, Y. K.; Zhao, J. C.; Ding, L.; Ge, W. K.; Wong, P. K. *Appl. Catal. A: Gen.* **2005**, *289*, 186–196.
- (206) Kang, X.; Chen, S. *J. Mater. Sci.* **2010**, *45*, 2696–2702.

- (207) Liu, J.; Qin, W.; Zuo, S.; Yu, Y.; Hao, Z. *J. Hazard. Mater.* **2009**, *163*, 273–278.
- (208) Zhao, B.; Chen, F.; Huang, Q.; Zhang, J. *Chem. Commun.* **2009**, *5115*–*5117*.
- (209) Xu, H.; Zhang, L. *J. Phys. Chem. C* **2009**, *113*, 1785–1790.
- (210) Paola, A. D.; Bellardita, M.; Ceccato, R.; Palmisano, L.; Parrino, F. *J. Phys. Chem. C* **2009**, *113*, 15166–15174.
- (211) Yu, J.; Xiong, J.; Cheng, B.; Liu, S. *Appl. Catal. B: Environ.* **2005**, *60*, 211–221.
- (212) Lopez, T.; Gomez, R.; Sanchez, E.; Tzompantzi, F.; Vera, L. *J. Sol-Gel Sci. Technol.* **2001**, *22*, 99–107.
- (213) Leytner, S.; Hupp, J. T. *Chem. Phys. Lett.* **2000**, *330*, 231–236.
- (214) Torimoto, T.; Nakamura, S.; Ikeda, S.; Ohtani, B. *Phys. Chem. Chem. Phys.* **2002**, *4*, 5910–5914.
- (215) Kawahara, T.; Konishi, Y.; Tada, H.; Tohge, N.; Nishii, J.; Ito, S. *Angew. Chem., Int. Ed.* **2002**, *41*, 2811–2813.
- (216) Gomez, P. R.; Borras, A.; Barranco, A.; Espinos, J.; Elipe, A. R. G. *ChemPhysChem* **2011**, *12*, 191–196.
- (217) Rosseler, O.; Shankar, M. V.; Du, M. K.; Shmidlin, L.; Keller, N.; Keller, V. *J. Catal.* **2010**, *269*, 179–190.
- (218) Scotti, R.; Bellobono, I. R.; Canevali, C.; Cannas, C.; Catti, M.; Arienzo, M. D.; Musinu, A.; Polizzi, S.; Sommariva, M.; Testino, A.; Morazzoni, F. *Chem. Mater.* **2008**, *20*, 4051–4061.
- (219) Hong, X.; Wang, Z.; Cai, W.; Lu, F.; Zhang, J.; Yang, Y.; Ma, N.; Liu, Y. *Chem. Mater.* **2005**, *17*, 1548–1552.
- (220) Liu, G.; Wang, X.; Chen, Z.; Cheng, H. M.; Lu, G. Q. *J. Colloid Interface Sci.* **2009**, *329*, 331–338.
- (221) Liu, G.; Wang, X.; Chen, Z.; Li, F.; Lu, G. Q.; Cheng, H. M. *J. Colloid Interface Sci.* **2009**, *334*, 171–175.
- (222) Li, W.; Liu, C.; Zhou, Y.; Bai, Y.; Feng, X.; Yang, Z.; Lu, L.; Lu, X.; Chan, K. Y. *J. Phys. Chem. C* **2008**, *112*, 20539–20545.
- (223) Zheng, Z.; Liu, H.; Ye, J.; Zhao, J.; Waclawik, E. R.; Zhu, H. *J. Mol. Catal. A: Chem.* **2010**, *316*, 75–82.
- (224) (a) Kamat, P. V. *J. Phys. Chem. B* **2002**, *106*, 7729–7744. *J. Phys. Chem. C* **2007**, *111*, 2834–2860. (b) Yu, J.; Yue, L.; Liu, S.; Huang, B.; Zhang, H. *J. Colloid Interface Sci.* **2009**, *334*, 58–64. (c) Xiang, Q.; Yu, J.; Cheng, B.; Ong, H. C. *Chem. Asian J.* **2010**, *5*, 1466–1474.
- (225) Subramanian, V.; Wolf, E. E.; Kamat, P. V. *J. Am. Chem. Soc.* **2004**, *126*, 4943–4950.
- (226) Shi, J.; Chen, J.; Feng, Z.; Chen, T.; Lian, Y.; Wang, X.; Li, C. *J. Phys. Chem. C* **2007**, *111*, 693–699.
- (227) Bosc, F.; Ayral, A.; Keller, N.; Keller, V. *Appl. Catal. B: Environ.* **2007**, *69*, 133–137.
- (228) Hidalgo, M. C.; Maicu, M.; Navio, J. A.; Colon, G. *Catal. Today* **2007**, *129*, 43–49.
- (229) Sclafani, A.; Herrmann, J. M. *J. Photochem. Photobiol. A: Chem.* **1998**, *113*, 181–188.
- (230) (a) Kim, S.; Choi, W. *J. Phys. Chem. B* **2002**, *106*, 13311–13317. (b) Sun, B.; Vorontsov, A. V.; Smirniotis, P. G. *Langmuir* **2003**, *19*, 3151–3156.
- (231) Christopher, P.; Ingram, D. V.; Linic, S. *J. Phys. Chem. C* **2010**, *114*, 9173–9177.
- (232) Bardos, E. S.; Czili, H.; Horvath, A. *J. Photochem. Photobiol. A: Chem.* **2003**, *154*, 195–201.
- (233) Orlov, A.; Jefferson, D. A.; Tikhov, M.; Lambert, R. M. *Catal. Commun.* **2007**, *8*, 821–824.
- (234) Tian, B.; Zhang, J.; Tong, T.; Chen, F. *Appl. Catal. B: Environ.* **2008**, *79*, 394–401.
- (235) Wu, Y.; Zhang, J.; Xiao, L.; Chen, F. *Appl. Catal. B: Environ.* **2009**, *88*, 525–532.
- (236) Wu, Y.; Liu, H.; Zhang, J.; Chen, F. *J. Phys. Chem. C* **2009**, *113*, 14689–14695.
- (237) Hidalgo, M. C.; Maicu, M.; Navio, J. A.; Colon, G. *Appl. Catal. B: Environ.* **2008**, *81*, 49–55.
- (238) Park, H.; Choi, W. *J. Phys. Chem. B* **2004**, *108*, 4086–4093.
- (239) Minero, C.; Mariella, G.; Maurino, V.; Pelizzetti, E. *Langmuir* **2000**, *16*, 2632–2641.
- (240) Minero, C.; Mariella, G.; Maurino, V.; Vione, D.; Pelizzetti, E. *Langmuir* **2000**, *16*, 8964–8972.
- (241) Mrowetz, M.; Sellli, E. *Phys. Chem. Chem. Phys.* **2005**, *7*, 1100–1102.
- (242) Yu, J.; Wang, W.; Cheng, B.; Su, B. L. *J. Phys. Chem. C* **2009**, *113*, 6743–6750.
- (243) Janczyk, A.; Krakowska, E.; Stochel, G.; Macyk, W. *J. Am. Chem. Soc.* **2006**, *128*, 15574–15575.
- (244) Tang, J.; Quan, H.; Ye, J. *Chem. Mater.* **2007**, *19*, 116–122.
- (245) Xu, Y.; Lv, K.; Xiong, Z.; Leng, W.; Du, W.; Liu, D.; Xue, X. *J. Phys. Chem. C* **2007**, *111*, 19024–19032.
- (246) Wang, Q.; Chen, C.; Zhao, D.; Ma, W.; Zhao, J. *Langmuir* **2008**, *24*, 7338–7345.
- (247) (a) Mrowetz, M.; Sellli, E. *New J. Chem.* **2006**, *30*, 108–114. (b) Cheng, X. F.; Leng, W. H.; Liu, D. P.; Xu, Y. M.; Zhang, J. Q.; Cao, C. N. *J. Phys. Chem. C* **2008**, *112*, 8725–8734.
- (248) Kim, J.; Lee, J.; Choi, W. *Chem. Commun.* **2008**, 756–758.
- (249) Hidalgo, M. C.; Maicu, M.; Navio, J. A.; Colon, G. *Appl. Catal. B: Environ.* **2008**, *81*, 49–55.
- (250) Nakajima, A.; Obata, H.; Kameshima, Y.; Okada, K. *Catal. Commun.* **2005**, *6*, 716–720.
- (251) Kormali, P.; Troupis, A.; Triantis, T.; Hiskia, A.; Papaconstantinou, E. *Catal. Today* **2007**, *124*, 149–155.
- (252) Park, H.; Choi, W. *J. Phys. Chem. B* **2003**, *107*, 3885–3890.
- (253) (a) Chen, C.; Lei, P.; Ji, H.; Ma, W.; Zhao, J.; Hidaka, H.; Serpone, N. *Environ. Sci. Technol.* **2004**, *38*, 329–337. (b) Lv, K.; Xu, Y. *J. Phys. Chem. B* **2006**, *110*, 6204–6212.
- (254) Saquib, M.; Tariq, M. A.; Faisal, M.; Muneer, M. *Desalination* **2008**, *219*, 301–311.
- (255) Muneer, M.; Qamar, M.; Saquib, M.; Bahnamann, D. W. *Chemosphere* **2005**, *61*, 457–468.
- (256) Haque, M. M.; Muneer, M. *J. Environ. Manage.* **2003**, *69*, 169–176.
- (257) Qamar, M.; Muneer, M.; Bahnamann, D. W. *J. Environ. Manage.* **2006**, *80*, 99–106.
- (258) Tariq, M. A.; Faisal, M.; Saquib, M.; Muneer, M. *Dyes Pigm.* **2008**, *76*, 358–365.
- (259) Saquib, M.; Tariq, M. A.; Haque, M. M.; Muneer, M. *J. Environ. Manage.* **2008**, *88*, 300–306.
- (260) Singh, H. K.; Saquib, M.; Haque, M. M.; Muneer, M. *J. Hazard. Mater.* **2007**, *142*, 425–430.
- (261) Qamar, M.; Saquib, M.; Muneer, M. *Desalination* **2005**, *171*, 185–193.
- (262) Singh, H. K.; Saquib, M.; Haque, M. M.; Muneer, M. *J. Hazard. Mater.* **2007**, *142*, 374–380.
- (263) Qamar, M.; Saquib, M.; Muneer, M. *Dyes Pigm.* **2005**, *65*, 1–9.
- (264) Singh, H. K.; Saquib, M.; Haque, M. M.; Muneer, M. *J. Mol. Catal. A: Chem.* **2007**, *264*, 66–72.
- (265) Syoufian, A.; Nakashima, K. *J. Colloid Interface Sci.* **2007**, *313*, 213–218.
- (266) Syoufian, A.; Nakashima, K. *J. Colloid Interface Sci.* **2008**, *317*, 507–512.
- (267) Neta, P.; Madhavan, V.; Zemel, H.; Fessenden, R. W. *J. Am. Chem. Soc.* **1977**, *99*, 163–164.
- (268) Devi, L. G.; Kumar, S. G.; Reddy, K. M.; Munikrishnappa, C. *qJ. Hazard. Mater.* **2009**, *164*, 459–467.
- (269) Devi, L. G.; Rajashekhar, K. E.; Raju, K. S. A.; Kumar, S. G. *J. Mol. Catal. A: Chem.* **2009**, *314*, 88–94.
- (270) Devi, L. G.; Kumar, S. G.; Reddy, K. M. *Cent. Eur. J. Chem.* **2009**, *7*, 468–477.
- (271) Devi, L. G.; Kumar, S. G.; Raju, K. S. A.; Rajashekhar, K. E. *Chem. Pap.* **2010**, *64*, 378–385.
- (272) Devi, L. G.; Raju, K. S. A.; Kumar, S. G. *J. Environ. Monit.* **2009**, *11*, 1397–1404.
- (273) Devi, L. G.; Raju, K. S. A.; Kumar, S. G.; Rajashekhar, K. E. *J. Taiwan Inst. Chem. Eng.* **2011**, *42*, 341–349.
- (274) Irmak, S.; Kusvaran, E.; Erbatur, D. *Appl. Catal. B: Environ.* **2004**, *54*, 85–91.

- (275) Devi, L. G.; Krishnamurthy, G. *J. Phys. Chem. A* **2011**, *115*, 460–469.
- (276) Devi, L. G.; Krishnamurthy, G. *J. Hazard. Mater.* **2009**, *162*, 899–905.
- (277) Devi, L. G.; Krishnamurthy, G. *J. Environ. Sci. Health Part A* **2008**, *43*, 553–561.
- (278) Diebold, U. *Surf. Sci. Rep.* **2003**, *48*, 53–229.
- (279) (a) Selloni, A. *Nat. Mater.* **2008**, *7*, 613–615. (b) Lv, K.; Xiang, Q.; Yu, J. *Appl. Catal. B: Environ.* **2011**, *104*, 275–281. (c) Sun, S.; Liu, L.; Selloni, A.; Lu, G. Q.; Smith, S. C. *J. Mater. Chem.* **2010**, *20*, 10319–10334. (d) Fang, W. Q.; Gong, X. Q.; Yang, H. G. *J. Phys. Chem. Lett.* **2011**, *2*, 725–734. (e) Yu, J.; Xiang, Q.; Ran, J.; Mann, S. *CrystEngComm.* **2010**, *12*, 872–879. (f) Wen, C. Z.; Jiang, H. B.; Qiao, S. Z.; Yang, H. G.; Lu, G. Q. *J. Mater. Chem.* **2011**, *21*, 7052–7061. (g) Liu, B.; Nakata, K.; Sakai, M.; Saito, H.; Ochiai, T.; Murakami, T.; Takagi, K.; Fujishima, A. *Langmuir* **2011**, *27*, 8500–8508.
- (280) Yang, H. G.; Sun, C. H.; Qiao, S. Z.; Zou, J.; Liu, G.; Smith, S. C.; Cheng, H. M.; Lu, G. Q. *Nature* **2008**, *453*, 638–641.
- (281) Amano, F.; Mahaney, O. O. P.; Terada, Y.; Yasumoto, T.; Shibayama, T.; Ohtani, B. *Chem. Mater.* **2009**, *21*, 2601–2603.
- (282) Yang, H. G.; Liu, G.; Qiao, S. Z.; Sun, C. H.; Jin, Y. G.; Smith, S. C.; Zou, J.; Cheng, H. M.; Lu, G. Q. *J. Am. Chem. Soc.* **2009**, *131*, 4078–4083.
- (283) Han, X.; Kuang, Q.; Jin, M.; Xie, Z.; Zheng, L. *J. Am. Chem. Soc.* **2009**, *131*, 3152–3153.
- (284) Xiang, Q.; Lv, K.; Yu, J. *Appl. Catal. B: Environ.* **2010**, *96*, 557–564.
- (285) Liu, S.; Yu, J.; Jaroniec, M. *J. Am. Chem. Soc.* **2010**, *132*, 11914–11916.
- (286) Zhang, D.; Li, G.; Yang, X.; Yu, J. C. *Chem. Commun.* **2009**, 4381–4383.
- (287) Liu, G.; Yang, H. G.; Cheng, L.; Pan, J.; Lu, G. Q.; Cheng, H. M. *J. Am. Chem. Soc.* **2009**, *131*, 12868–12869.
- (288) Xiang, Q.; Yu, J.; Wang, W.; Jaroniec, M. *Chem. Commun.* **2011**, *47*, 6906–6908.
- (289) Liu, G.; Sun, C.; Smith, S. C.; Wang, L.; Lu, G. Q.; Cheng, H. M. *J. Colloid Interface Sci.* **2010**, *349*, 477–483.
- (290) Yu, J.; Dai, G.; Xiang, Q.; Jaroniec, M. *J. Mater. Chem.* **2011**, *21*, 1049–1057.
- (291) Xiang, Q.; Yu, J.; Jaroniec, M. *Phys. Chem. Chem. Phys.* **2011**, *13*, 4853–4861.
- (292) Liu, G.; Yu, J. C.; Lu, G. Q.; Cheng, H. M. *Chem. Commun.* **2011**, *47*, 6763–6783.
- (293) Yu, J.; Fan, J. J.; Lv, K. *Nanoscale* **2010**, *2*, 2144–2149.
- (294) Pan, J.; Liu, G.; Lu, G. Q.; Cheng, H. M. *Angew. Chem., Int. Ed.* **2011**, *50*, 2133–2137.